

**PL-TR-96-2022**

**DESIGN, EVALUATION, AND  
CONSTRUCTION OF TEXESS AND  
LUXESS, AND RESEARCH IN MINI-ARRAY  
TECHNOLOGY AND USE OF DATA  
FROM SINGLE STATIONS AND SPARSE  
NETWORKS: PHASE V**

**Eugene Herrin  
Paul Golden  
Herbert Robertson**

**Southern Methodist University  
Dallas, TX 75275**

**October 1995**

**Scientific Report No. 5**

**FOUO QUALITY INSPECTED 2**

**APPROVED FOR PUBLIC RELEASE; DISTRIBUTION UNLIMITED**



**PHILLIPS LABORATORY  
Directorate of Geophysics  
AIR FORCE MATERIEL COMMAND  
HANSCOM AFB, MA 01731-3010**

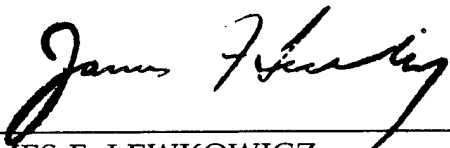
**19960408 142**

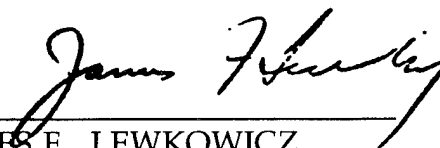
SPONSORED BY  
Advanced Research Projects Agency (DoD)  
Nuclear Monitoring Research Office  
ARPA ORDER No. A-128

MONITORED BY  
Phillips Laboratory  
CONTRACT No. F19628-93-C-0057

The views and conclusions contained in this document are those of the authors and should not be interpreted as representing the official policies, either express or implied, of the Air Force or the U.S. Government.

This technical report has been reviewed and is approved for publication.

  
\_\_\_\_\_  
JAMES F. LEWKOWICZ  
Contract Manager  
Earth Sciences Division

  
\_\_\_\_\_  
JAMES F. LEWKOWICZ  
Director  
Earth Sciences Division

This report has been reviewed by the ESC Public Affairs Office (PA) and is releasable to the National Technical Information Service (NTIS).

Qualified requestors may obtain additional copies from the Defense Technical Information Center. All others should apply to the National Technical Information Service.

If your address has changed, or if you wish to be removed from the mailing list, or if the addressee is no longer employed by your organization, please notify PL/IM, 29 Randolph Road, Hanscom AFB, MA 01731-3010. This will assist us in maintaining a current mailing list.

Do not return copies of this report unless contractual obligations or notices on a specific document requires that it be returned.

REPORT DOCUMENTATION PAGE			Form Approved OMB No. 0704-0188	
Public reporting burden for this collection of information is estimated to average 1 hour per response, including the time for reviewing instructions, searching existing data sources, gathering and maintaining the data needed, and completing and reviewing the collection of information. Send comments regarding this burden estimate or any other aspect of this collection of information, including suggestions for reducing this burden, to Washington Headquarters Services, Directorate for Information Operations and Reports, 1215 Jefferson Davis Highway, Suite 1204, Arlington, VA 22202-4302, and to the Office of Management and Budget, Paperwork Reduction Project (0704-0188), Washington, DC 20503.				
1. AGENCY USE ONLY (Leave blank)	2. REPORT DATE October 1995	3. REPORT TYPE AND DATES COVERED Scientific No. 5		
4. TITLE AND SUBTITLE Design, Evaluation and Construction of TEXESS and LUXESS & Research in Mini-Array Technology & Use of Data from Single Stations and Sparse Networks: Phase V		5. FUNDING NUMBERS PE: 62301E PR NM93 TA GM WU AK  Contract F19628-93-C-0057		
6. AUTHOR(S) Eugene Herrin Paul Golden Herbert Robertson				
7. PERFORMING ORGANIZATION NAME(S) AND ADDRESS(ES) Southern Methodist University Dallas, TX 75275		8. PERFORMING ORGANIZATION REPORT NUMBER		
9. SPONSORING/MONITORING AGENCY NAME(S) AND ADDRESS(ES) Phillips Laboratory 29 Randolph Road Hanscom AFB, MA 01731-3010  Contract Manager: James Lewkowicz/ GPE		10. SPONSORING/MONITORING AGENCY REPORT NUMBER PL-TR-96-2022		
11. SUPPLEMENTARY NOTES				
12a. DISTRIBUTION/AVAILABILITY STATEMENT  Approved for public release; distribution unlimited		12b. DISTRIBUTION CODE		
13. ABSTRACT (Maximum 200 words) In a discrimination study corollary to the AR method, phase-matched-filtering techniques were used to analyze Rg dispersion from mine blasts. Short-period surface waves from chemical explosions were used to obtain reliable dispersion curves for surface waves being generated, and to establish any azimuthal variations in relative Rg (fundamental-mode, short-period Rayleigh wave) energy at azimuths around the quarry, including the quarry pit's influence on these energy variations. Observed dispersion curves were interpreted using theoretical dispersion curves that consider estimated values of Poisson's ratio (0.35-0.4) for the central Texas' upper crust. The Rg dispersion has 3 sections; an inversely dispersed branch complicated by the presence of higher modes (at periods less than 0.6 seconds), a group velocity minima (at periods between 0.6 and 0.7 seconds), and normally dispersed Rg (between 0.7 and 3.0 seconds with an inflection point near 1.7 seconds). In the period interval between 0.7 and 1.5 seconds, multipathing complicates interpretation of the dispersion curve by creating spectral holes in multiple filter analysis (MFA), a single station routine for calculating group velocity dispersion. Spectral holes must be dealt with before interpreting the final dispersion curve, which is then used to extract Rg from the complex wave train by phase match filtering (PMF). Rg extracted from paths not traversing the open pit of the quarry have more energy than paths influenced by the open pit. Likewise, higher-mode energy exceeds fundamental-mode energy only when the propagation path includes the open pit.				
14. SUBJECT TERMS  Rg dispersion Spectral holes Phase-matched filtering techniques		15. NUMBER OF PAGES 96		
		16. PRICE CODE		
17. SECURITY CLASSIFICATION OF REPORT Unclassified	18. SECURITY CLASSIFICATION OF THIS PAGE Unclassified	19. SECURITY CLASSIFICATION OF ABSTRACT Unclassified	20. LIMITATION OF ABSTRACT SAR	

## CONTENTS

Summary	1
Objectives	1
Technical Problem	2
General Methodology	2
Technical Results	3
Important Findings and Conclusions	3
Significant Hardware Development	4
Special Comments	4
Implications for Further Research	4
CLIN 1 - RESEARCH	5
Array Research	5
Calibration Studies	6
Discrimination Research	6
Acoustic Research	8
CLIN 2 - DESIGN, EVALUATION, AND CONSTRUCTION OF TEXESS AND LUXESS	8
Experimental Array Program	8
TEXESS and LUXESS	8
Acquisition of Hardware and Software	9
Array Hardware	9
Computer Hardware	9

## CONTENTS

Software	9
Install TXAR	9
Layout	9
Installation	9
Perform Site Survey and Choose Locations for LUXESS	10
Test TEXESS Prior to De-Installation	10
De-Install TEXESS	10
Additional Tasks	11
Appendix A. -- Azimuthal Variations of Rg Energy in Central Texas	13
Appendix B -- Seismo-Acoustic Synergy	41
Appendix C. -- Seismo-Acoustic Research	73

## ILLUSTRATIONS

1. TXAR map showing new site designations	11
---	----

## SUMMARY

Personnel contributing to this contract are: (1) Dr. Eugene Herrin, Principal Investigator, (2) Paul Golden, Director of Geophysical Laboratory, (3) Karl Thomason, Chief Engineer, (4) Nancy Cunningham, Director - Computer Laboratory, (5) David Anderson, Systems Analyst, (6) Dyann Anderson Slosar, Administration, (7) Herbert Robertson, Consultant, (8) Jack Swanson, Consultant, and (9) Dr. Gordon G. Sorrells, Consultant. Ph. D. students include: (1) Chris Hayward, (2) Relu Burlacu, (3) Zenglin Cui, (4) Jessie Bonner, and (5) Ileana Tibuleac.

### Objectives

Objectives of the contract are twofold: (1) to conduct research in seismic-array technology and use of data from single stations and sparse networks, and (2) to design, evaluate, and construct two experimental arrays, TEXESS in Southwest Texas and LUXESS (Luxor Experimental Seismic System), which is northeast of Luxor, Egypt. These two tasks are dubbed CLIN 1 and CLIN 2.

The original CLIN 1 objectives were to: (1) conduct research in the use of single station and sparse network data in detecting and identifying small seismic events, (2) conduct research to develop optimum configurations and processing techniques for a nine-element experimental array, and (3) to continue development of an unmanned intelligent seismic station. These objectives have been revised by the Project Office in April 1994 as described on page 4 under Implications for Further Research. The contract has subsequently been revised to include acoustical research as a CLIN1 objective.

CLIN 2 objectives are to: (1) acquire hardware and software, (2) install TEXESS, (3) perform site surveys and choose location for LUXESS, (4) test TEXESS and perform verification tests prior to de-installation, (5) de-install TEXESS, (6) complete civil work in Egypt, (7) install and test LUXESS, (8) de-install data acquisition, analysis and archiving equipment and ship to Helwan, Egypt, data center, and (9) install and test data acquisition, analysis and archiving equipment at Helwan data center. The contract is in the process of being extended to include additional tasks under CLIN2 regarding the

establishment of the Egyptian array. TEXESS has recently been designated TXAR, which will be used when appropriate in the remainder of this report.

## Technical Problem

The German Experimental Seismic System was dedicated in 1992 and represents an upgrade for regional arrays. Although GERESS was technologically advanced over NORESS and ARCESS, which were earlier regional arrays, because of greater sensitivity and wider dynamic range, there was a considerable effort that resulted in increased costs for pier and vault construction and trenching for power cabling. Now, in TXAR, innovations in emplacement techniques, such as the installation of sensors in shallow boreholes instead of vaults and the use of solar power at each site to eliminate cabling from a central-power source, that have reduced array-installation costs by an order of magnitude. Other innovations are discussed below. TXAR is, therefore, a proposed design for a GSE-Alpha station because of these cost-cutting innovations. In addition to design, construction, installation, and operation, of TXAR, research will be undertaken to develop new means of taking data and handling the data.

## General Methodology

In GSE/US/84, February 1993, entitled "Technical Concepts for an International Data Exchange System," the GSE established the design goals of a future system. Goals are as follows:

1. Provide prompt access to all essential data
2. Provide convenient access to all available data
3. Provide direct access to all data at authorized national and global facilities
4. Accomplish goals with realistic manpower and budget resources.

The new concept of a global system for data exchange calls for an Alpha Network of 40-60 stations, primarily arrays; plus much greater than 60 Regional or Beta Stations; plus Local and National Networks or Gamma Stations.

SMU began research on experimental-array technology in 1991 on a previous contract. The proposed design was along the lines of an Alpha Station consisting of an array containing nine sites. Advancements over the GERESS design included the following:

1. The placement of seismometers and electronics in boreholes to greatly reduce construction costs for piers and vaults
2. The use solar power at each site rather than a central-power source
3. The use GPS receivers for time data at each seismometer site to replace central timing from the Hub
4. The employment of radio links from seismometer sites to the Hub to replace cable links and associated construction costs
5. The use of modular equipment to facilitate the installation and maintenance of the array.

Four shallow boreholes about 7 meters deep and 11-5/8 in. in diameter were drilled and cased with standard 8-in. pipe. Special equipment and techniques were developed to lower and level seismometers in the boreholes. A prototype solar power array and directional antenna were also developed for installation at LTX.

### Technical Results

The limited program described above was successful and SMU was granted a contract to design, evaluate, and construct two nine-element experimental arrays: TEXESS and LUXESS.

### Important Findings and Conclusions

The SMU mini-array research program that was begun in 1991 under the previous contract proved the feasibility of the proposed design and methodology described above.



## Significant Hardware Development

Preliminary research has led to the following hardware developments:

1. The development of seismometer emplacement techniques in boreholes, including remote seismometer locking eliminated the need for vaults
2. Advancements in computer applications and radio modems allow all necessary electronic components to fit inside a 8-in. casing to provide physical protection and a more stable environment for the electronics
3. The use of Global Positioning Satellite (GPS) receivers to obtain timing accurate to within 10 ms of world time assuring time synchronization of the array
4. The use of modern digital radio modems allows the system to perform as a local area network referred to as a RAN (Radio Area Network); radio polling software provides wide bandwidth intra-array communications while requiring two base-station radios; the need for expensive buried fiber-optic cable is eliminated
5. A NEMA enclosure is mounted on top of the borehole and is used to house the batteries and as a mount for the solar-power array; the GPS receiver and radio antenna are mounted above it.

## Special Comments

The task of adapting the solar-panel arrays at Lajitas to the LUXOR environment is simplified somewhat in that both TXAR and LUXESS are at approximately the same latitude, 30 deg North; both are in arid climatic zones; and both have about 3,500 annual hours of sunshine. As a result, there would be no need to modify the prototypic TXAR design because of differing environmental conditions at LUXESS.

## Implications for Further Research

CLIN 1 objectives were revised by the Project Office in April 1994 to: (1) conduct research to develop optimum configurations and processing techniques for nine- and sixteen-element short-period arrays, (2) conduct research in discrimination of nuclear events using autoregressive (AR) modeling techniques on Lg data, and (3) conduct research in measuring 20-

second Rayleigh waves at regional distances using high-resolution, wide-dynamic-range, short-period, seismic-array data and broadband KS 36000 data.

## CLIN 1 -- RESEARCH

### Array Research

**Conduct research to develop optimum configurations and processing techniques for nine-and-sixteen element short-period arrays,**

In Scientific Report No. 1, PL-TR-94-2106, ADA284580, we discussed the problems of the large scatter of the order of  $\pm 15$  deg of azimuth estimates at GERESS after f-k processing. In order to address this problem, SMU research has concentrated on developing a time-domain processing techniques to reduce this statistic using the nine-element TXAR array. The array-processing technique is similar to that described by Bernard Massinon in his paper entitled "The French seismic network -- current status and future prospects," which he presented at the GERESS Dedication and Symposium on 24 June 1992. The processing algorithm developed by SMU using GERESS D-ring data, which approximates the proposed 9-element TEXESS array, was presented in SMU-R-92-396, p. 14-17.

In Scientific Report No. 2, PL-TR-94-2258, ADA292546, array-processing research is described in Appendix 1. Specifically, Appendix 1 describes work on time-domain processing of GERESS and TXAR data to decrease azimuthal-error statistics with respect to that obtained by f-k processing. Time-domain processing has resulted in a reduction of azimuthal standard deviations from  $\pm 15$  degrees with f-k processing to  $\pm 1.4$  degrees with time-domain processing of TXAR data. The plan is to integrate the time-domain process with a detector that is being developed by Chris Hayward in order to automate array processing. Code is being developed as part of a joint-research project with Mission Research, Inc.

## Calibration Studies

Calibration research at TXAR was addressed in Appendix A of Scientific Report No. 4, PL-TR-95-2091. A modified version of the correlation method described by Cansi, Plantet and Massinon in their 1993 paper entitled "Earthquake location applied to a mini-array: K-Spectrum versus correlation method" in *Geophysical Research Letters*, vol 17, p. 1819-1822 was used to estimate azimuth and horizontal phase velocity of 36 events recorded at TXAR for which we had USGS  $m_b$  values. Modifications to the correlation method include Fourier interpolation of the data by a factor of 8 to obtain a virtual sample rate of 320/sec, use of an L-1 technique (least absolute deviation) to obtain estimates of azimuth and phase velocity, and a moving window display to indicate those portions of the waveform that show strongest correlation across the array. Observed bias in estimated azimuth as large as  $15^\circ$  was found to be dependent on both distance and true azimuth.

This paragraph includes recent corrections not included in Appendix A of Scientific Report No. 4, PL-TR-95-2091. Corrections have been forwarded to AFTAC and CMO. Based on 150 well located events (USGS), we have determined to the first order the attitude of the MOHO beneath TXAR to be:

Strike azimuth 111 deg (ESE)

Dip 10 deg north

This result is consistent with the tectonic setting for the area.

This structure leads to bias in estimates of back azimuth and phase velocity (or slowness) using TXAR arrival data. The following corrections should be made to the estimates:

Azimuth correction (dZ)

Add to the estimated back azimuth ( $Z'$ ) in degrees

$$dZ = -7.44 \cos (Z' - 111.2)$$

Phase velocity correction (dV)

Add to the estimated phase velocity ( $V'$ ) in order to  
correct to the IASPI standard crustal model

$$dV = - [0.44 + 0.86 \cos (Z' + 0.12)]$$

We have also determined regional and teleseismic magnitude formulas for TXAR that are calibrated to mb (USGS) as follows:

For corrected phase velocity less than 8.6 km/sec:

$$m = \log A + 2.4 \log D - 3.95$$

For corrected phase velocity 8.6 km/sec or greater:

$$m = \log A + 2.4 \log D - 4.39,$$

Where A is maximum O - P amplitude in nanometers in the first 5 sec, and D is the epicentral distance in km.

### Discrimination Research

Conduct research in discrimination of nuclear events using autoregressive (AR) modeling techniques on Lg data

In the framework of a Comprehensive Test Ban Treaty (CTBT), discrimination between low-yield or decoupled nuclear explosions, economic explosions and small shallow earthquakes using the characteristics of the seismic waves becomes very important. Some of the economic explosions are multiple-source events with a time and space pattern dependent upon the type of application. The superposition of the seismic motion in the time domain leads to regular amplification and suppression of spectral power in the frequency domain. As, in general, single events (single explosions or earthquakes) do not exhibit spectral modulations, their presence can be used in the discrimination between single and multiple events. The aim of the present study is to develop a fast and robust method of discriminating between earthquakes and economic explosions based on differences observed in the spectral content of the regional waveforms. The method is based on the parametric estimation of the power-spectral density (PSD) using the autoregressive (AR) Burg algorithm of order 3, which provides a fast method to emphasize the spectral differences.

In Scientific Report No. 2, PL-TR-94-2106, ADA284850, AR modeling is described in Appendices 2 and 4. The initial data set (see Table 1 of said report) includes about 30 mine explosions and earthquakes from the

Vogtland area of Czechoslovakia about 200 km northwest of GERESS. The frequency and reciprocal pole position of the complex pole in the AR (3) models were calculated using the Lg arrival for the Vogtland events recorded at GERESS in Table 1 of Scientific Report No. 3, PL-TR-95-2023, ADA295787. Figure 1 of Scientific Report No. 3, shows a clear separation of explosions and earthquakes with the latter having broad spectra with "weak" poles above 6 Hz whereas the explosions all show much "stronger" poles at frequencies less than 5 Hz. The AR (3) method appears to be an effective discriminant for small explosions and small earthquakes. Further work will be to answer questions regarding the method: (1) its effectiveness in other areas such as the Middle East, (2) its effectiveness using larger events, and (3) why the method works as well as it does?

In a corollary discrimination study, phase-matched-filtering techniques were used to analyze Rg dispersion from mine blasts. Appendix A is a paper by Jessie Bonner, Eugene Herrin, and Tom Goforth of Baylor University entitled "Azimuthal Variations of Rg Energy in Central Texas."

Conduct  $M_S:m_b$  research by measuring 20-second Rayleigh waves at regional distances using high-resolution, wide-dynamic-range, short-period, seismic-array data and broadband KS 54000 data.

The  $M_S:m_b$  discriminant has been investigated by a number of researchers for both regional and teleseismic events and explosions. Bases for the discriminant are (1) that explosions emit more energy in the form of high-frequency body waves and (2) that earthquakes emit more energy in surface waves having low frequency radiation; therefore, an  $M_S:m_b$  plot displays a significant separation of the two populations. The problem with the method is that of identifying small explosions; that is, the problem boils down to seismograph sensitivity. With the installation of new high-dynamic-range seismographs at TXAR, planned research includes the determination of  $M_S$  from small earthquakes at regional distances using the TXAR array data recorded by short-period GS-13 seismometers and a posthole, broadband KS 54000 seismometer. In Scientific Report No. 2,  $M_S:m_b$  studies were described in Appendices 3 and 4, and were excerpted in this section of Scientific Report No. 3, PL-TR-95-2023.

## Acoustic Research

During the week of 21 September, a microbarograph pipe array was installed at TXAR, collocated with the posthole broadband system at the hub. The array consists of six, 50-ft-long hoses, each with multiple ports, feeding into a common collector, dubbed the bomb, wherein the summed acoustic output is then fed into a single, solid hose containing a condenser microphone, which is suspended in a borehole. The microphone has been replaced by a pressure transducer, and its output is recorded on one channel of the CIM. Microbarograph data are being continuously transmitted to SMU for evaluation.

This is the first phase of a research program to analyze the origins of seismo-acoustic signals recorded at TXAR. Appendix B of this report is a paper by Eugene Herrin and others entitled "Seismo-Acoustic Synergy," which provides background information on the advantages of collocating infrasonic and seismic sensors. Appendix C is a paper by G. G. Sorrells entitled "Seismo-Acoustic Research," which addresses the present research program.

## CLIN 2 -- DESIGN, EVALUATION, AND CONSTRUCTION OF TXAR AND LUXESS

### Experimental-Array Program

Information on the experimental-array program at SMU on the previous contract was presented in SMU-R-92-396, and in Scientific Report No. 1, PL-TR-94-2106, ADA284580.

### TXAR AND LUXESS

Information on CLIN 2 has been presented in Scientific Report No. 1, PL-TR-94-2106, Scientific Report No. 2, PL-TR-94-2258, ADA292546, and Scientific Report No. 3. Since the submission of Scientific Report No. 3, an extension to the contract has been granted to install LUXESS because of unavoidable delays. As a result, six additional tasks have been added.

## Acquisition of Hardware and Software

The First and Second Quarterly R & D Status Reports cover the acquisition of hardware and software. TEXESS and LUXESS equipment are discussed in Scientific Report No. 1, PL-TR-94-2106. Instructions for the installation of the Posthole 54000 seismometer are presented in Appendix 5 of Scientific Report No. 2.

## Array Hardware

Hardware is discussed in the Scientific Report No. 1, PL-TR-94-2106, ADA284580.

## Computer Hardware

Computer equipment is discussed in the Scientific Report No. 1, PL-TR-94-2106, ADA284580.

## Software

Acquisition of software was addressed in Scientific Report No. 1, PL-TR-94-2106, ADA284580.

## Install TXAR

## Layout

TXAR layout is discussed in Scientific Report No. 1, PL-TR-94-2106, ADA284580, and the relocation of C1 was discussed in Scientific Report No. 4, PL-TR-95-2091. Since then, the A, B, and C site prefixes have been superseded by TX prefixes as shown in Figure 1.

As mentioned in Scientific Report No. 4, information about TXAR, which has been compiled by Chris Hayward of SMU, can now be accessed on Internet via the World Wide Web at:

[http://inge.css.gov:65123/WebIDC/About\\_TXAR/](http://inge.css.gov:65123/WebIDC/About_TXAR/)

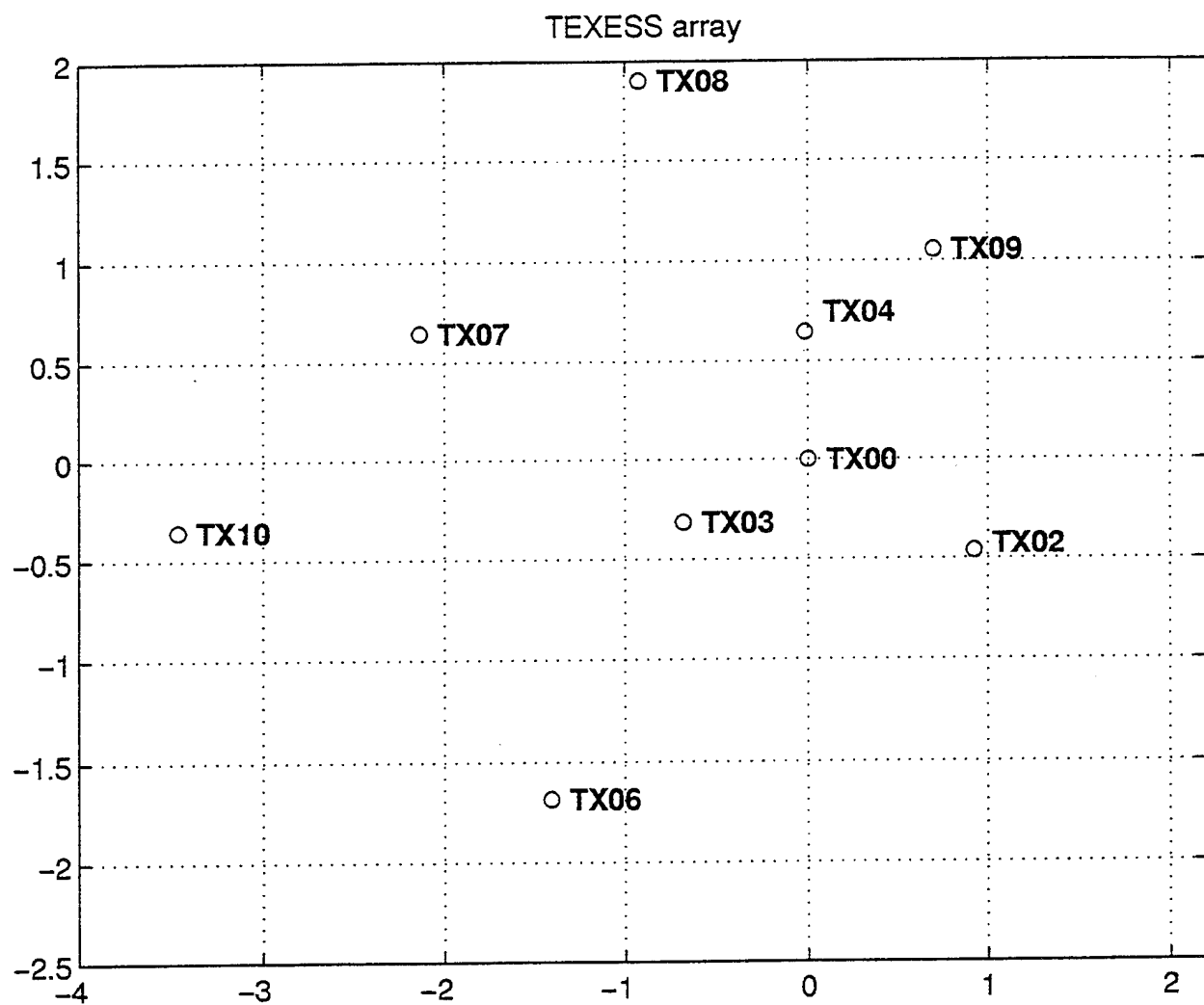


Figure 1 TXAR map showing new site designations.



## Installation

Installation is discussed in the Scientific Report No. 1, PL-TR-94-2106, ADA284580.

## Perform Site Surveys and Choose Locations for LUXESS

As mentioned in Scientific Report No. 3, PL-TR-95-2023, two locations have been identified from satellite photos and maps for LUXESS, which are on granitic bodies located north of the road between Luxor and Quseir. Figure 4 of Scientific Report No. 3 is a digitally-enhanced LandSat image of the two circular granitic intrusions. The specific site for LUXESS will be selected by a team composed of SMU and Egyptian scientists.

## Test TXAR Prior To De-installation

TXAR has been operational since 30 August 1993, but outages as discussed in this section of Scientific Report No. 3, PL-TR-95-2023, have led to reconfigurations as discussed in this Scientific Report No. 4, PL-TR-95-2091, which should improve overall reliability.

Addition changes at TXAR have recently been made including CIM modification at TX01, AIM repair at TX07, installation of the microbarograph array as mentioned previously, and site retrofit.

## De-install TXAR

The present plan is to de-install all equipment except the seismometers, and transport said equipment to LUXESS. Equipment tagged for shipping includes the AIMs, radios, antennas, solar panels, batteries, NEMA enclosures, CIMs, and UPS.

## Additional Tasks

Additional tasks such as training of Egyptian representatives, spare parts for LUXESS, and the broadband system were covered in Scientific Report No. 4, PL-TR-95-2091, pages 13 and 14.

## APPENDIX A -- AZIMUTHAL VARIATIONS OF RG ENERGY IN CENTRAL TEXAS

Jessie Bonner, Eugene Herrin, and Tom Goforth

### Abstract

In this article, we present the results of a study of short-period surface waves from chemical explosions at a limestone quarry 40 km west of Waco, Texas. Our purpose is twofold; first, to obtain reliable dispersion curves for the surface waves being generated, and second, to establish any azimuthal variations in relative Rg (fundamental-mode, short-period Rayleigh wave) energy at azimuths around the quarry, including the quarry pit's influence on these energy variations. Observed dispersion curves were interpreted using theoretical dispersion curves that consider the estimated values of Poisson's ratio (0.35-0.4) for the upper crust of central Texas. The Rg dispersion essentially has three different sections; an inversely dispersed branch complicated by the presence of higher modes (at periods less than 0.6 seconds), a group velocity minima (at periods between 0.6 and 0.7 seconds), and normally dispersed Rg (between 0.7 and 3.0 seconds with an inflection point near 1.7 seconds). In the period interval between 0.7 and 1.5 seconds, multipathing complicates the interpretation of the dispersion curve by creating spectral holes in the multiple filter analysis (MFA), a single station routine for calculating group-velocity dispersion. Spectral holes must be dealt with before interpreting the final dispersion curve, which is then used to extract Rg from the complex wave train by phase match filtering (PMF). Rg extracted from paths not traversing the open pit of the quarry have more energy than paths influenced by the open pit. Likewise, higher-mode energy exceeds fundamental-mode energy only when the propagation path includes the open pit. Implications for these observations are discussed.

## Introduction

The presence of short-period fundamental-mode Rayleigh waves (Rg) often observed on seismograms from explosions is an indication of shallow source depth (Bath, 1975; Kafka, 1990). The Rg dispersion may be used to investigate crustal velocity structure (McEvilly and Stauder, 1965; Herrmann, 1969; Anderson and Dorman, 1973; Kocaoglu and Long, 1993; Bonner, 1993). Unfortunately, the ability to extract Rg can be problematic because of the complexity of short-period local seismograms recorded at distances less than 200 km.

On short-period seismograms in Central Texas, Rg waves are most prominent at epicentral distances of 8 to 175 km where propagation paths traverse strata characterized by the low-velocity sediments deposited during the Cretaceous period. At distances greater than 175 km, Rg is no longer observed probably because of modal convergence into Lg. This modal convergence begins much earlier in the propagation paths on some records, an effect that was first noted when using Rg as a depth discriminant between chemical explosions and microearthquakes along the Mexia Fault Zone in Central Texas (Goforth and Bonner, 1995). Goforth and Bonner observed a correlation between the presence or absence of Rg in the quarry blast seismograms and the alignment of the quarry faces relative to the propagation paths to the recording sites.

In this article, we investigate seismograms from explosions at the Chemical Lime (Chemlime) limestone quarry, 40 km west of Waco, Texas, by evaluating which Rayleigh wave modes are generated by the explosions and by examining the azimuthal variation of relative Rg energy in relation to the open pit of the quarry. Dispersion curves are calculated by multiple filter analyses (MFA) (Herrmann, 1973; Dziewonski, et. al, 1969), a single-station method of determining group-velocity dispersion. These observed curves are compared with theoretical dispersion curves to determine the modes present in the surface-wave train and especially to determine the observed bandwidth of Rg. These dispersion curves are then used to extract Rg from the waveform through use of the phase-match filtering (PMF) technique

(Herrin and Goforth, 1977) . The relative energy in the extracted Rg is then compared for azimuths around the quarry.

### Data Acquisition

This study involves seismograms from three blasts at Chemline on June 28, July 12, and July 17, 1994. The June 28 (Table A1) and July 12 blasts were shot on a northwest trending (azimuth  $325^{\circ}$ ) face of limestone (Edwards formation of Cretaceous age) approximately 12 meters high above the quarry floor (Figure A1). The July 17 detonation (Table A1) occurred on a wall approximately perpendicular to the previous one (azimuth  $55^{\circ}$ ) in the same stratigraphic unit.

Table 1. Parameters for Chemline quarry blasts

Blast parameters	28 Jun '94	12 Jul '94	12 Jul '94
Number of holes	42	40	28
Total ANFO (lb)	6964	6540	4856
Powder factor	0.32	0.30	0.32
Rocks moved (tons)	21,157	21,246	14,872

Seismograms were to be recorded on ten Sprengnether 6000 three-component, 2 Hz geophones connected to Reflection Technologies (REFTEK) DAS 72-0A systems. A Teledyne Geotech PDAS 100 system, placed at the quarry, recorded the origin time for each event. Ten sites were selected to surround the quarry at a distance of approximately 10 km. At this distance, the surface wave train consists of a complex mix of higher and fundamental-mode surface waves. Field logistics and accessibility resulted in a skewed network (Figure A2) with the seismometers ranging from 9.2 km (B7, B8) to 12.85 km (B10) from the quarry. At each site, the seismometer was buried in a 1-2 meter deep hole, and the recorder was set up to use STA/LTA trigger. Disk failure at two sites (B6 and B4) reduced the active network to eight sites. Additional failures on the dates of the blasts resulted in seven stations recording the June 28 and July 17 blasts, and six recording the July 12, blast.

Sample rates were 100 samples per second for the June 28 blast, and 125 samples per second for the July 12 and July 17 blasts. The data were transferred to a workstation and corrected for the instrument response. Because the bandwidth for Rg (0.2 to 2.75 seconds period) includes the 2 Hz (0.5 seconds period) instrument corner frequency where the maximum phase shift occurs, both amplitude and phase corrections were applied prior to phase-matched filtering. The correction was made by dividing the complex Fourier transform (FT) of the signal by the complex seismometer response. The inverse FT of the result is the corrected waveform used in the study.

### **Modal Characterization of Central Texas Surface Waves**

Each vertical component seismogram was studied to determine the characteristics of all prominent phases, with the emphasis on the surface wave train. A previous study by Gupta and Hartenberger (1981) considered the seismic phases recorded at 0.5 to 3.0 km from a quarry blast along a propagation path in sedimentary rocks. They noted five distinct phases on each record: the P-wave first arrival; a complex wave train consisting of higher-mode Rayleigh waves; a precursor to the air-blast wave; the air blast wave; and the air-coupled Rayleigh waves. Records from the June 28 blast show similar results, even though the paths are at least three times longer. In Figure B3, each record, corrected for the instrument response, is shown as a function of distance from the quarry and is scaled to the same amplitude scale in cm/sec. Each record has an emergent P-wave first arrival and coda, followed by a complex surface wave train. Figure A3 does not show the observed air blast and associated air-coupled Rayleigh waves that arrive some 30 seconds after the origin of the blast.

Gupta and Hartenberger (1981) noted that only higher-mode surface waves were observed in their data at 0.5 to 3 km. Without filtering, the same conclusion might be drawn from the June 28 data (Figure A3). Filtering each trace with a 3 pole, Butterworth, bandpass filter between 0.4 and 2 Hz will show the presence of low frequency energy (Rg) in the signal, that is not obvious from Figure A3; however, it will be shown later that this bandwidth does not accurately represent the entire Rg signal. The seismograms from the July 12 and July 17 blasts (Figures A4 and A5) are also presented.

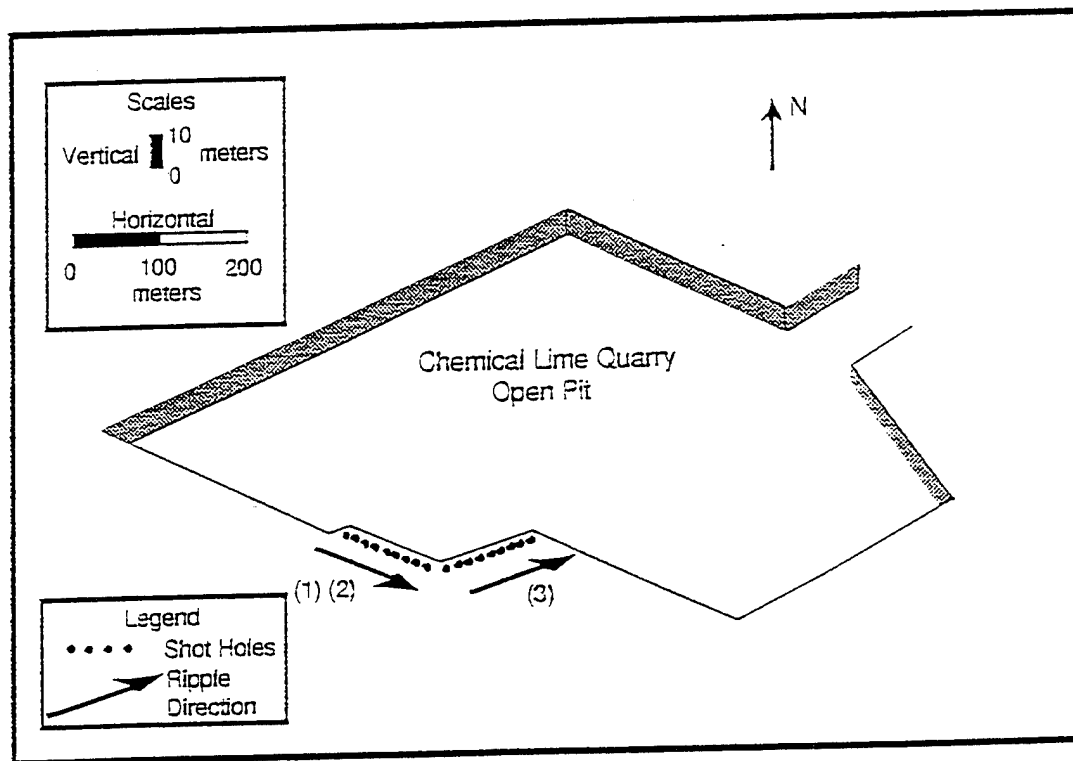


Figure A1. Schematic representation of the Chemical Lime (Chemlime) quarry pit 40 km west of Waco, Texas showing the approximate size and shape of the quarry. The stratigraphic unit being quarried is the Edwards Formation, a Cretaceous limestone of approximately 32' thickness at this location. Three explosions were recorded at this quarry; (1) June 28, 1994 (2) July 12, 1994, and (3) July 17, 1994. The direction of the ripple firing is shown for each blast.

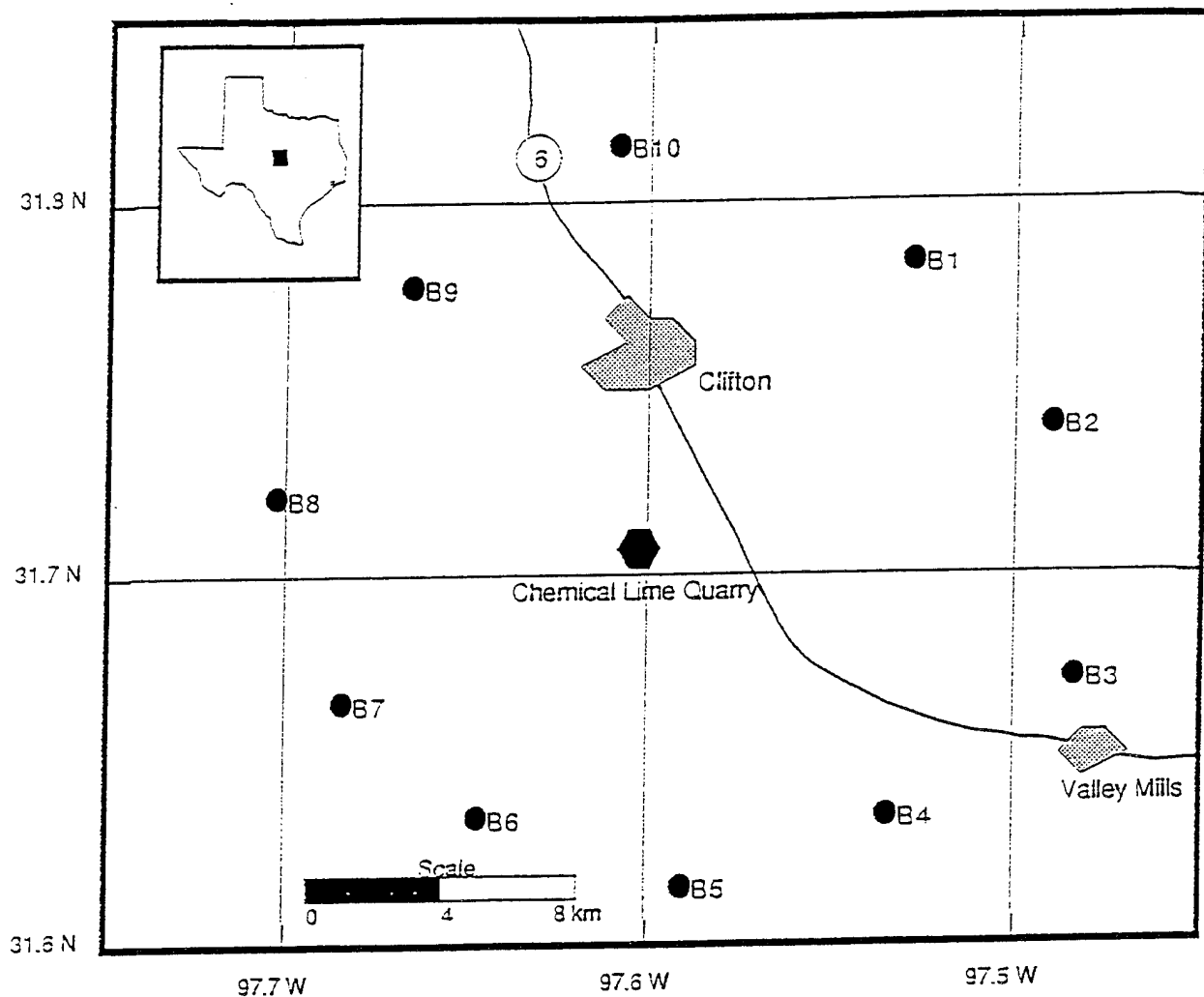


Figure A2. Portable network of seismometers used to record three chemical explosions from the Chemlime quarry. Each site was selected based upon site accessibility and geologic makeup. All sites have several feet of well defined soil to allow seismometer burial of at least 1-2 m, with the exception of B1, which was located in the characteristic rocky soils associated with the Edwards formation.

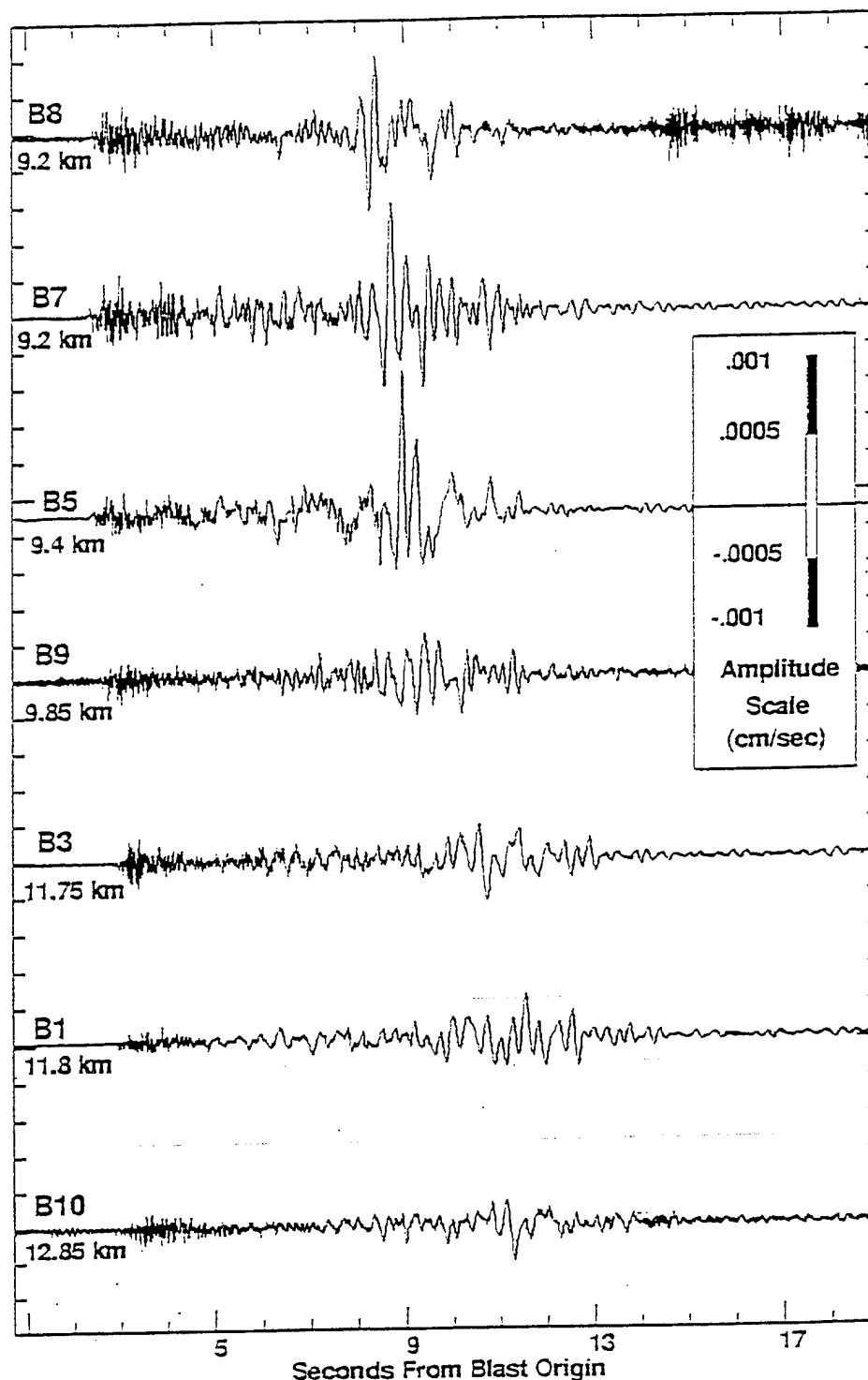


Figure A3. The vertical-component seismograms, corrected for the instrument response, from the June 28, 1994, Chemlime explosion shown at the same amplitude and time scales. The waveforms are plotted as a function of distance from the quarry. At this distance,  $R_g$  is not well defined, due to the presence of coda, higher modes, and other arrivals, unless band-pass filtering is done in the  $R_g$  bandwidth (approximately 0.23 to 2.75 seconds period).



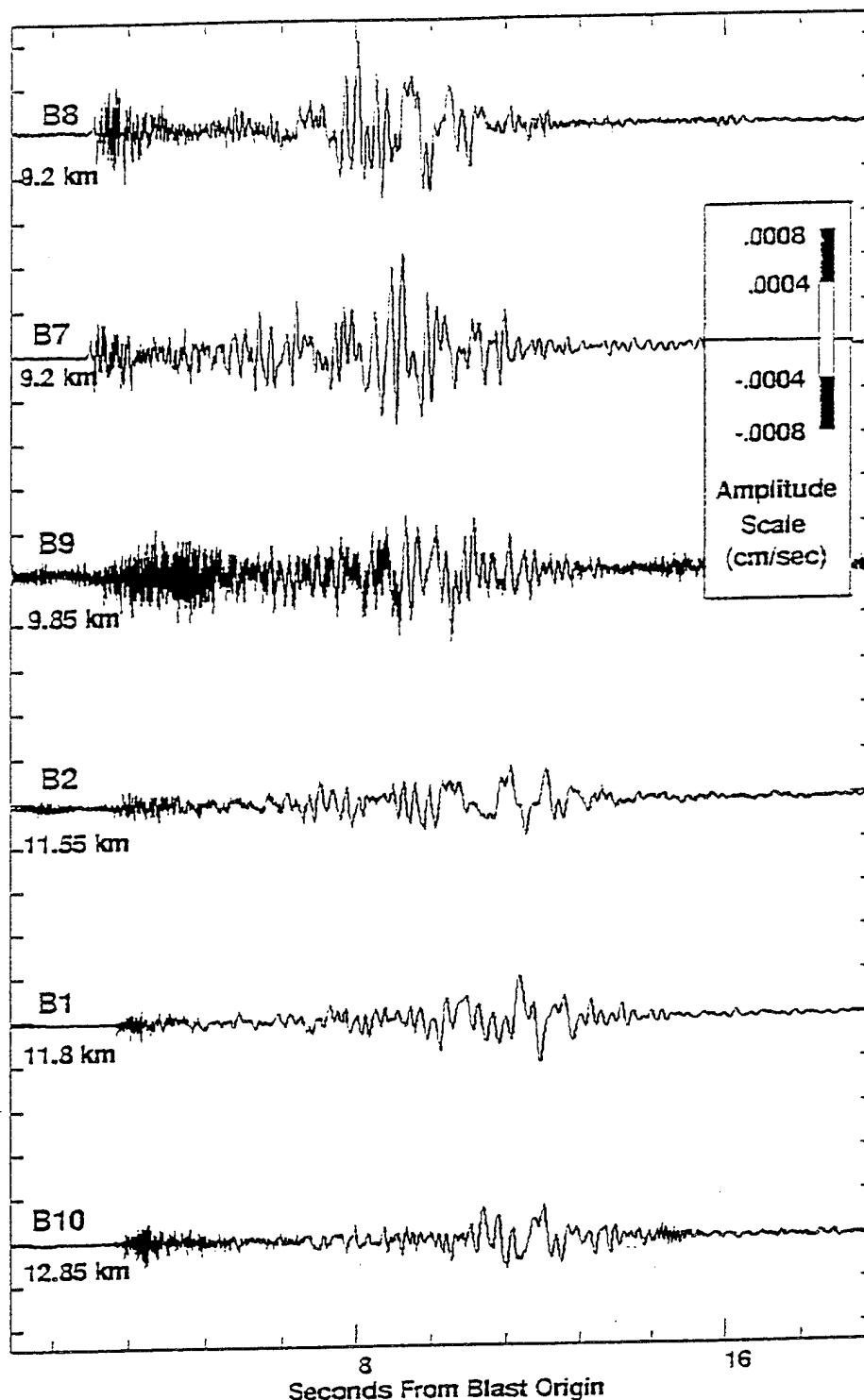


Figure A4. The vertical-component seismograms, corrected for the instrument response, from the July 12, 1994, Chemlime explosion shown at the same amplitude and time scales. Station B2, which did not trigger for the June 28 blast, is the first station to note the presence of Rg (seen on the waveform between 9 and 13 seconds) without filtering.

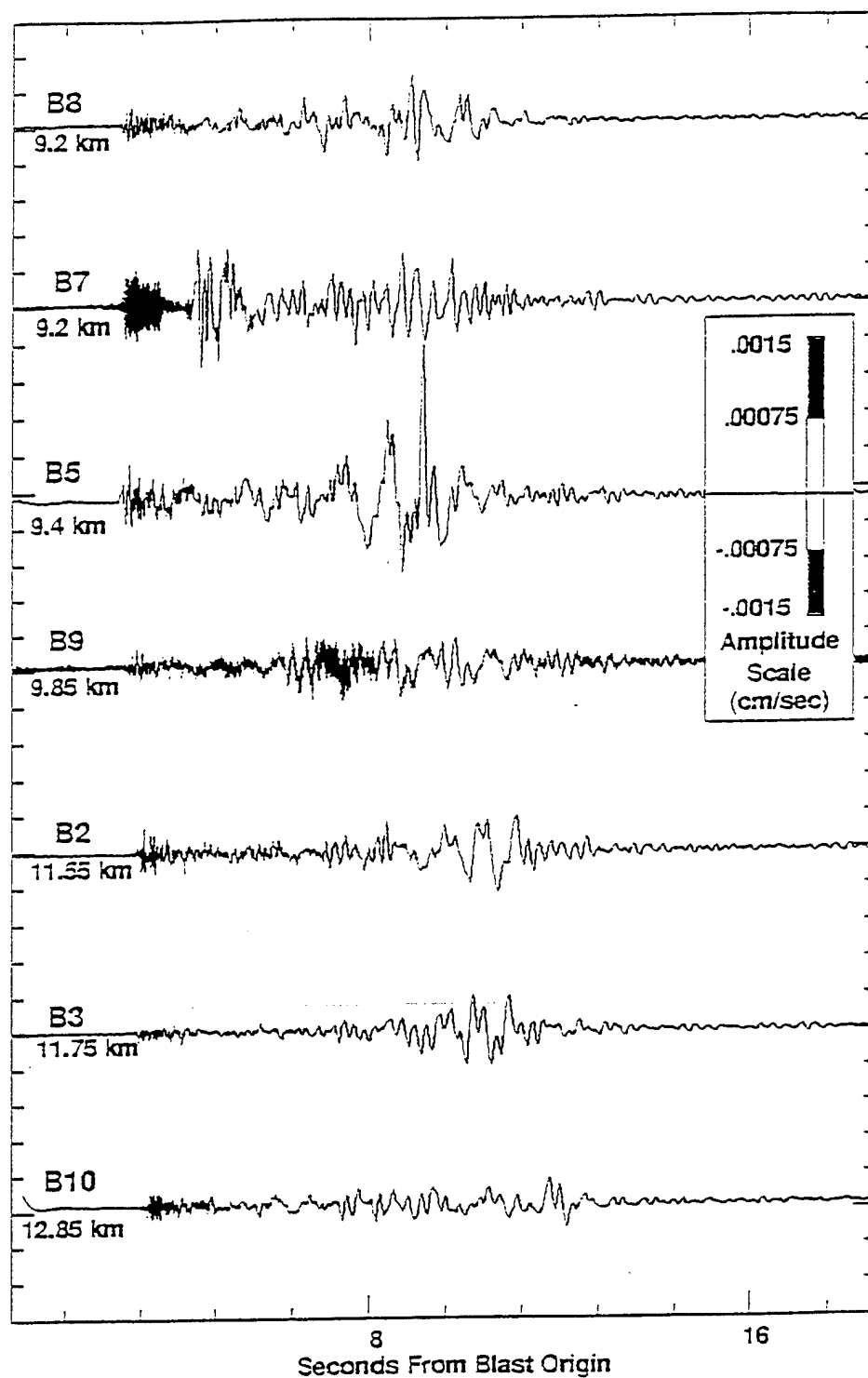


Figure A5. The vertical-component seismograms, corrected for the instrument response, from the July 17, 1994, Chemlime explosion shown at the same amplitude and time scales. Note that station B5 recorded very strong Rg that is clearly visible in the unfiltered seismograms.

In Figure A3, the seismograms from stations B8, B7, B5, and B9 have more energy in the signal than other stations recording the same blast. A similar appearance is seen for the other two blasts (Figures A4 and A5). Spectral comparisons of these records show that the differences are confined to frequencies of 16 Hz or less (Figure A6), while the spectra are similar at frequencies than 16 Hz except in cases where artificial noise was generated (i.e. Texas longhorn cattle licking the white, salt-block appearing seismometer case). These differences can not be explained as attenuation effects with increasing distance, but instead are the result of a combination of source effects. Ripple direction and duration, scattering, reflection of energy by the working face, and the existence of the open pit are several factors that might lead to this asymmetrical relative energy proportioning.

## Modeling

The first arrival (Pg), (Langston, 1982) is emergent and clearly observed on most records, and at local distances, Pg travels in the upper crust. The group velocities of Pg arrivals in this study range from 2.5 to 3.0 km/sec, less than the average velocities (3.8 to 4.2 km/sec) determined for the upper crust of Central Texas in a previous study (Bonner, 1993). Any discrepancy results from the shorter propagation paths (i.e., shallower penetration depths) in this study. The group velocities of Pg arrivals in Bonner (1993) are in accordance with values for sedimentary rocks in Oklahoma (Trygvasson and Qualls, 1967).

The low-dipping strata of Central Texas consist of a layer of low-velocity, fractured, Cretaceous shales, limestones, and sands over a half space of crystalline limestones and dolomites (Paleozoic) as well as high-velocity basement granites (Greenvillian). Compressional and shear wave data interpreted using Chemlime and five other quarries in the area recorded at Baylor University's seismic observatory (BUTX) suggest that the low-velocity surface layers have a Poisson's ratio ( $s$ ) of 0.35-0.40. Surface wave propagation occurs within this low velocity, high  $s$  layer.

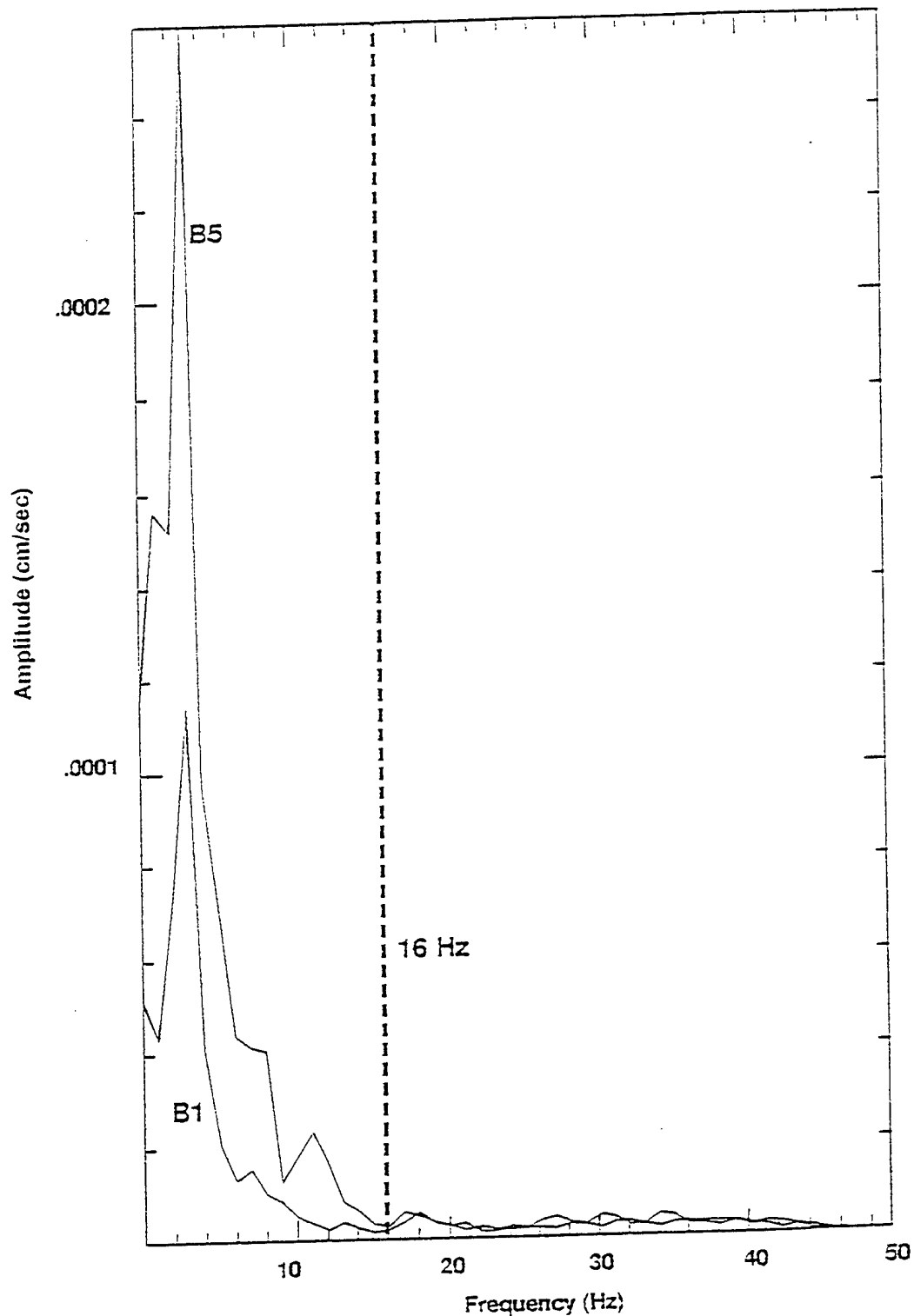


Figure A6. Spectral comparison of the recorded blasts at stations B5 and B1 for the June 28, 1994, Chemlime blast. The Fourier transformed data, smoothed with a 1 Hz window, shows similar spectra beyond 16 Hz. At frequencies less than frequencies of 16 Hz though, the spectra vary as the result of the asymmetric nature of energy propagation from the quarry blast.

Mooney and Bolt (1966) studied the dispersive characteristics of surface waves for general cases where Poisson's ratio is high in a sedimentary basin that is similar to this study's location in the southeastern margin of the Fort Worth basin. Using a 3 km layer over a half space and a value of  $s$  of 0.35, group velocity minima appeared at 4.4 sec for the fundamental mode, 1.6 sec for the first higher mode, and 1 sec for the second higher mode. In another case, even higher values of  $s$  (0.40) were used to simulate surface wave dispersion for a 100-m layer of alluvium. An extremely complicated dispersion pattern resulted from this model. The fundamental-mode group-velocity curve had two steeply rising limbs separated by an inflection point, and a slow travelling fundamental-mode Airy phase. The first and second higher modes had a least three group velocity minima. Based on dispersion curves already obtained in this region (Bonner, 1993), a mixture of both models is needed to distinguish which modes are being observed.

An alluvium model with a thin, low-velocity, high  $s$  layer was combined with a sedimentary model with one, thicker, low-velocity, high  $s$  layer. These two layers were over a half space (Table A2). The dispersion curves for several modes were calculated (Herrmann, 1985) and plotted (Figure A7) along with the crustal model assigned to the Central Texas crust. As reported by Mooney and Bolt (1966), the fundamental mode has two limbs separated by an inflection point at approximately 1.25 sec period. The steepness of the rising limbs depends upon the velocity contrast between the layer and the half space. Because the velocity contrast is not large between any of the layers in the model, the dispersion is slight between 1.5 and 3.0 seconds. The higher modes have at least two group velocity minima, different from Mooney and Bolt's alluvium model that had at least three. The dispersion curves for this Central Texas model may be used to understand the modes in the surface wave train of the recorded Chemlime explosions.

Table A2. Velocity model for upper crust of Central Texas.

Thickness (km)	Vp (km/sec)	Vs ((km/sec)	Density (g/cu cm)
0.3	3	1	1.5
0.7	3.1	1.18	1.6
Half Space	5	1.32	2.5

## Processing

The Multiple Filter Analysis technique (MFA), first developed by Dziewonski and others (1969), and implemented using a set of computer programs (Herrmann, 1985, 1987, 1988), provides a fast, efficient method of analyzing multiply dispersed signals (Dziewonski, et. al., 1969). In this method, a set of narrow band Gaussian filters are applied to the input spectra. The envelope of the filtered time signal is then searched for the occurrence of the four largest envelope amplitudes. Each of these amplitude maxima has an associated time from the origin of the event, and when combined with the distance from the quarry, a group velocity can be estimated for each one (Herrmann, 1973). These amplitudes are then contoured and displayed. Figure A8 shows the result of using the MFA on the vertical component of the June 28 blast, recorded at station B1. Analysis was restricted to periods of 0.23 and 3.0 seconds. For periods below 0.23 seconds, the surface wave train analysis is complicated by the occurring P-wave coda, while periods greater than 3 seconds are contaminated with microseisms and instrument noise.

## Interpretation

In Figure A8, the prominent feature of the MFA is the contoured, dispersed Rg arrival between 0.5 and 2.0 sec period. The dispersion is subtle between periods of 0.7 to 1.5 sec and flat after periods of 1.5 sec, suggesting very little change in velocity in the layers greater than 1-km deep.

A spectral hole is evident in the MFA between 2.5 and 3.0 sec period. Spectral holes may be the result of destructive interference of two wave trains. Refracted/reflected phases, higher modes, and multipathing are possible causes of destructive interference in the surface wave train. The exact cause of the hole in the case of B1 (Figure A8) was never distinguished, while other spectral holes important to processing surface waves in this study occurred in the 0.7 to 1.5 sec period range. The cause of these spectral holes was shown by phase match filtering to be due to multipathing. After extracting Rg by phase matched filtering, the MFA was performed again on the residual waveform, which showed the multi-path surface waves to have similar dispersion curves

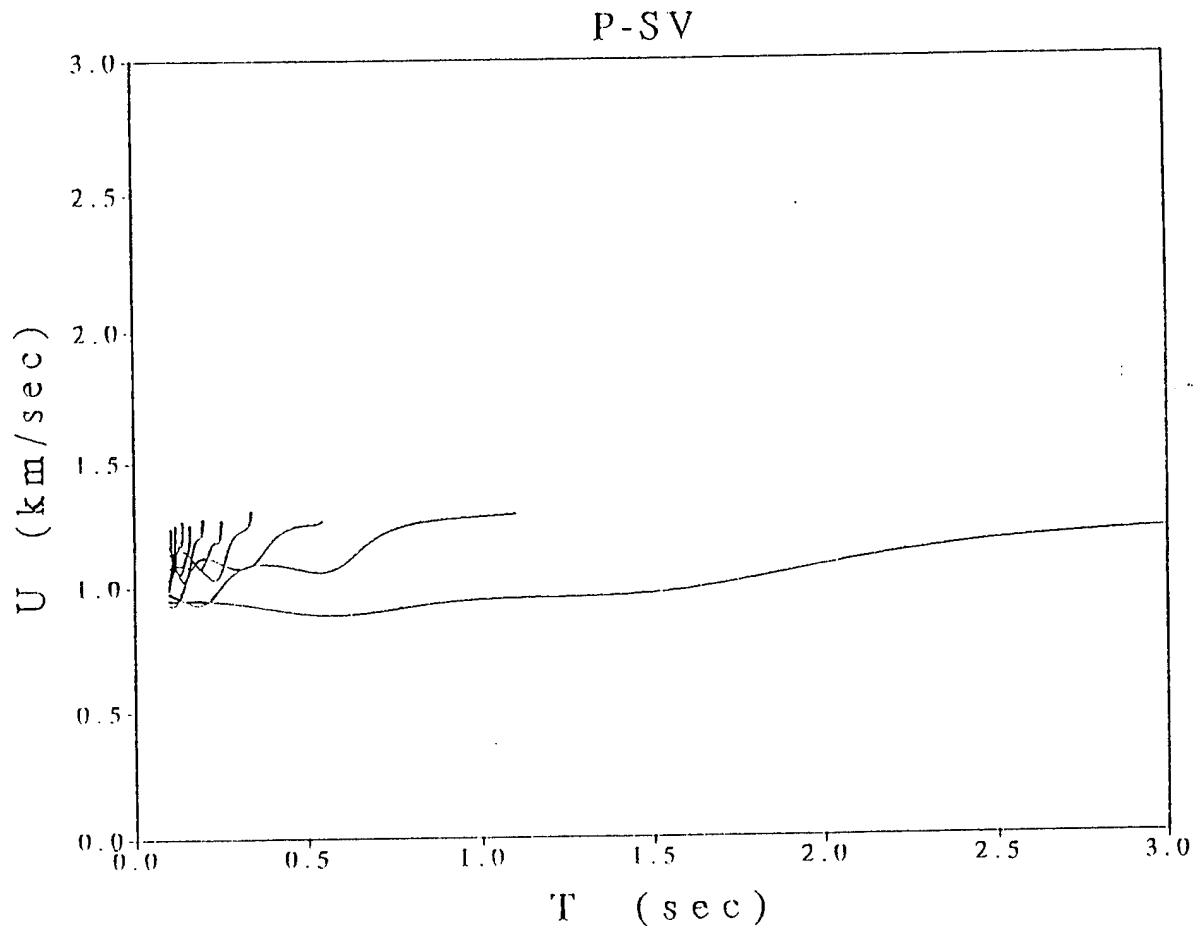


Figure A7. Short-period Rayleigh wave dispersion curves generated for the shallow crustal structure of Central Texas.  $R_g$ , the fundamental-mode Rayleigh, exists for all periods between 0.2 and 3.0 seconds. The next nine higher modes are also plotted, and demonstrate the complexity of the surface wave arrivals at periods less than 0.6 seconds period. The  $R_g$  dispersion curve consists of three branches, the normally dispersed branch between periods of 0.7 and 3.0 seconds, which is separated by an inflection point near 1.2 seconds period. The second branch represents the fundamental-mode Airy phase at approximately 0.6 seconds period. Finally, the third section of dispersion exists at periods less than 0.6 seconds and is inversely dispersed.

that are slightly delayed due to longer propagation paths. In the presence of spectral holes, the dispersion curve was drawn through the hole to mimic data interpreted at the of stations without spectral holes..

As the model predicts, the MFA becomes more complicated at periods less than 0.6 seconds. For these periods, the model-dispersion curves (Figure A7) illustrates that many higher modes will be present with group velocities ranging only between 0.95 and 1.3 km/sec, greatly complicating the interpretation. Based on the model, the fundamental-mode Airy phase should travel at 0.9 km/sec with period 0.6 sec. Data (Figure A8) have a group velocity minimum (Airy Phase) at 0.69 seconds period and 0.88 km/sec

and the branch is inversely dispersed for periods less than 0.69 seconds. The data also shows the intersection of the first higher mode and the fundamental mode near a period of 0.5 seconds, slightly different than the model predicts. Similar interpretations, such as this for station B1 (Figure A9), were made for the MFA of each record to ensure the most accurate starting model for the PMF technique.

### **Azimuthal Variation of Rg Energy**

The dispersion curves carefully determined by modeling and MFA serves as the input to the phase match filtering (PMF) technique (Herrin and Goforth, 1977). The PMF procedure starts with an initial estimate of dispersion, generally from the MFA, and by an iterative technique finds and applies a filter that is phase-matched to the particular mode or arrival of a surface wave, Rg in this study. The relative energy of the extracted Rg can then be calculated.

#### **Processing**

Cross-correlation of a signal  $s(t)$  with a filter  $f(t)$  can be represented in the frequency domain as:

$$s(t) \times f(t) = |S(w)| |F(w)| \exp(i(d(w)-j(w))),$$



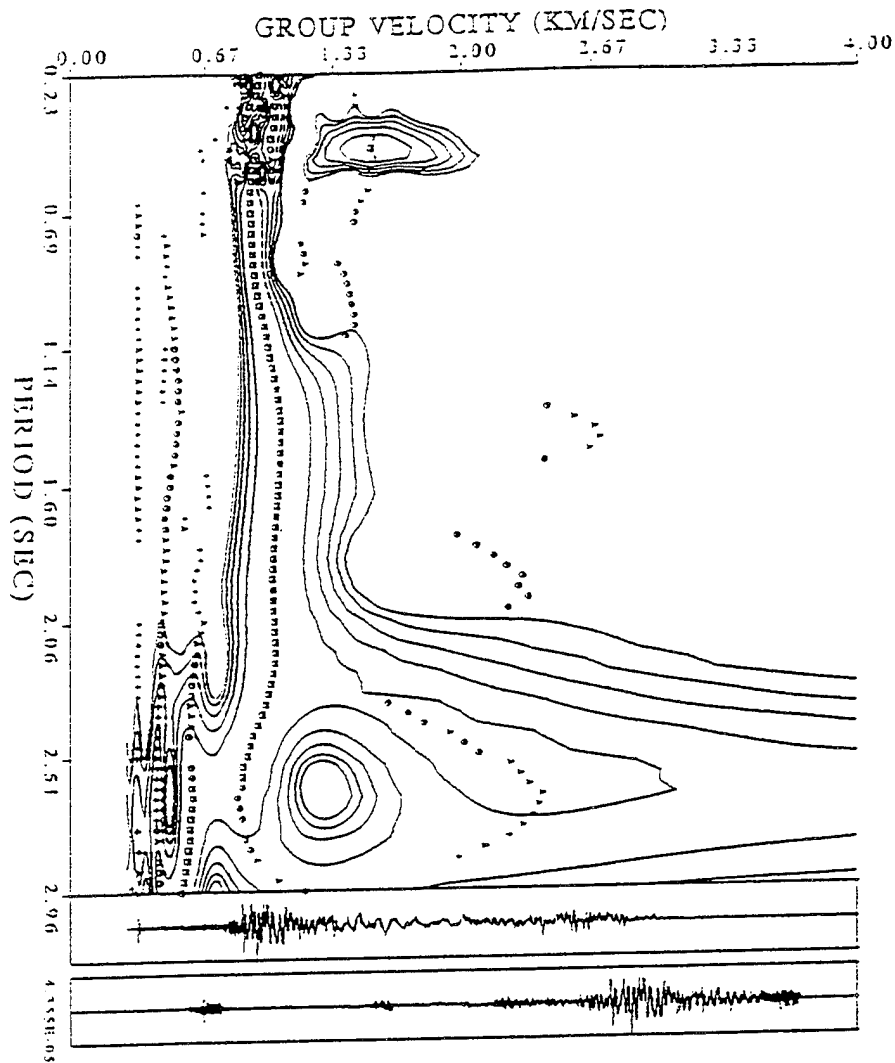


Figure A8. The Multiple Filter Analysis (MFA) of the recorded June 28, 1994, blast at station B1. The largest amplitudes of the envelope are plotted as squares, then circles, triangles, and pluses for corresponding lesser amplitudes. The seismic trace on the far left is the waveform, while the inner trace represents the waveform scaled linearly versus apparent group velocity. The normalized contours of this MFA plot show the dispersed Rg between periods of 0.7 and 2.10 seconds. At periods less than 0.7 seconds, the MFA is complicated by the appearance of higher modes. At periods greater than 2.10 seconds, a spectral hole (the closed, circular contours on the graph) is diverting the peak amplitudes of the envelope (denoted by squares) around the hole.

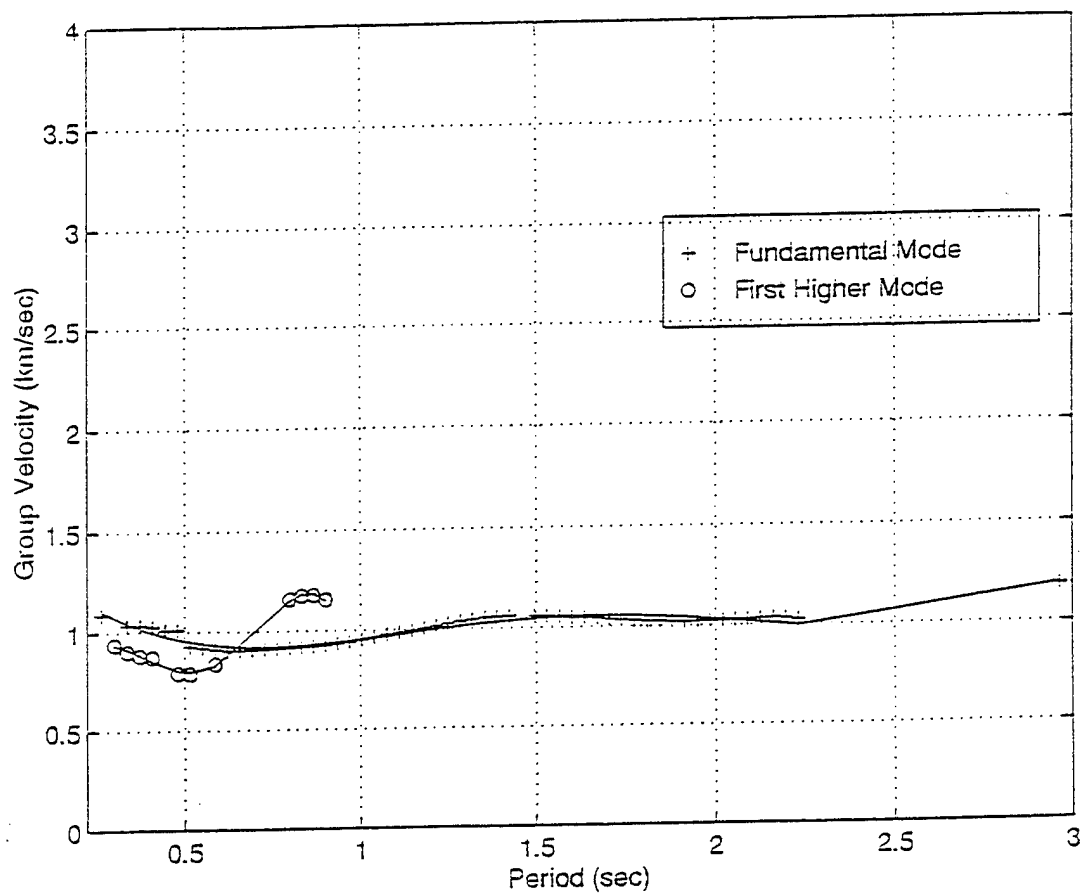


Figure A9. The interpreted MFA of the recorded June 28, 1994, blast at station B1. By studying the theoretical dispersion curves for the Central Texas crust, the nature of the observed dispersion curve was established and interpreted as shown. The complicated higher-mode region was delineated, although not in true accordance with the model, as was the region affected by the spectral hole. Similar interpretations were completed for each station's dispersion data.

where  $d(w)$  and  $j(w)$  are the phase spectrums of  $s(t)$  and  $f(t)$  respectively. If  $f(t)$  is chosen such that the Fourier phase is the same as that of  $s(t)$ , then  $f(t)$  is a phase-matched filter with respect to  $s(t)$ . For a more complete discussion of the PMF technique, the reader is referred to Herrin and Goforth (1977), who originally defined this class of linear filters. The advantage of using the PMF is that the final results are less contaminated by higher modes and multipathing arrivals. Thus, the complex spectrum of the primary signal can be recovered from multiple arrivals. With this in mind, the PMF represents a method of extracting  $R_g$  from the waveform in order to establish any azimuthal variations in the energy.

### Experimental Results

Two approaches were used to calculate the phase-matched filter of each  $R_g$  record for the June 28, 1994, Chemlime blast. The first method used one dispersion curve (obtained from the MFA of B8) to initialize the phase-matched filters for all seismograms in the network. This approach required more iterations to obtain a reliable PAF, and in some cases never converged to a trustworthy solution. Minor differences in the crustal velocity structure along each path forced a second approach for initializing the PMF technique that considered a different dispersion curve for each station. This method, although requiring each MFA to be interpreted as described previously, produced more reliable estimates for the desired filter.

Referring again to Figure A1, note that the June 28 and the July 17 blast are not along the same wall, but are instead along walls that are almost perpendicular to one another. The distances between the blasts, no more than 300 meters at most, were enough to cause differences in the dispersion analyses between the two blasts. These discrepancies are the result of lengthening or shortening propagation paths by very small amounts (less than 300 m), resulting in destructive interference. As noted previously, these holes greatly complicate the dispersion analysis. As an example, the June 28 blast has a spectral hole at 1.2 sec period on station B8, while the dispersion is smooth and continuous for the same station's July 17 blast seismogram. The result was that slightly different dispersion curves were interpreted and used

for each station and each blast, even though the propagation paths were similar.

Using PMF, the Rg waveforms in each record was extracted. Figure A10 shows the low-pass filtered (3 Hz), vertical component from station B7, June 28, blast and the PMF estimated Rg. The Rg consists of a normally dispersed signal between 0.7 and 2.0 seconds period with inversely dispersed higher frequency arrivals superposed. Similar results are found for all other data processed in this study. By subtracting the estimated signal from the waveform, the residual waveform can be examined (Figure A10). The residuals show several events that are higher modes and/or multipathing, depending upon their time delay. The PMF extracted Rg are plotted in Figures A11, A12, and A13 to show the amplitudes scaled to constant values, filtered in the forward and reverse directions with a band-pass filter such that the inversely dispersed branch is not shown. Previous seismograms from this same quarry recorded at greater distances do not show the inversely dispersed branch.

The squared sum of the amplitudes of Rg, what we are terming relative energy, for all three blasts was then determined and plotted (Figure A14). The relative energies (relative to station B10 in each graph) are shown as a function of travel path either crossing or not crossing the open pit. The results show that azimuthal variations of Rg energy are present, and are related to the open pit of the quarry. Rg that propagates through the open pit has less relative energy than Rg for paths that do not cross the pit.

For example, notice the PMF extracted Rg for station B8, which was recorded for all three blasts (Figure A14). For the June 28 and July 12 blasts, B8 sits behind the face of the quarry being mined, and has relative Rg energy greater than any values propagating across the open pit. But, when the working face is changed, as in the case of the July 17 blast, and the propagation path to B8 now involves a small part of the pit, the relative energy decreases. Modal scattering and/or conversion (i.e. from Rg energy to higher mode energy/shorter wavelength energy) may be occurring in the open pit. Numerical modeling studies are now needed to explain these results.

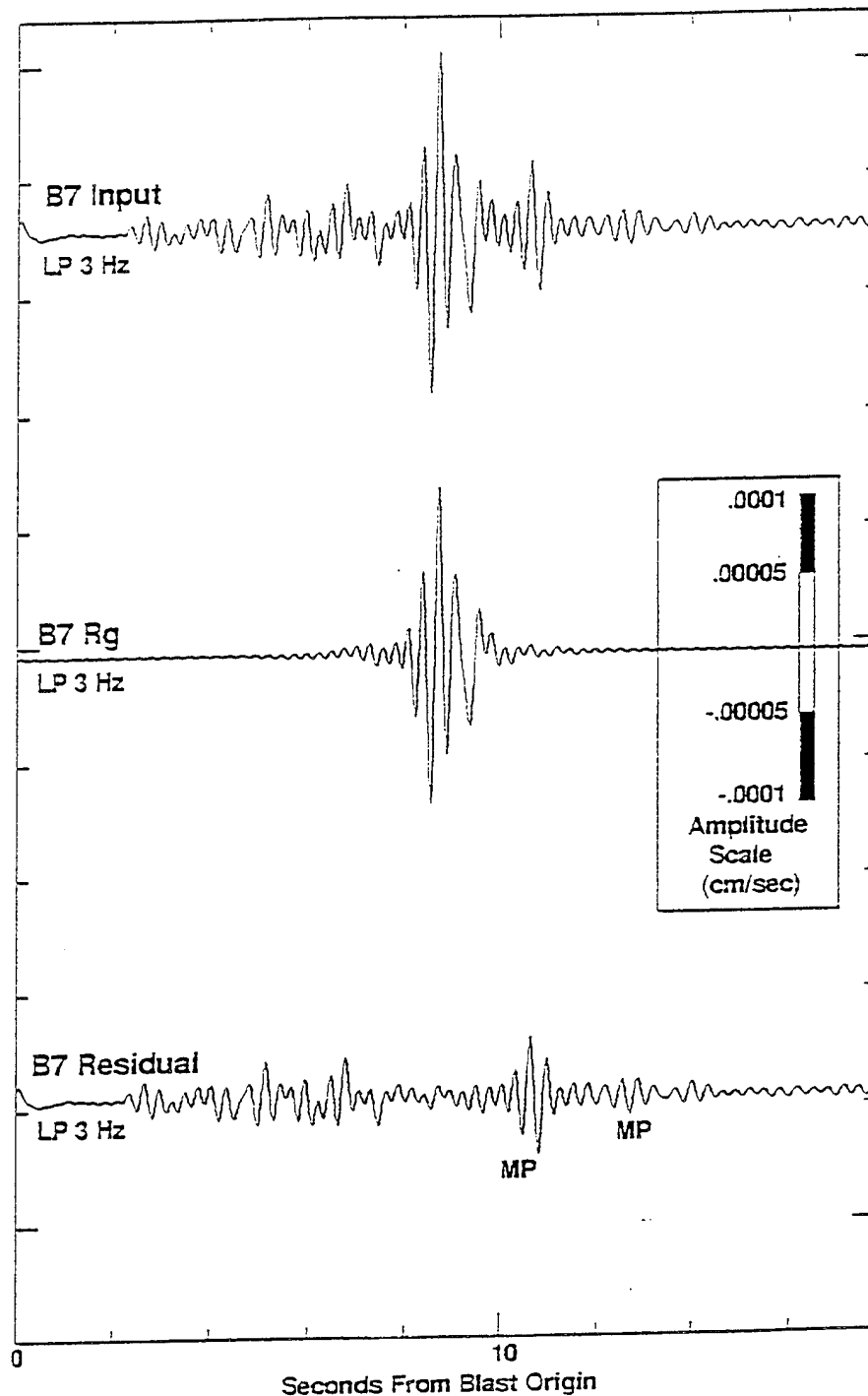


Figure A10. The results of the Phase Match Filtering (PMF) technique on the June 28 blast data at station B7. The top trace shows the lowpass (3 Hz) filtered input trace characterized by the Rg signal at approximately 9 seconds from the origin of the blast. The middle trace shows the PMF extracted Rg which, although not easily seen, consists of reversely dispersed Rg superposed on normally dispersed Rg with periods between 0.7 and 2.75 seconds. The final plot shows the residual trace, obtained by subtracting the middle trace from the top. The result is that Rg has been removed leaving only multipaths (MP) and higher-modes in the remaining surface wave train.

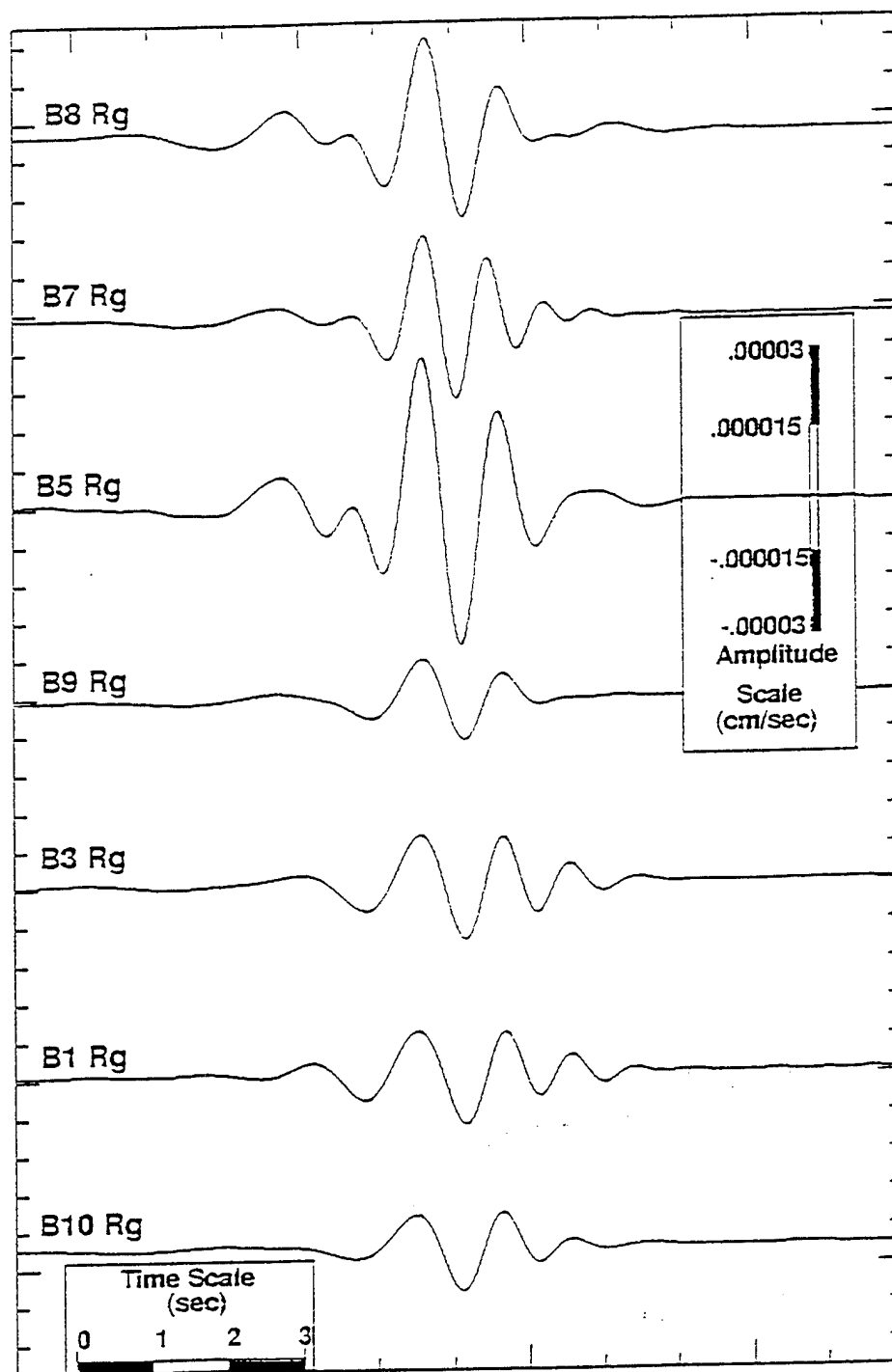


Figure A11. PMF extracted Rg from the June 28, 1994 Chemlime explosion, bandpass filtered in the forward and reverse directions. Traces have been arbitrarily shifted to align the most prominent pulse.

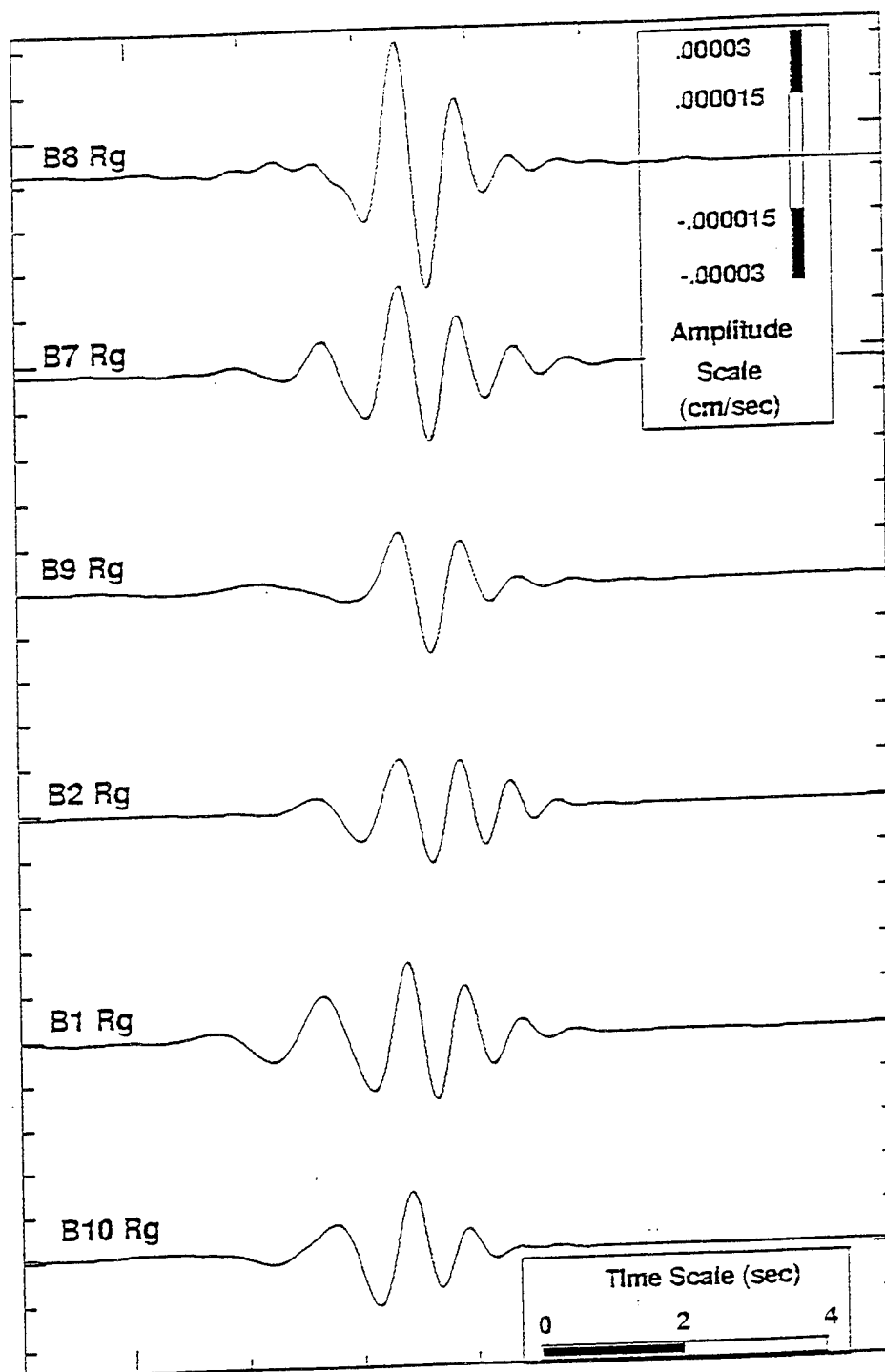


Figure A12. PMF extracted Rg from the July 12, 1994 Chemline explosion, bandpass filtered in the forward and reverse directions. Traces have been arbitrarily shifted to align the most prominent pulse.

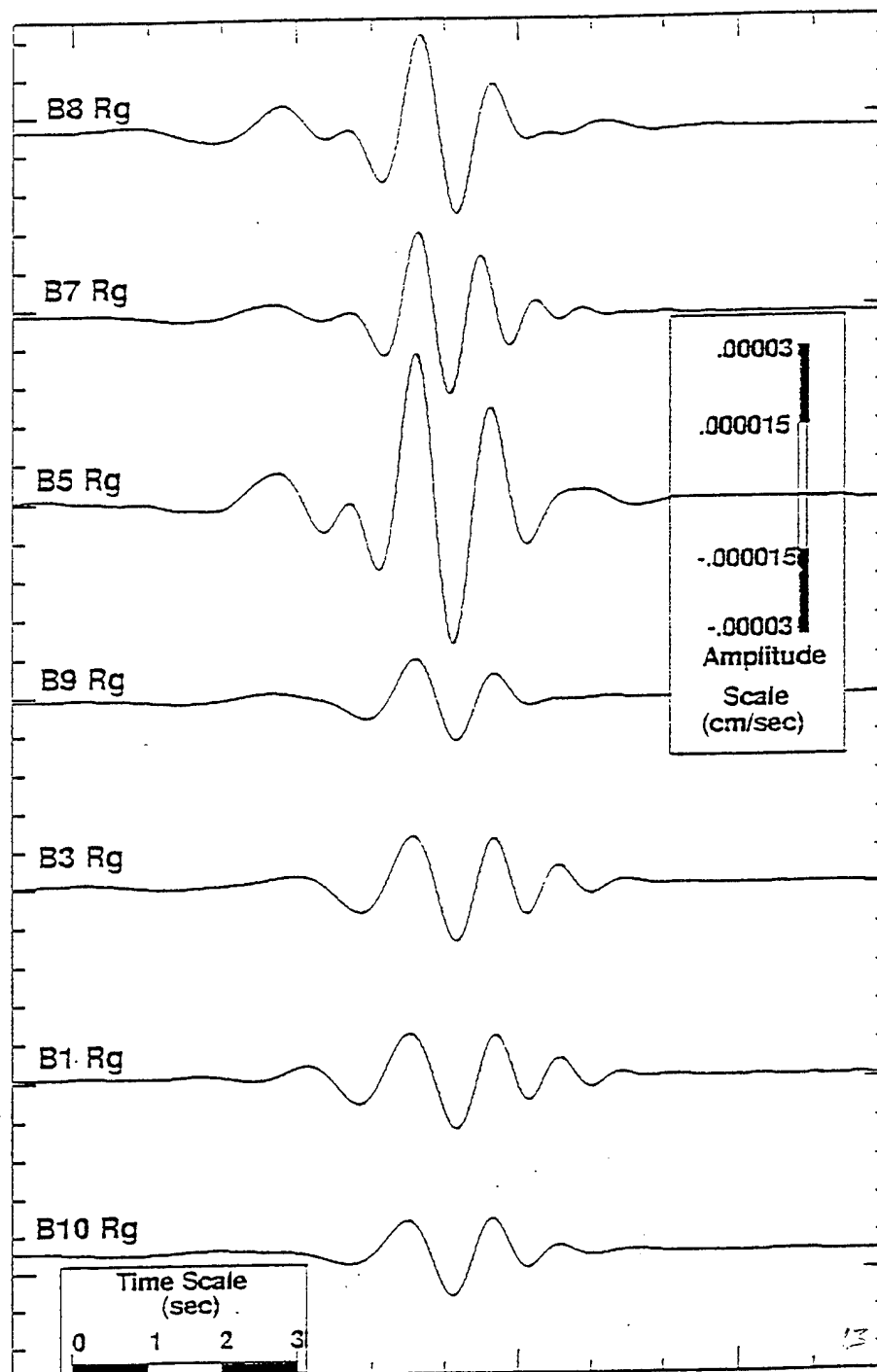


Figure A13. PMF extracted Rg from the July 17, 1994 Chemline explosion, bandpass filtered in the forward and reverse directions. Traces have been arbitrarily shifted to align the most prominent pulse.



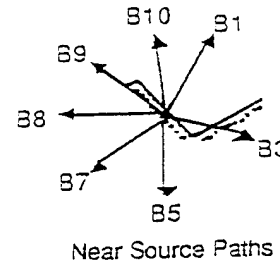
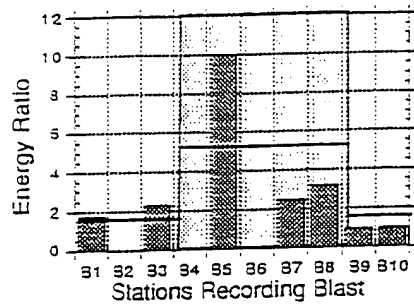
After the extraction of Rg from the signal, higher-mode surface waves still exist in the residual seismogram. By using time-domain windows inferred from the group velocities of these higher modes, the relative energy in the higher modes was calculated. Remarkably, the only place where the residual higher-mode energy exceeded the Rg energy was at stations B1 and B2, both having the propagation paths affected by the open pit. This suggests the possibility that Rg is converting some energy into higher modes.

The open pit may not be the only cause of such azimuthal variations in relative energy. We note that the ripple direction may have an effect. The ripple fire direction for the July 17 direction was almost directly in line to station B2. Even though the path was across the open pit of the quarry, the relative energies of Rg were greater for this blast at B2 than the same station's record for the July 12 blast, where the ripple direction was parallel to the station. Even so, the open pit hypothesis seems to complement the energy variations somewhat better than dependence upon ripple fire direction.

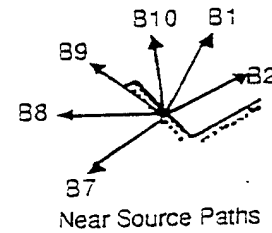
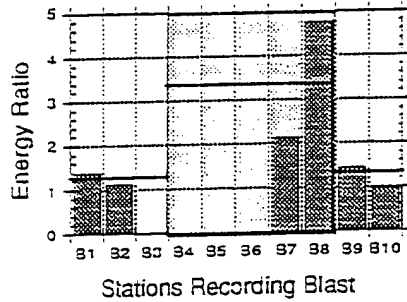
### Conclusions

1. The upper crust in Central Texas has a high value of Poisson's ratio ( $\nu$ ), estimated to be between 0.35 and 0.40, such that the dispersion curves for short-period Rayleigh waves are very complex.
2. The dispersion curve for the fundamental-mode Rg consists of two limbs separated by an inflection point, an Airy phase, and an inversely dispersed branch. One limb has bandwidth 1.5 to 2.75 seconds period and a subtle dispersion. The second limb, between 0.7 and 1.5 sec period has more noticeable dispersion. The Airy phase travels at 0.9 km/sec and has a period of 0.6-0.7 sec. The inversely dispersed branch is complicated by the arrival of the first higher mode, but can be distinguished when models for the dispersion are considered.
3. Spectral holes in the Multiple Filter Analysis (MFA) are localized near 0.9 sec period in this study, and are caused by multipathing of surface waves. If these spectral holes are not accounted for, considerable error in group-velocity dispersion curves can occur. Dispersion curves in this study were obtained by projecting the curve through the holes.

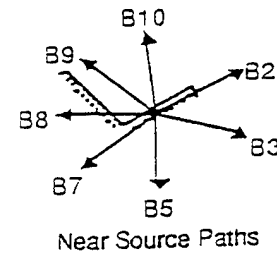
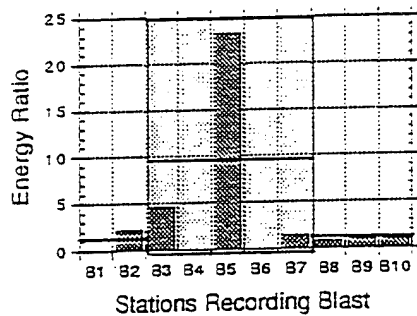
### June 28, 1994 Chemlime Blast



### July 12, 1994 Chemlime Blast



### July 17, 1994 Chemlime Blast



- ☒ Paths that do not cross the open pit of the quarry
- ☐ Paths that do cross the open pit of the quarry

Figure A14. Azimuthal variation of relative energy in Rg around the Chemlime quarry for three separate blasts. The squared sum of the amplitudes of Rg for each station, compared relative to station B10, are plotted as a series of bar graphs for each blast on the left, and the near source paths to each recording station is shown schematically on the right. Stations B4 and B6, inoperable due to disk failure during the entire experiment, and other sites failing to perform are plotted to show the extent of the coverage desired, but not obtained in the experiment. Even with the lack of desired data, there does seem to be a relationship between the relative energy that varies azimuthally around the quarry and the open pit.

4. The Phase Match Filter (PMF) technique is a reliable means of separating Rg from a complicated surface wave train when the dispersion curve used to initiate the technique is accurate.
5. Relative energy in extracted Rg from this study shows that Rg contains more energy on paths not crossing the open pit of the quarry than those propagation paths that do.
6. Relative energy in the remaining higher-mode surface waves show higher mode energy exceeding Rg only on paths that cross the open pit.
7. The fact that paths involving the open pit in some cases have half the Rg energy than those that do not suggest modal convergence of Rg to Lg will occur much earlier than the 175 km distance usually noted in Central Texas. Also, it is possible that this can explain numerous examples in which seismograms from the same quarry look remarkably different from blast to blast. Based on this study, it would be possible for the quarry to move its blasting operations to the opposite side of the quarry and change the nature of the Rg seismogram recorded at a permanent station.

### Acknowledgements

We thank Chris Hayward and Herbert Robertson for helpful discussion and comments on the manuscript. We also thank Beth Rinard, Fred Nawrocki, Jeff Gephardt, and the other members of the Baylor Geology Department Geophysics Summer Field Course for their help in deploying the portable network. Finally, without the support of Freeman Mullins and Robert "Squeaky" Shannon at Chemlime, this study would not have been completed. This work was sponsored by the Advanced Research Projects Agency, Nuclear Monitoring Office, ARPA orders A128 and C325, under Phillips Lab contracts F19628-93-C-0057 and F19628-95-C-0184.

### References

- Anderson, J., and Dorman, J. (1973). Local geologic effects on short-period Rayleigh waves around New York City, *Bull. Seism. Soc. Am.* **63**, 1487-1497.

- Bath, M. (1975). Short-period Rayleigh waves from near-surface events, *Phys. EarthPlanet. Inter.* **10**, 369-376.
- Bonner, J. (1993). Crustal velocity structure of Central Texas. M.S. Thesis, Baylor University, Waco, Texas, 125 pp.
- Boore, D. Harmsen, S., and Harding, S. (1981). Wave scattering from a step change in surface topography. *Bull. Seism. Soc. Am.* **71**, 1731-1741.
- Dziewonski, A., Bloch, S., and Landisman, M. (1969). A technique for the analysis of transient seismic signals, *Bull. Seism. Soc. Am.* **59**, 427-444.
- Goforth, T. and Bonner, J. (1995). Characteristics of Rg waves recorded in Central Texas, *Bull. Seism. Soc. Am.* **85**, 1232-1235.
- Gupta, I. and Hartenberger, R. (1981). Seismic phases and scaling associated with small high-explosive surface shots, *Bull. Seism. Soc. Am.* **71**, 1731-1741.
- Herrin, E. and Goforth, T. (1977). Phase-matched filters: application to the study of Rayleigh waves, *Bull. Seism. Soc. Am.* **67**, 1259-1275.
- Herrmann, R. B. (1969). The structure of the Cincinnati arch as determined by short period Rayleigh waves, *Bull. Seism. Soc. Am.* **59**, 399-407.
- \_\_\_\_\_ (1984). Some aspects of band-pass filtering of surface waves, *Bull. Seism. Soc. Am.* **63**, 663-671.
- Kafka, A. (1990). Rg as depth discriminant for earthquakes and explosions: a case study in New England, *Bull. Seism. Soc. Am.* **80**, 373-394.
- Kocaoglu, A. and Long, L.T. (1993). Tomographic inversion of Rg wave group velocities for regional near-surface structure, *J. Geophys. Res.* **98**, 6579-6587.
- Langston, C.A. (1982). Aspects of Pn and Pg propagation at regional distances, *Bull. Seism. Soc. Am.* **72**, 457-472.

- McEvilly, T.V., and Stauder, W. (1965). Effect of sedimentary thickness on short-period Rayleigh wave dispersion, *Geophys.* 30, 198-203.
- Mooney, H. and Bolt, B. (1966). Dispersive characteristics of the first three Rayleigh modes for a single surface layer, *Bull. Seism. Soc. Am.* 56, 43-67
- Trygvasson, E. and Qualls, B. (1967). Seismic refraction measurements of crustal study in Oklahoma, *J. Geophys. Res.* 72, 3738-3740.

## APPENDIX B – SEISMO-ACOUSTIC SYNERGY

Eugene Herrin, Valeriu Burlacu, Ileana Tibuleac, Chris Hayward, Jessie Bonner, Paul Golden and G.G. Sorrells

### INTRODUCTION

In CD/NTB/WP.225 Working Group I of the Ad Hoc Committee on a Nuclear Test Ban (UN Conference on Disarmament) suggested on 13 March 1995 that the IMS include "...a [infrasonic monitoring] network designed to provide uniform global coverage with a high probability of detecting a 1 kt nuclear explosion in the atmosphere, taking full advantage of synergy with other systems...." They further state that "The experts propose a system of between 60 and 70 infrasound stations...." Proposed plans by several expert groups for this system call for many of the infrasound stations to be collocated with primary IMS seismic stations. Clearly there would be a net reduction in cost and operational complexity with the collocated systems sharing the required infrastructure and communication channels. It is the purpose of this paper to demonstrate that there are additional advantages to collocation; namely, important data for event characterization will be generated because of seismo-acoustic synergy.

Over two decades ago Donn and others (1971) reported the observation of air-coupled seismic waves at long range from Apollo launchings. Using microphones and seismographs collocated in arrays in Georgia, USA, they recorded simultaneous acoustic and seismic waves from launchings of Apollo 13 and 14, a distance of 374 km to the south, at times appropriate to the arrival of acoustic waves from these sources.

At a recent GSE Workshop (26-29 June, Baltimore, USA), Dr. Michael Jost discussed outages at GERESS (FRG) caused by summer thunderstorms and showed records of seismic signals resulting from thunder-induced acoustic waves. We have observed similar seismo-acoustic signals at TXAR. In May 1991, a connector failure in a GS 13 Z seismometer at the Lajitas seismic station (TXAR) caused the instrument to respond to electromagnetic pulses from lightening in nearby thunderstorms. Figure C1a shows sharp pulses

caused by lightning (indicated by flags) followed by ground motion caused by the following acoustic signal (thunder). The spectra shown in Figure C1b show that thunder induced ground motion is well above ambient noise at frequencies greater than about 0.5 Hz.

### THE THOMPSON HOLLOW EXPERIMENT

Because of the developing interest in using collocated infrasonic and seismic stations in the IMS, we began this year to investigate carefully the relationship between acoustic waves and induced ground motion, particularly for frequencies between 0.5 and 10 Hz. An experiment was carried out at a site called Thompson Hollow in Central Texas. A small pipe array with a B & K microphone was collocated with a Sprengnether S-6000 vertical seismometer at a distance of 9.75 km from the Chemline quarry. The rock properties at Thompson Hollow are shown in the following stratigraphic section.

Surface		
Clay	Walnut fm.	$V_p = 1 \text{ km/s}$
and	and	$V_s = 0.5 \text{ km/s}$
20 m sand	Paluxy fm.	$\rho = 1.4 \text{ gm/cc}$
Layer		
Half Space		
Limestone	Glen Rose fm.	$V_p = 2.6 \text{ km/s}$
		$V_s = 1.5 \text{ km/s}$
		$\rho = 2.5 \text{ gm/cc}$

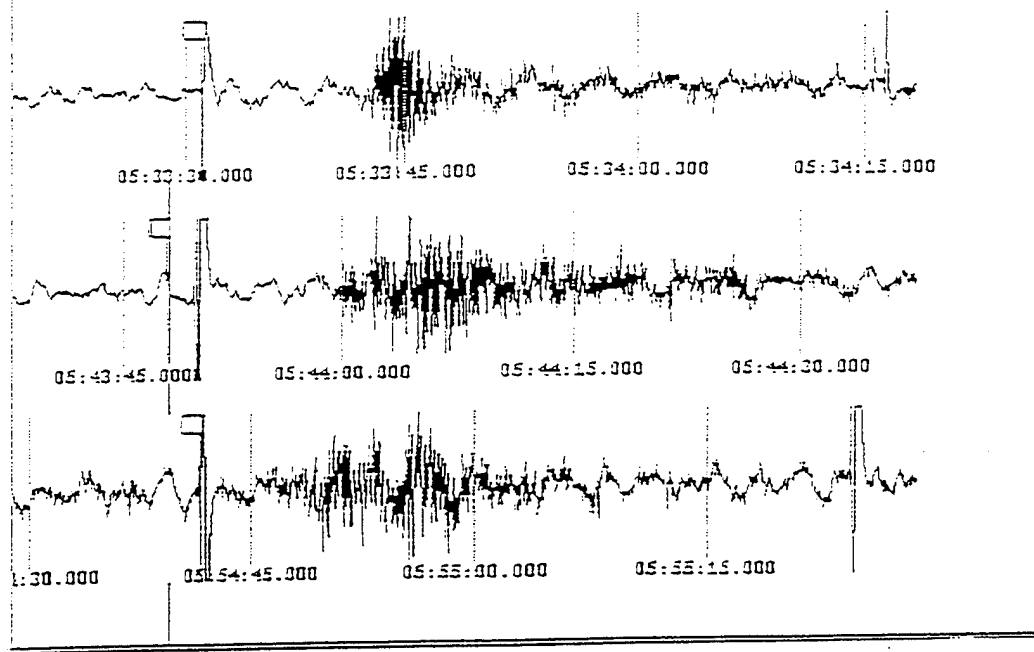


Figure B1a. Short-period vertical seismograms illustrating lightning-triggered EM pulses followed by seismic signals presumably generated by the passage of the atmospheric waves caused by the lightning. These data were recorded at LTX in 1991 during a period of local thunderstorm activity.

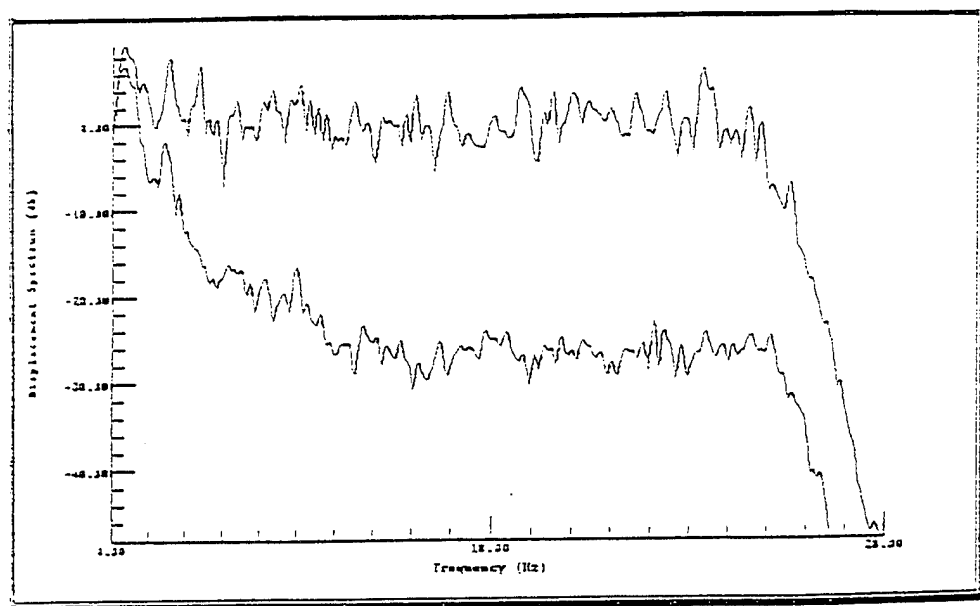


Figure B1b. Comparison of the ambient-noise spectrum with the spectrum of a representative short-period vertical seismic signal in the middle trace of figure B1a. The comparison shows that this type of source can generate power levels that are substantially above the ambient background at frequencies greater than about 0.5 Hz.



Using a theoretical analysis developed by Sorrells (1971) and Sorrells and Goforth (1973), a predicted transfer function for Thompson Hollow (Figure B2) shows nanometers displacement divided by acoustic pressure in microbars as a function of frequency. In the frequency band of interest, ground motion was predicted to be about 2 nm per mbar pressure change. Figures B3 through B5 show filtered waveforms on the microphone and seismic channels for the acoustic arrival from the Chemline quarry blast. Figure B6 shows the crosscorrelation between ground acceleration and sound pressure level. As predicted, the two signals are 180° out of phase indicating that an increase in sound pressure causes a downward acceleration of the ground. The observed relations between sound pressure and ground motion compared with the predicted values (Figure B2) are as follows:

<u>Frequency Band</u>	<u>Predicted</u> (nanometers/microbars)	<u>Observed</u>
1-2 Hz	2.0	2.3
2-4 Hz	1.8	2.0
4-8 Hz	1.8	1.0

The agreement between the theoretical and observed seismo-acoustic coupling is very good considering that the velocities and densities used in the calculations were approximate values. The Thompson Hollow experiment supported the theoretical model providing confidence that calculations made for the Lajitas, Texas, area (TXAR) and the Pinedale, Wyoming, area (PDAR) would prove to be reliable.

#### IDENTIFICATION

Explosions in quarries or open-pit mines are distributed in space and time in order to minimize collateral damage from air blast and ground motion and to make the most cost-effective use of explosives. These distributed explosions, sometimes referred to as ripple-fired or row-fired shots, provide a shear-wave source that has a relative long time duration resulting in a low-frequency peak in the Sn-Lg spectrum observed at regional distances. Because this peak

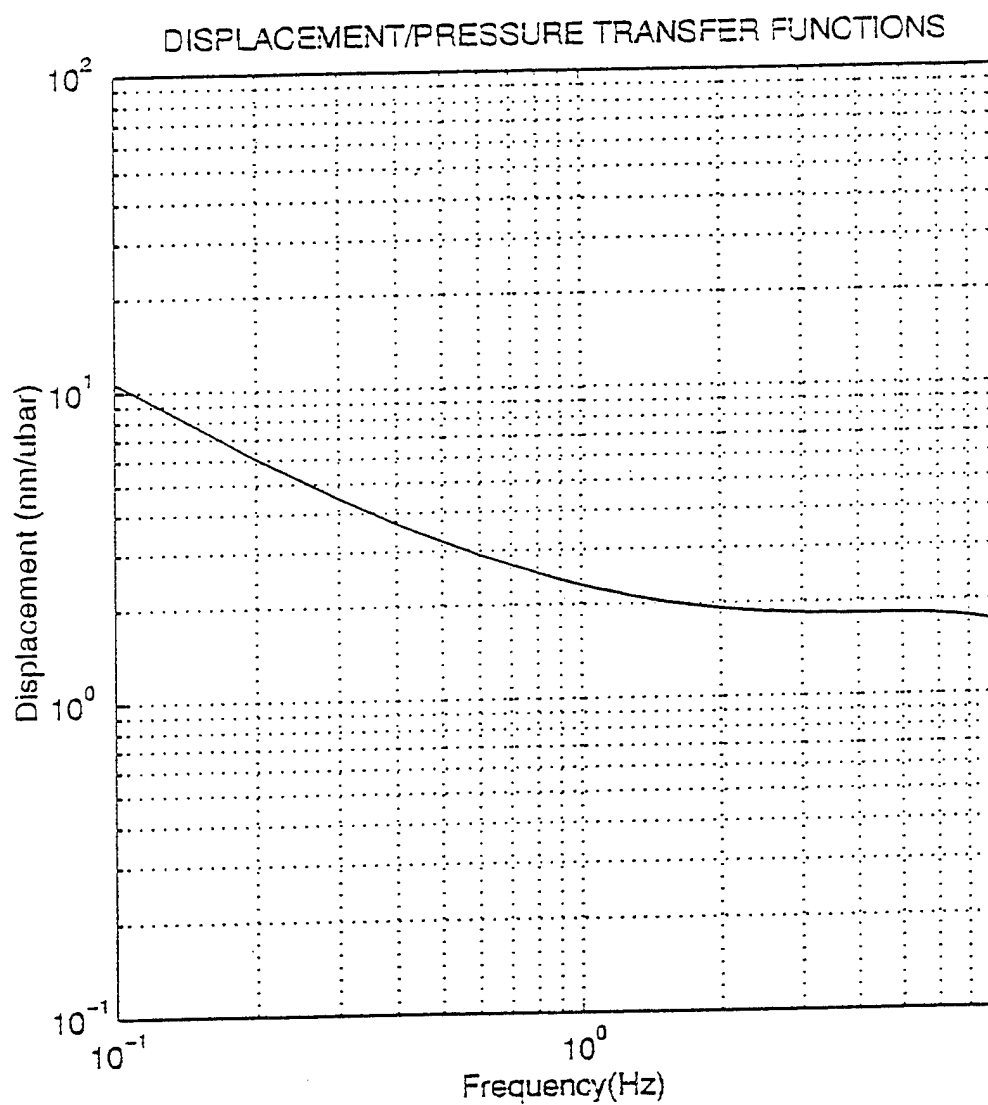


Figure B2. Predicted ground motion at Thompson Hollow induced by acoustic waves as a function of frequency.

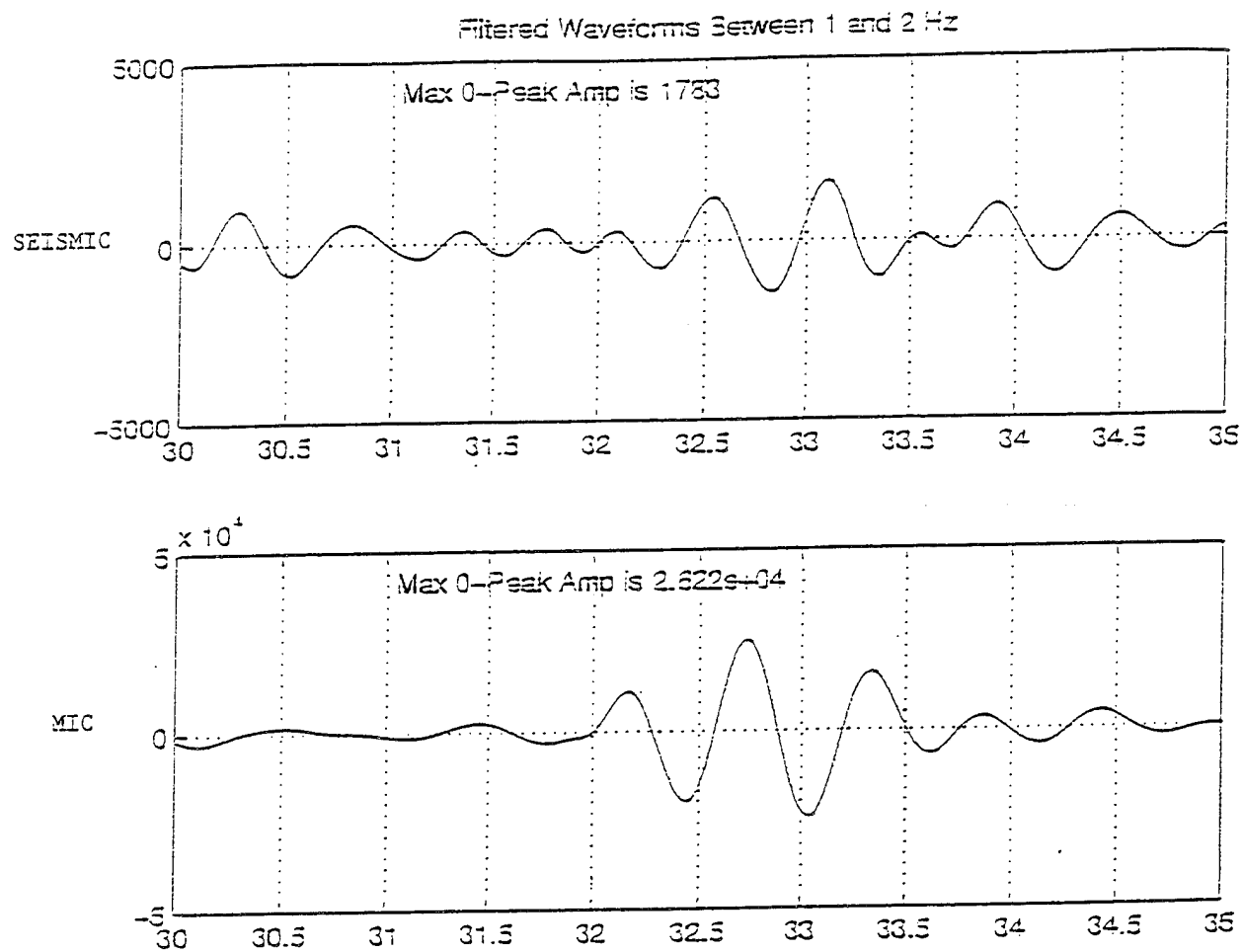


Figure B3. filtered seismograms recorded from the march 17 Chemline blast. The signals were filtered using a three-pole Butterworth BP filter between 1 and 2 Hz.

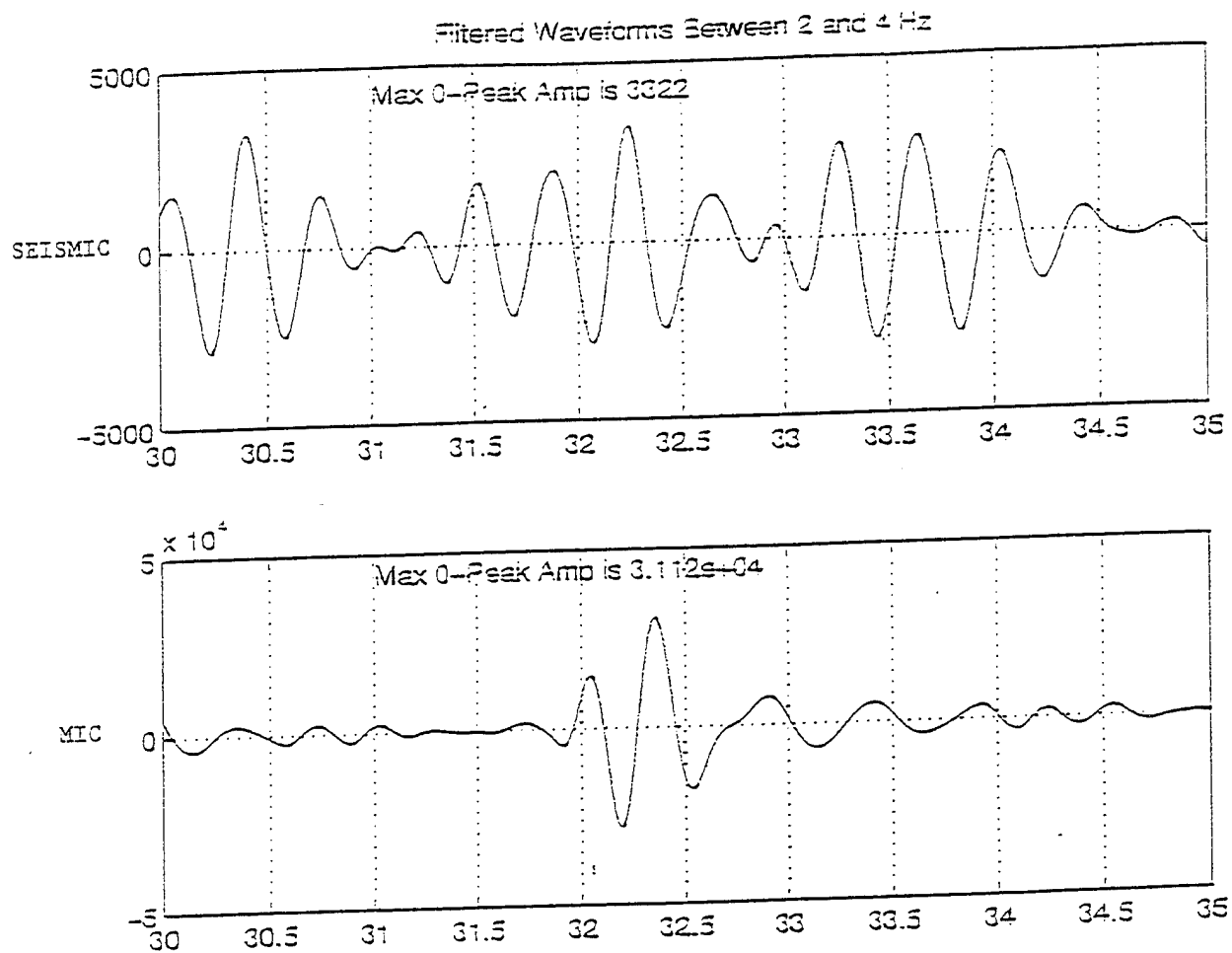


Figure B4. filtered seismograms recorded from the march 17 Chemline blast. The signals were filtered using a three-pole Butterworth BO filter between 2 and 4 Hz.

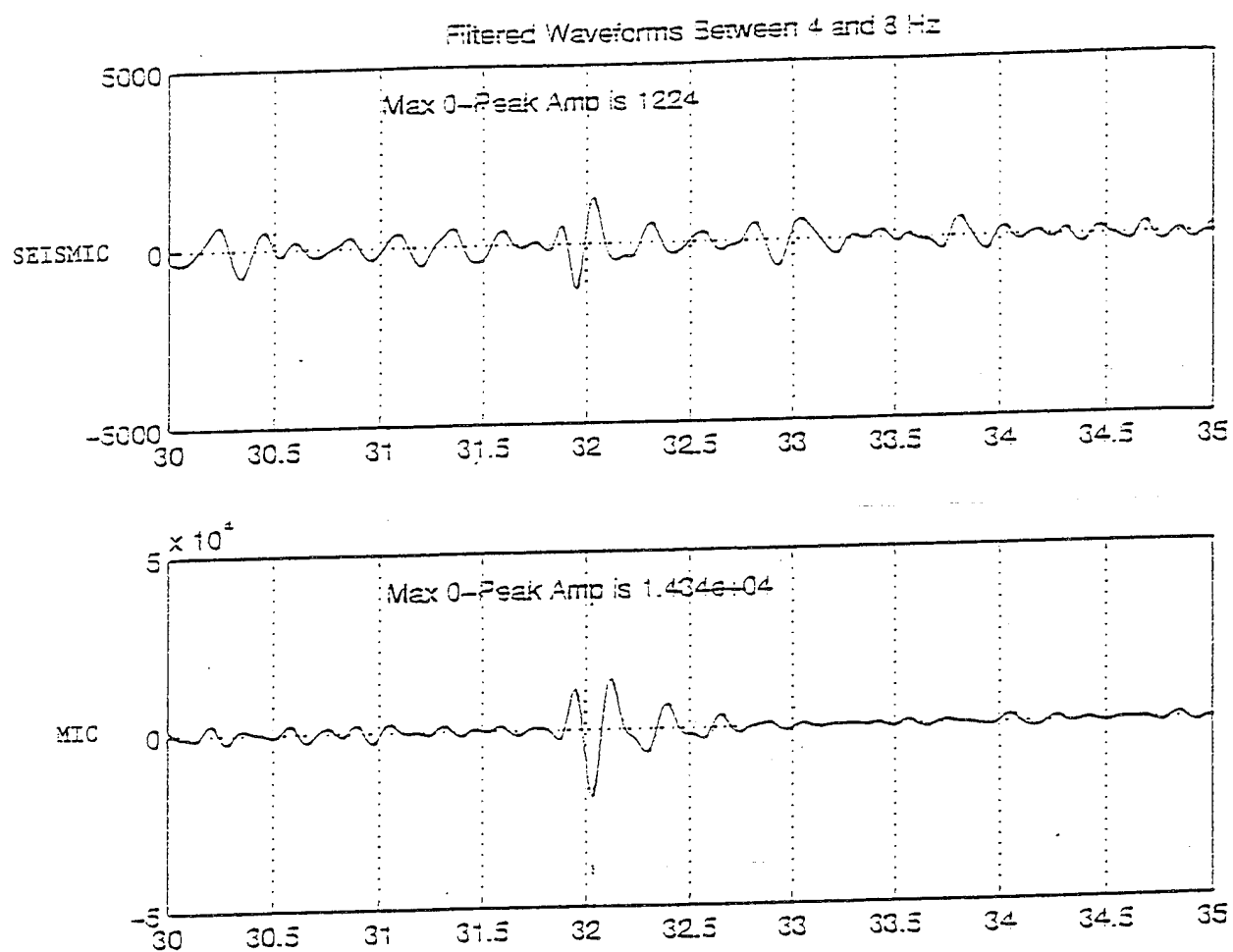


Figure B5. filtered seismograms recorded from the march 17 Chemline blast. The signals were filtered using a three-pole Butterworth BP filter between 4 and 8 Hz.

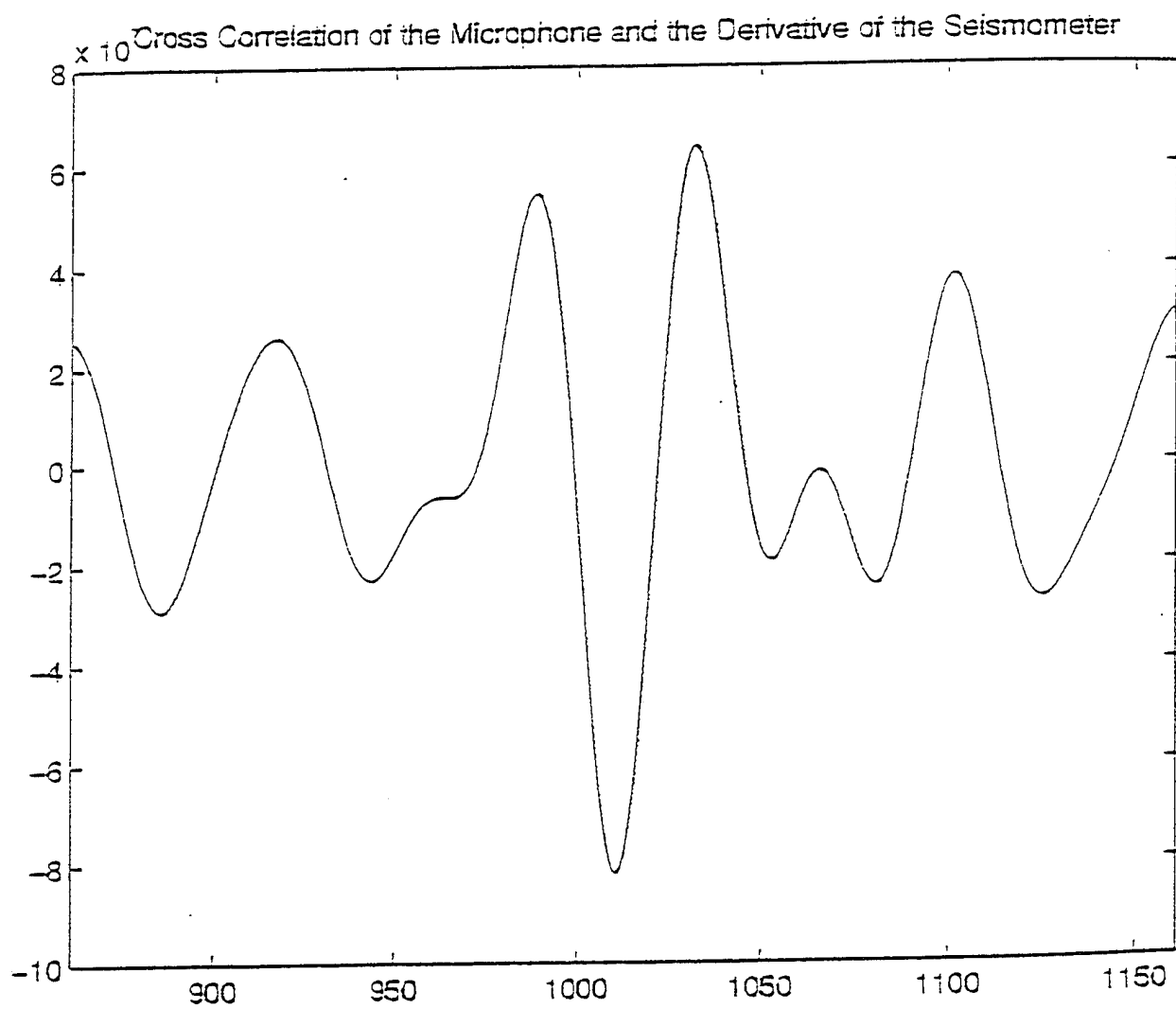


Figure B6 Cross correlation between ground acceleration and sound pressure that shows the expected  $180^\circ$  phase difference.

dominates the spectrum, an auto-regressive model is appropriate to identify the spectral characteristics of commercial explosions.

Figure B7 shows the mathematical model for an auto-regressive (AR) or all-pole process of order  $p$ . In order to determine the most dominant spectral feature of a regional waveform, we have used an order 3 AR model. This model has one real pole and a pair of conjugate complex poles. For an AR process to be stable the complex poles must lie outside the unit circle in the complex  $z$ -plane. In Figure C8 we plot the reciprocal of the pole position relative to the unit circle. Angular position is determined by the frequency between 0 and  $\pi$  radians. In our data, the real pole always lies at zero radians because of the effect of a strong anti-alias filter. The closer the pole is to the unit circle, the stronger the spectral peak represented by the pole.

Figure B9 shows the waveform and AR(3) spectrum for Lg from an explosion in the Vogtland region of Eastern Europe recorded at GERESS. The sharp peak at 2 Hz comes from a strong complex pole, only positive frequencies being considered. In Figure B10, frequency and pole position relative to the unit circle are shown for a moving window 200 points wide (5 sec.) that is advanced through the waveform with 50% overlap. As the window moves into the Lg wavetrain, the frequency associated with the complex pole drops well below 5 Hz and pole strength increases, as the reciprocal pole position approaches the unit circle. This pattern in the moving window display is seen only for distributed surface explosions.

Figure B11 shows the waveform and AR(3) spectrum for the Lg phase from an earthquake in the Vogtland region recorded at GERESS. Note the broad spectral peak centered at about 8 Hz. In the moving window display shown in Figure B12, the frequency associated with complex pole stays around 10 Hz as the window moves through the Lg wavetrain and the reciprocal pole position does not approach the unit circle. For the Vogtland data set, a discrimination rule can be applied. Explosions all show reciprocal pole positions greater than 0.7 and frequencies less than 5 Hz. Figure B13 is a summary of pole positions for AR(3) models of Lg arrivals from the Vogtland region. The stars are earthquakes and the solid dots are explosions all recorded at GERESS. The

## AR (ALL POLE) PROCESS

$$x(n) = - \sum_{k=1}^p a(k)x(n-k) + u(n)$$

$p$  is the order of the process.

$a(k)$  are the coefficients, generally complex.

$u(n)$  is the driving process, here assumed to be white noise.

Figure B7. Mathematical model for an auto-regressive (AR) or all-pole process of order  $p$ .



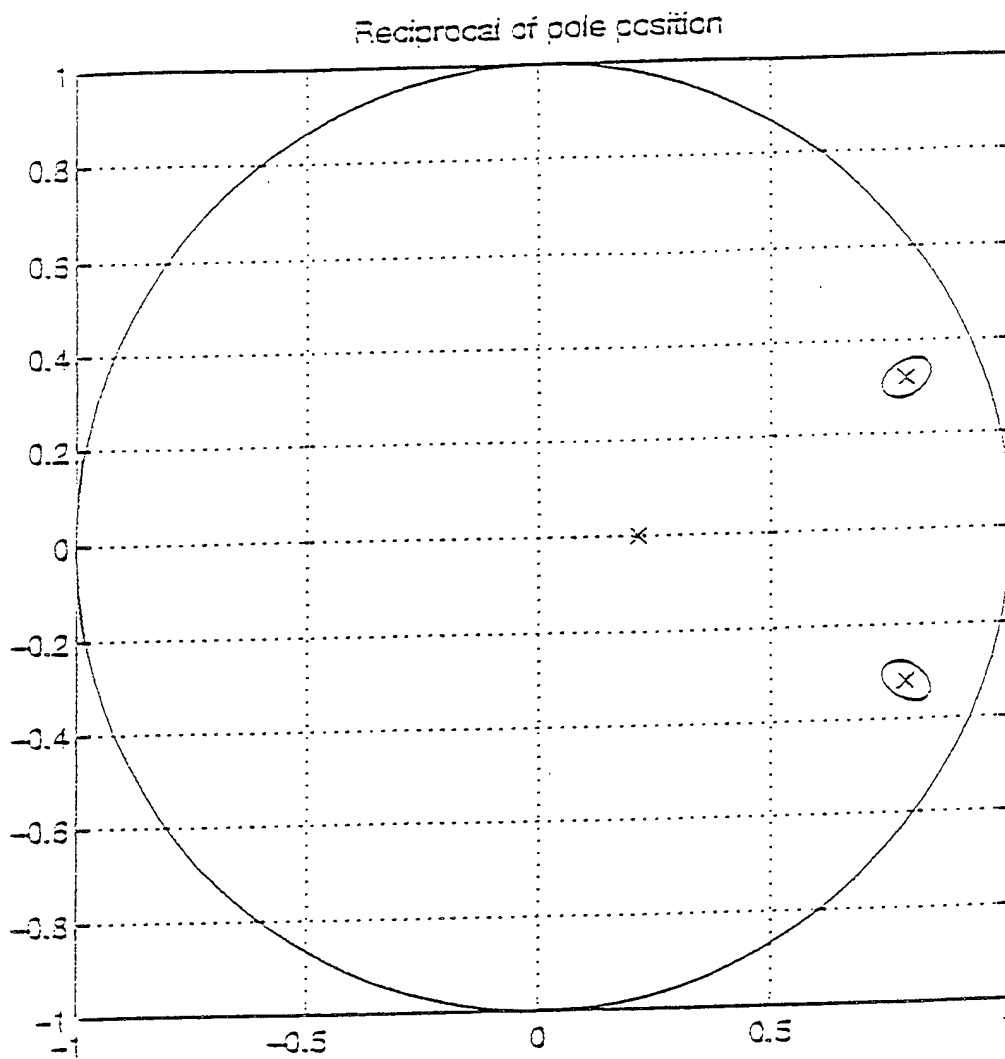


Figure B8 Three reciprocal poles in the complex plane.

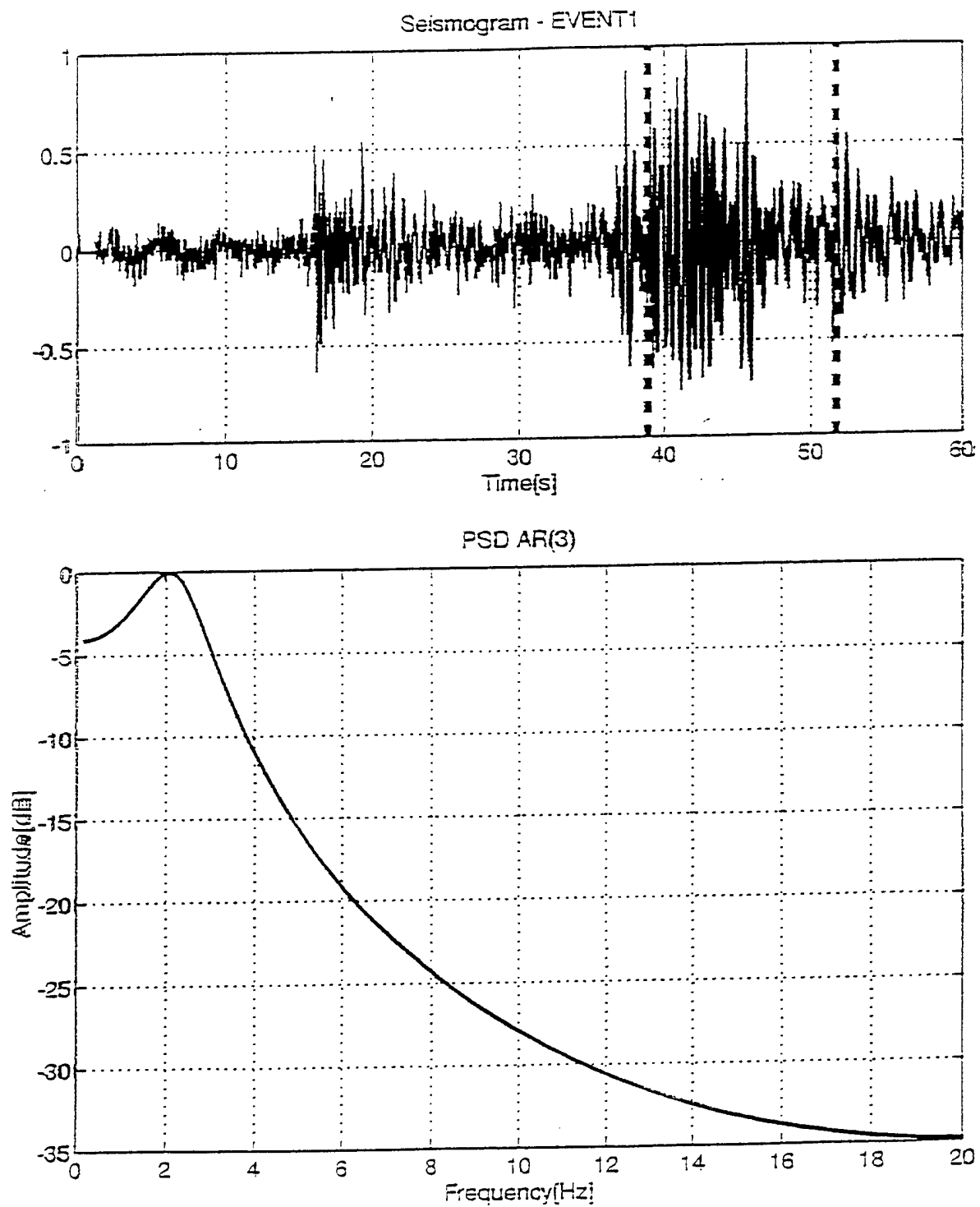


Figure B9. Waveform and AR(3) spectrum for a commercial explosion in the Vogtland region.

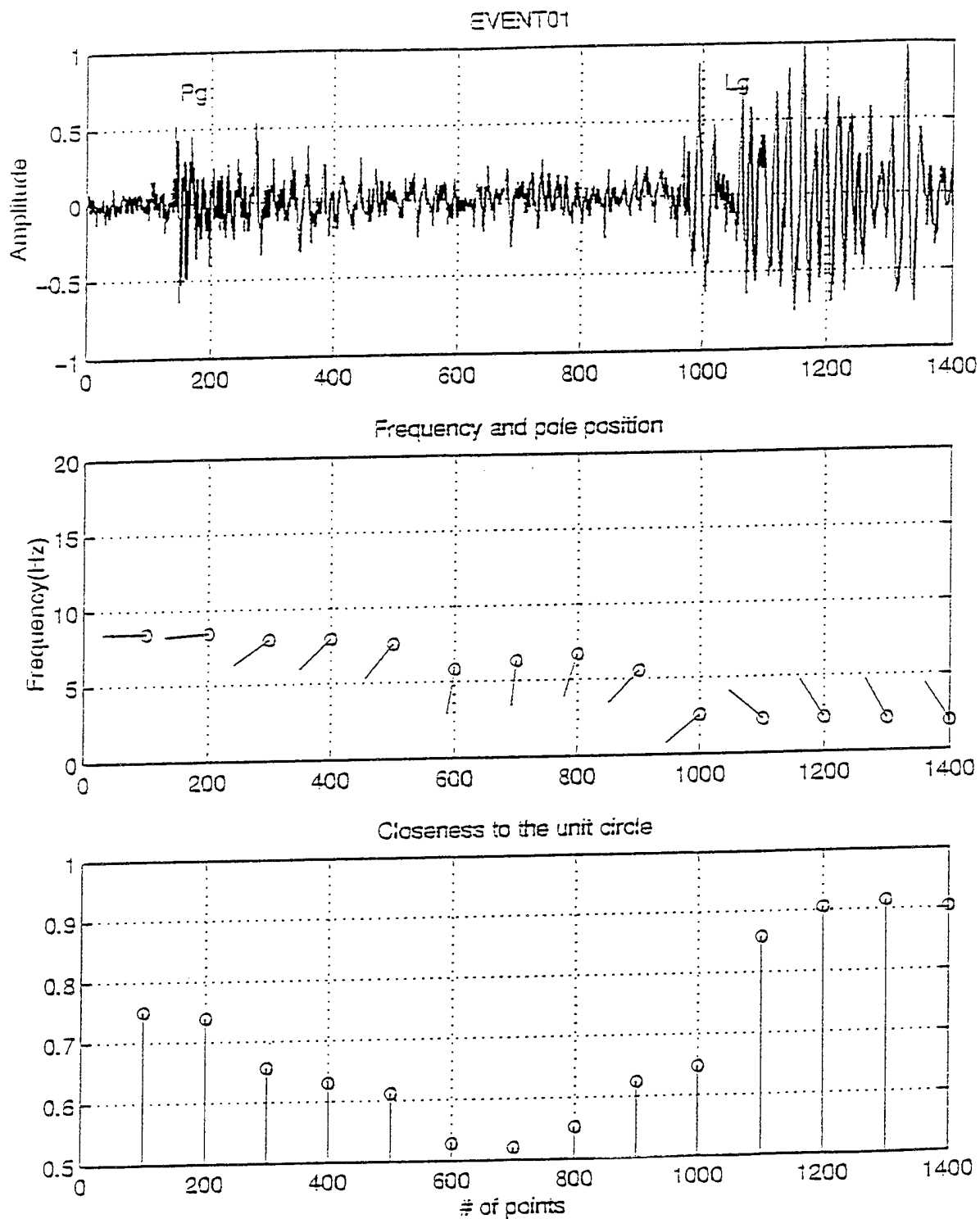


Figure B10. Moving window display showing the complex-pole position for the explosion shown in Figure B9.

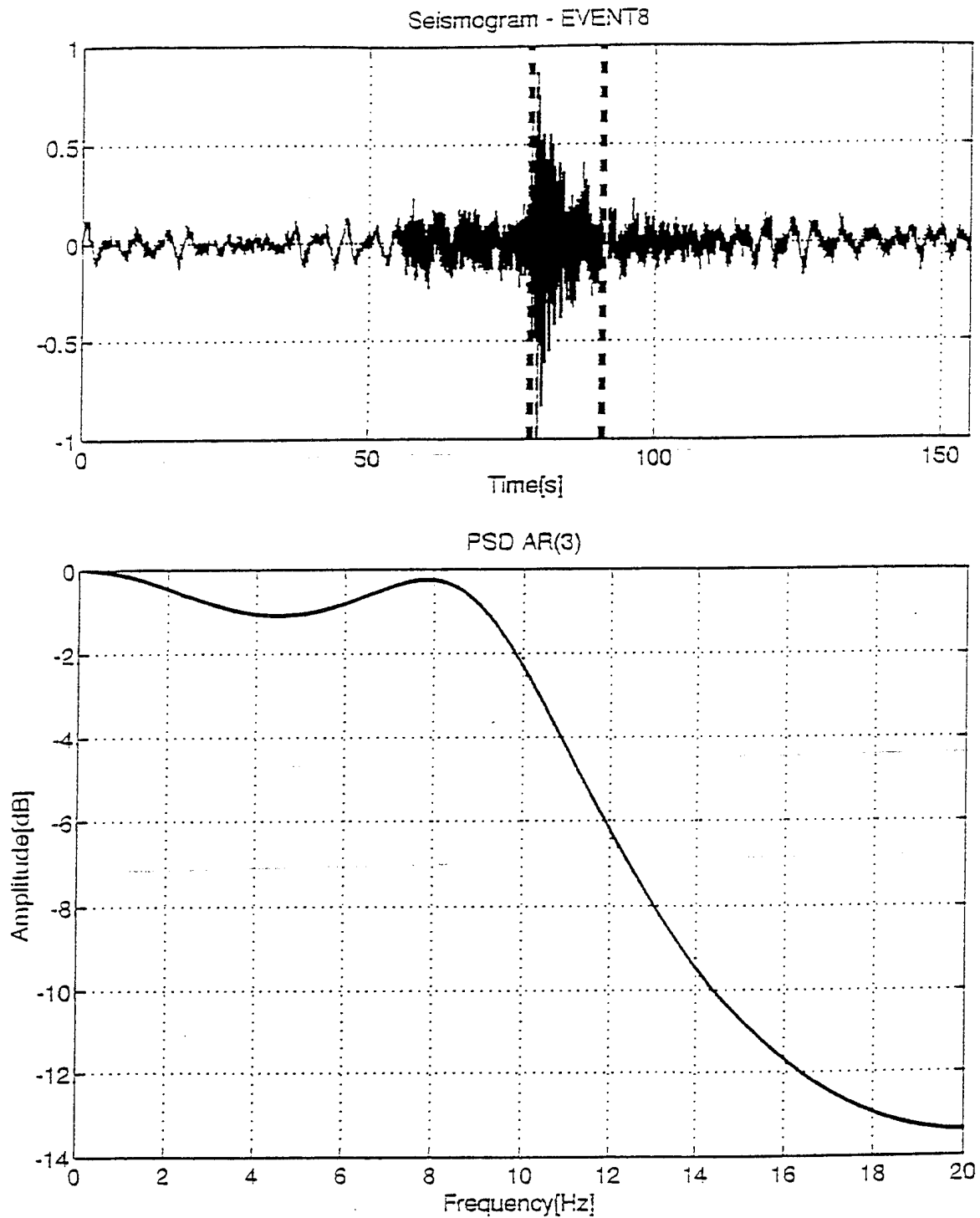


Figure B11. Waveform and AR(3) spectrum for an earthquake in the Vogtland region.

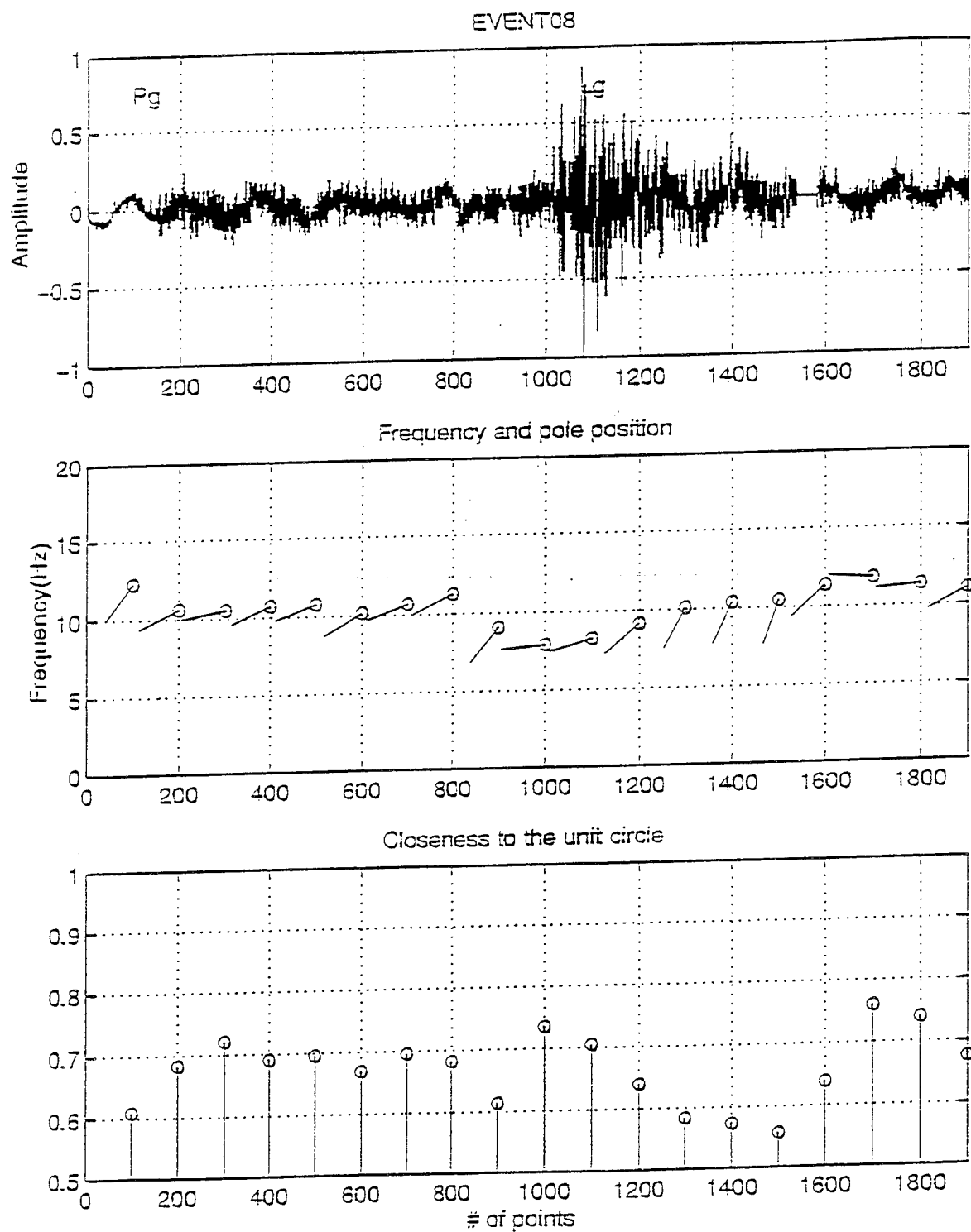


Figure B12. Moving window display showing the complex pole position for the earthquake shown in Figure B11.



open circles are explosions in the Southern Caucasus of Russia recorded at GUM.

Not all events are as clearly discriminated as those in the Vogtland data base. Figure B14 shows the moving window display from an earthquake in the Steigen region of Norway recorded at ARCESS. Pole position and frequency are intermediate relative to those of the explosions and earthquakes in the Vogtland set; however, the position does not move below 5 Hz or above 0.9 as the window enters the Lg wave train. The AR(3) method is useful as a "screen" or one-sided discriminant. Whenever the characteristic pattern for the AR(3) moving window display seen in Figure B10 is observed for a regional signal, the event is a distributed surface explosion. Otherwise, the event cannot be classified by this method.

#### OBSERVATIONS AT TXAR

Figure B15 shows waveforms from the TXAR array for  $m_b$  1.9 event on 30 March 1995 from Northern Coahuila, Mexico, about 325km east-southeast of the station. The moving window display for this event in Figure B15 does not show the pattern expected for a distributed, surface explosion (compare Figure B16 with Figure B14). TXAR waveforms shown in Figure B17 are from an event on 17 February 1995 close to the location of the 30 March event. The AR(3) moving window display seen in Figure B18 for 17 February event clearly shows the pattern indicative of a commercial explosion. This event was located 319 km from TXAR near Villa Unión, south of Piedras Negras, Mexico, where there are numerous surface coal mines. Figure B19 shows the acoustic signal from this blast as seen on the vertical seismometers at TXAR. The time of arrival is consistent with the acoustic wave travel time from Villa Unión to TXAR and the delays across the array are appropriate to sonic velocities. Figure B20 shows the 3-component, broadband seismo-acoustic signal at TXAR for this event. Without the data from the array, this arrival would almost surely be called "lonesome Lg," an Lg arrival from an event too small for the P wave arrivals to be seen. The acoustical arrival from this explosion was barely detected by the seismic systems at TXAR. Had data from a collocated infrasonic station been available, crosscorrelation of the seismic and acoustic signals would have verified the nature of the arrival.

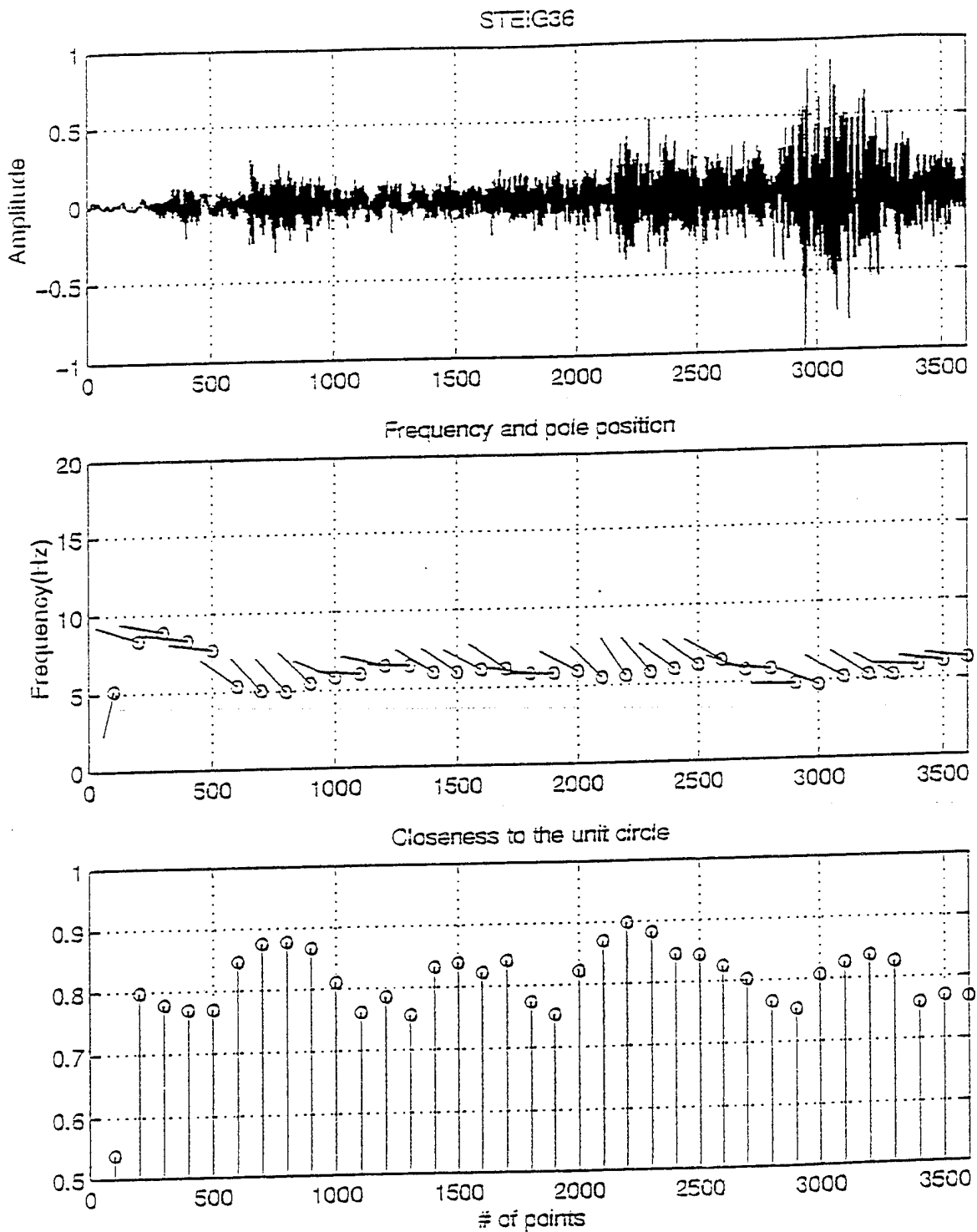


Figure B14. Moving window display showing the AR(3) complex pole position for a Steigen earthquake.



Mar 1995  
20:01:11.671

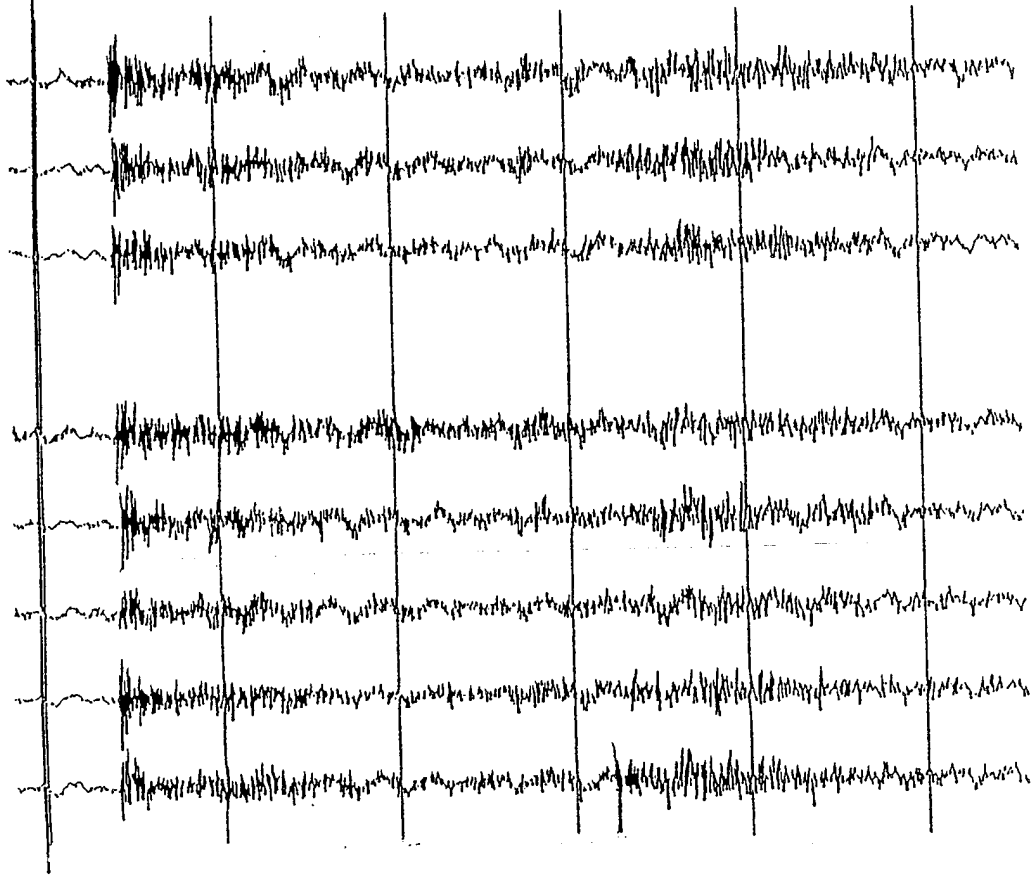


Figure B15. TXAR waveforms for an event of 30 MArch 1995.  $Z=109^\circ$ ,  $D=325$  km,  $mb=2.2$

Mar 1995  
01:14.671

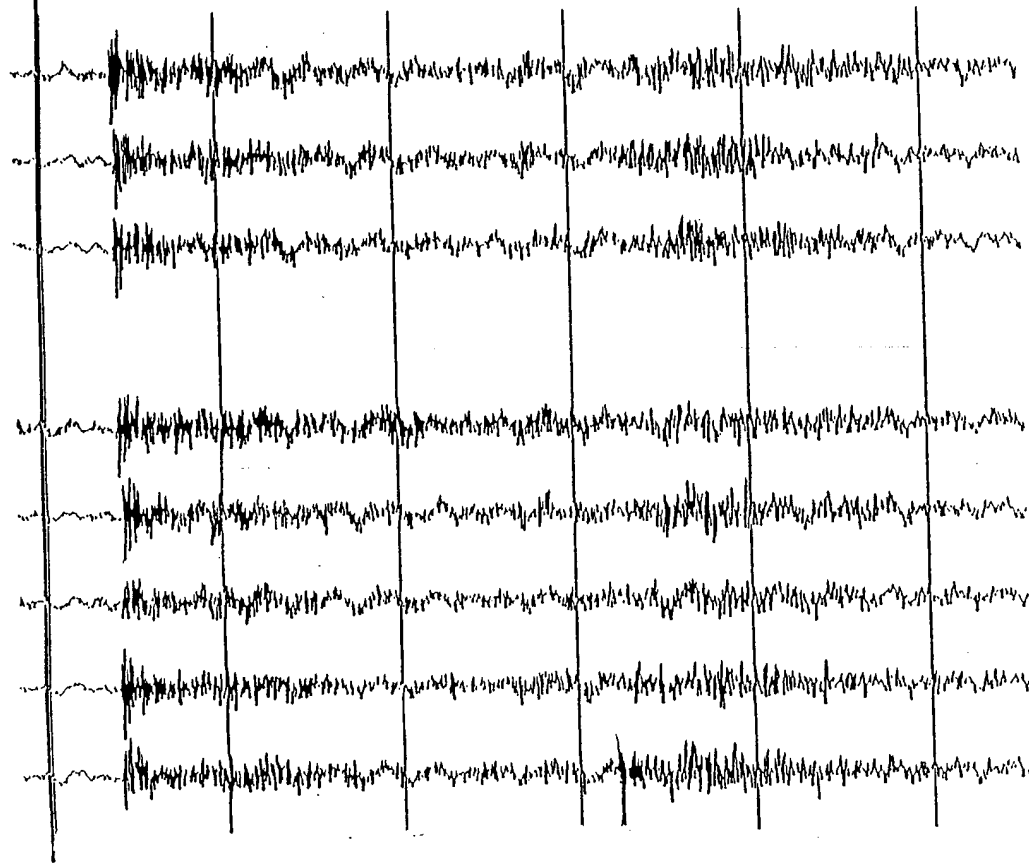


Figure B15. TXAR waveforms for an event of 30 MArch 1995.  $Z=109^\circ$ ,  $D=325$  km,  $mb=2.2$

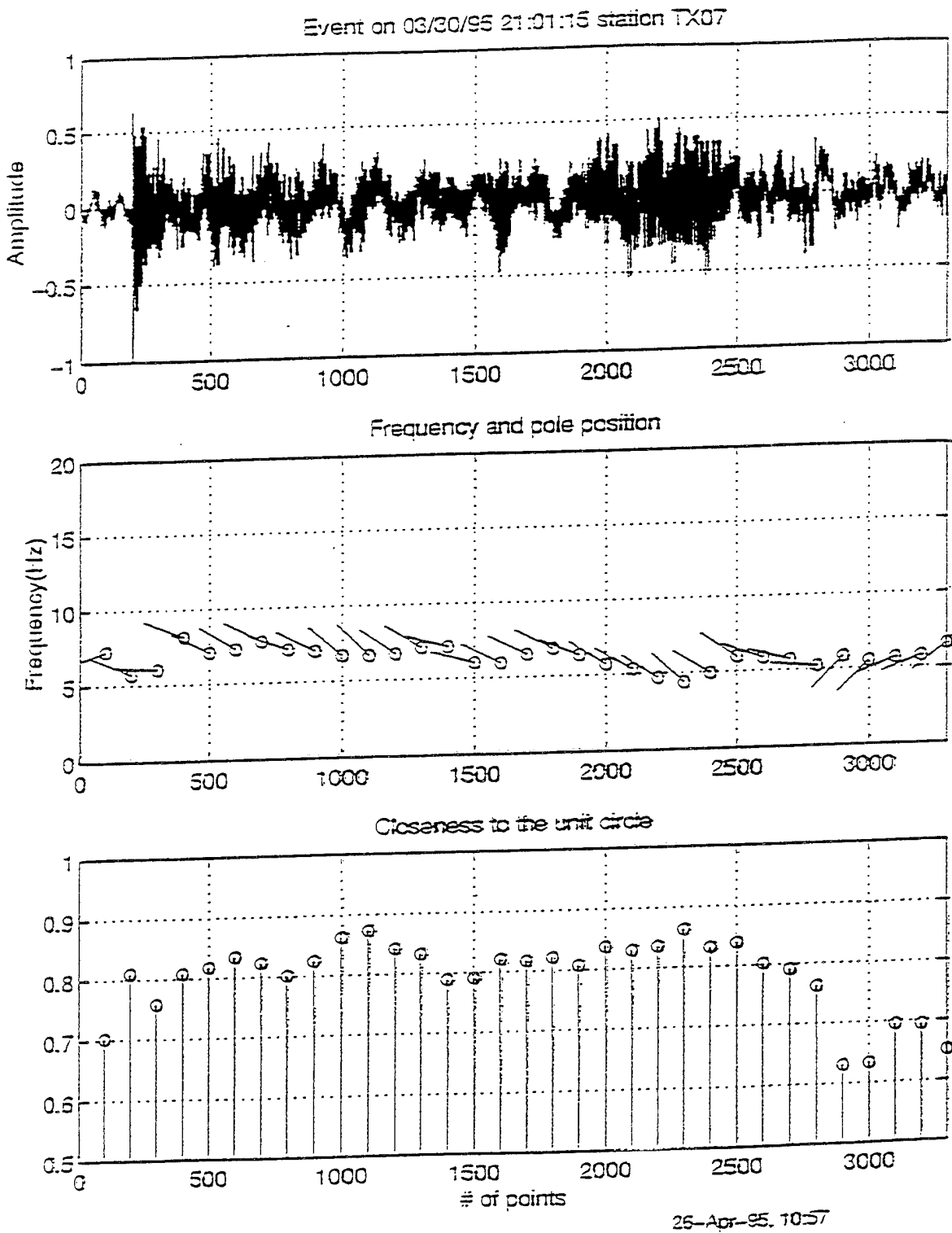


Figure B16. AR(3) moving window display for the event shown in Figure B15. This pattern of pole positions is only seen for explosions.

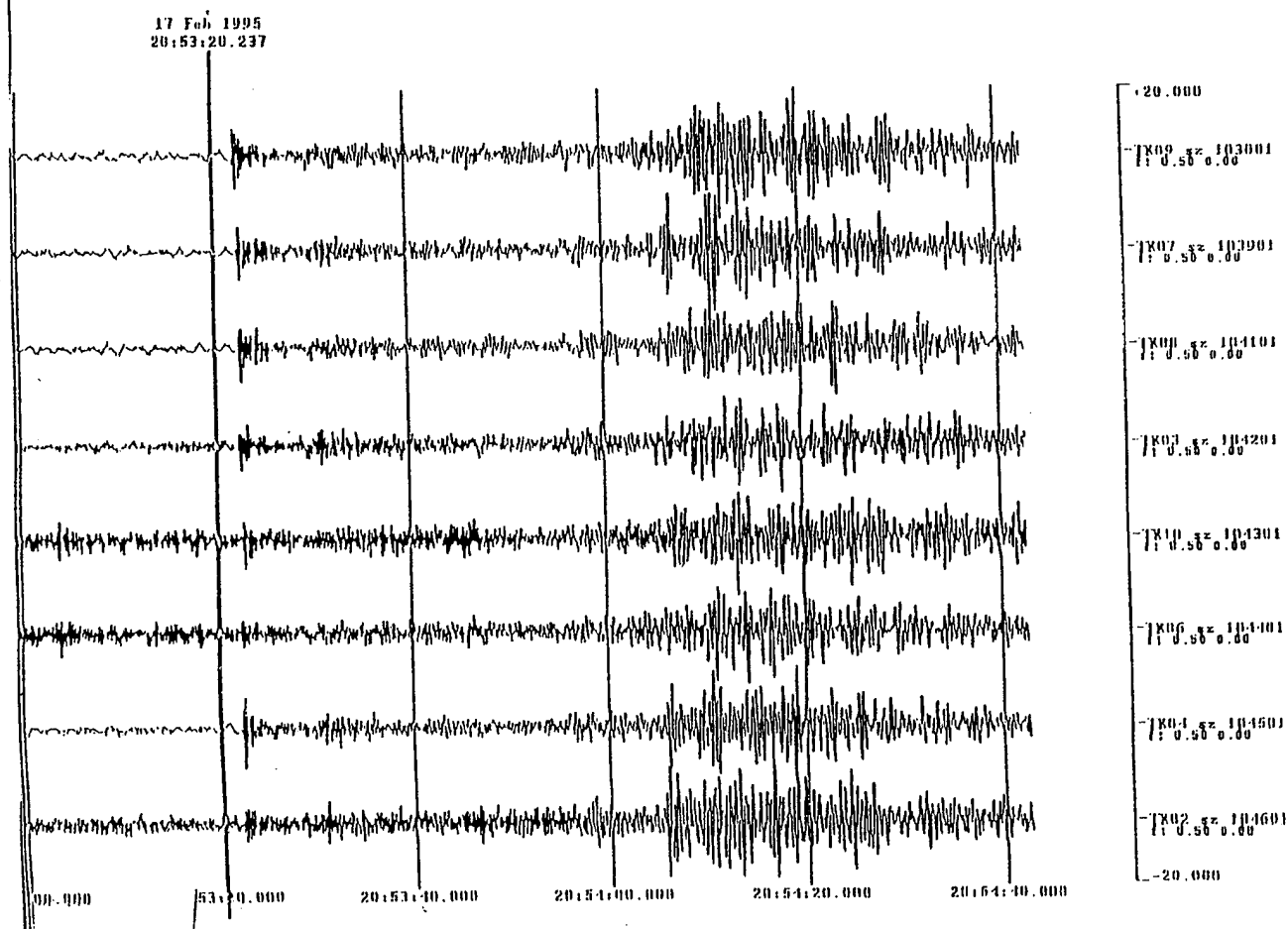


Figure B17. TXAR waveforms for an event on 17 February 1995.  $Z=112^\circ$ ,  
 $D=319$  km,  $mb=1.9$ .

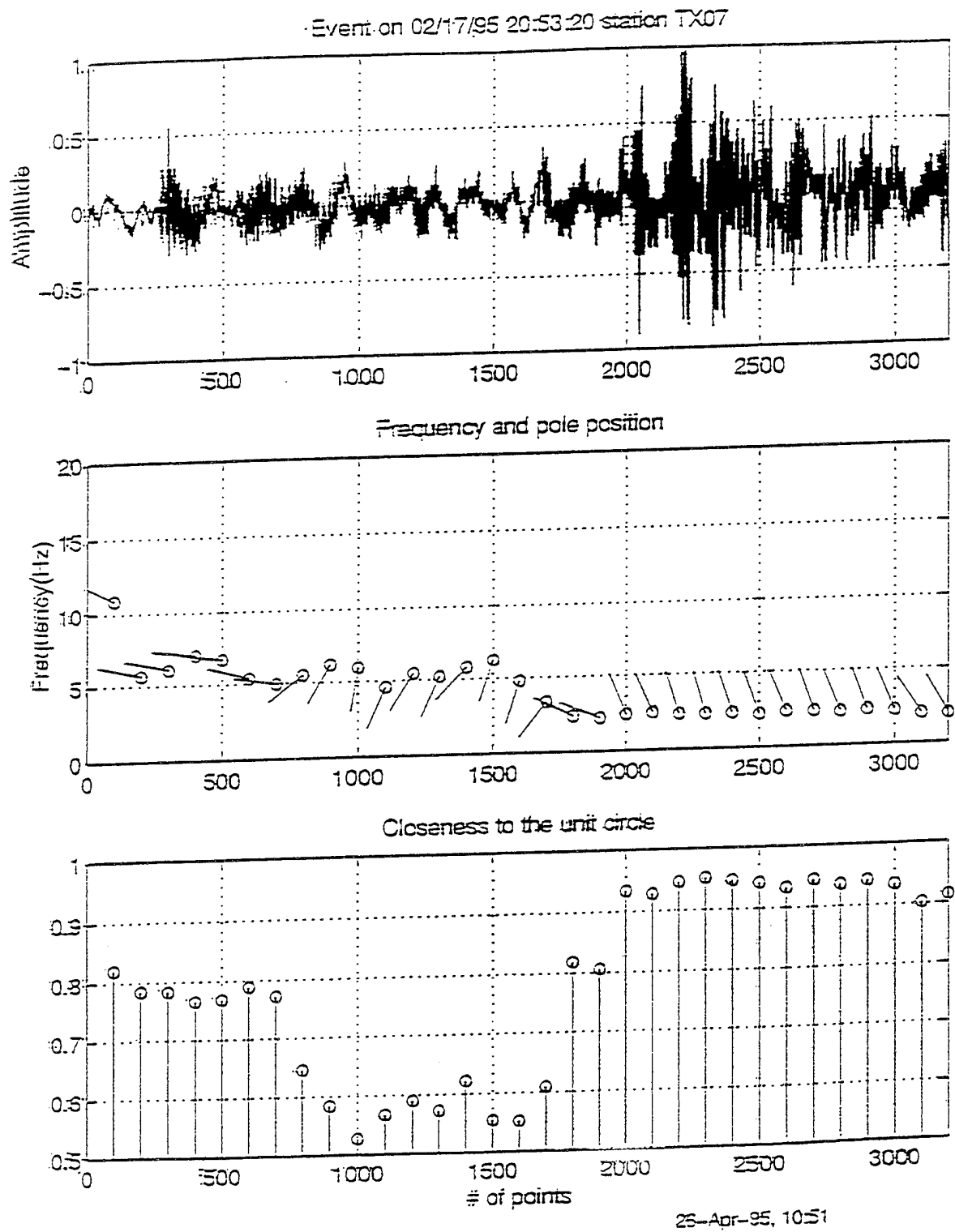


Figure B18. AR(3) moving window display for the event shown in Figure B17. This pattern of pole positions is only seen for explosions.

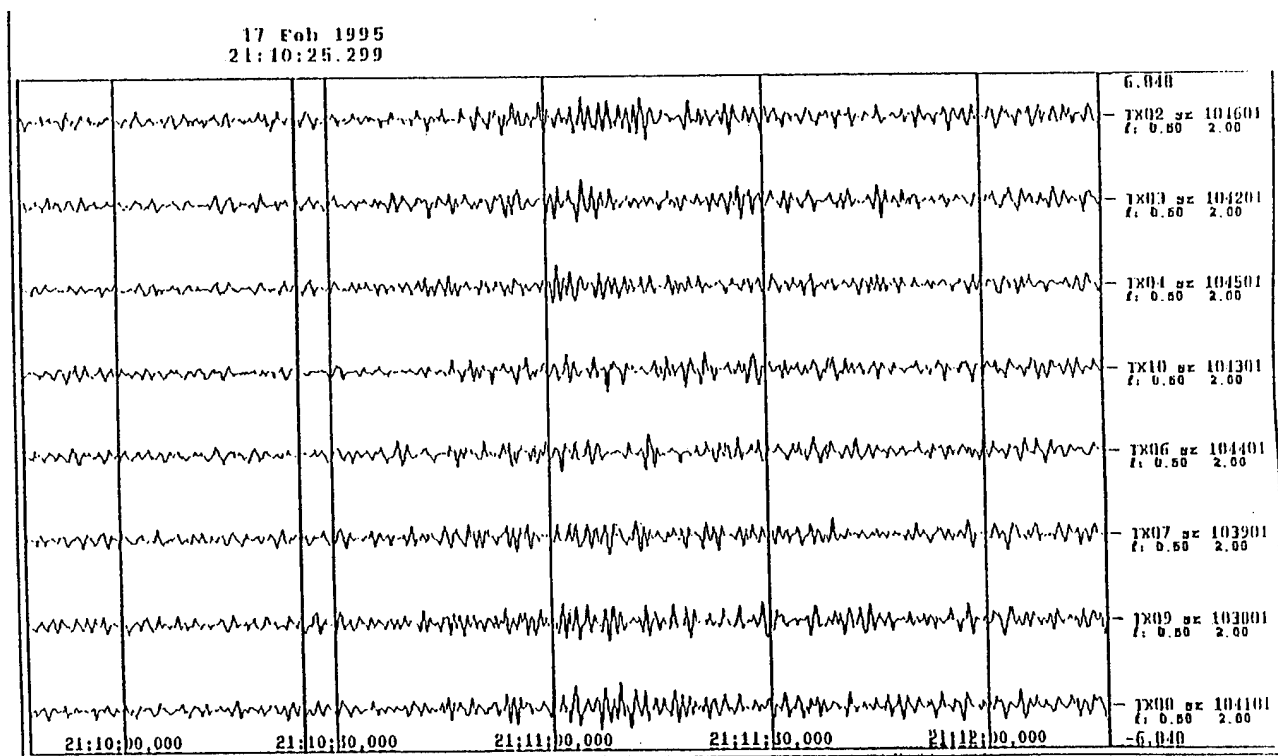


Figure B19. TXAR waveforms at expected time of arrival of acoustic waves from the explosion of 17 February shown in Figures B17 and B18.

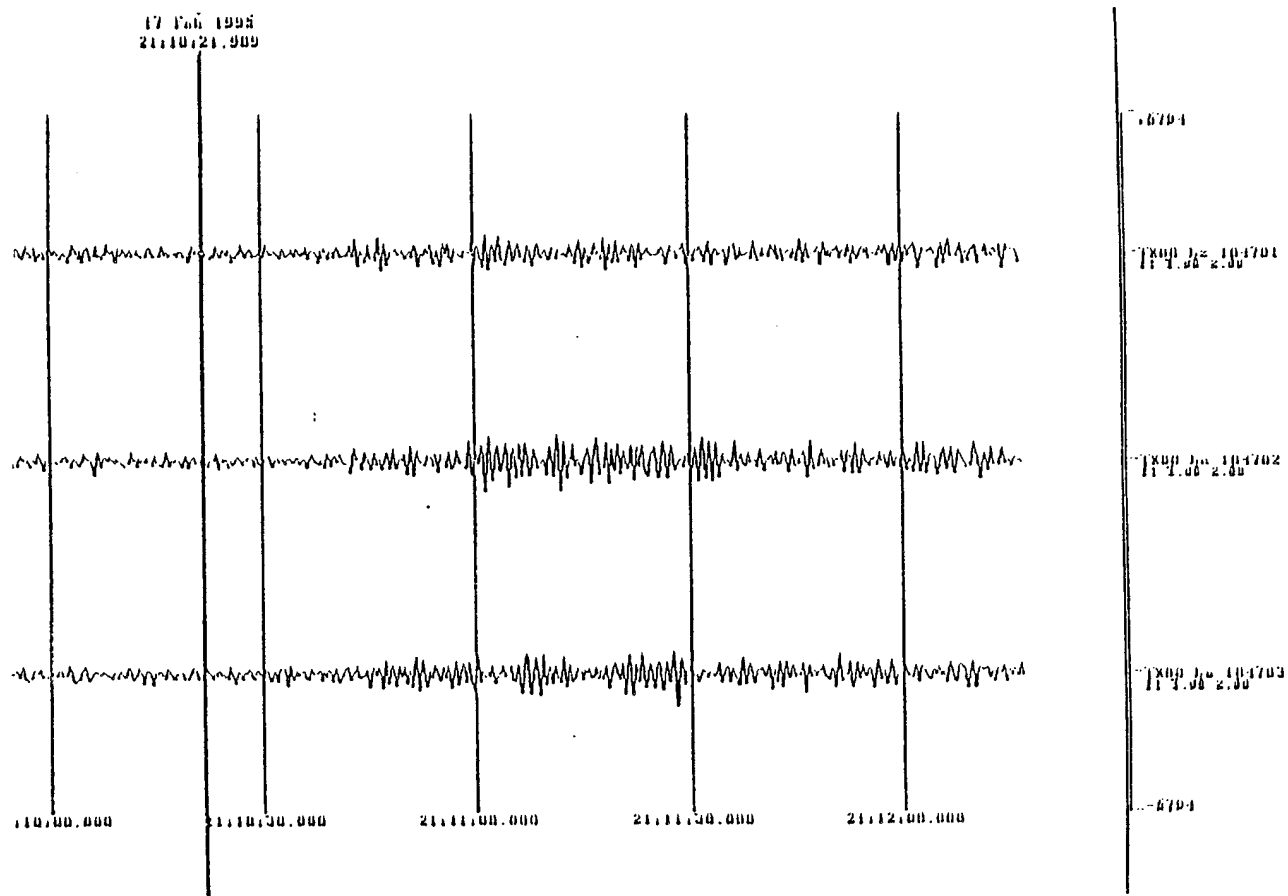


Figure B20. TXAR 3-component, broadband wave forms for the acoustical arrival shown in Figure B19.

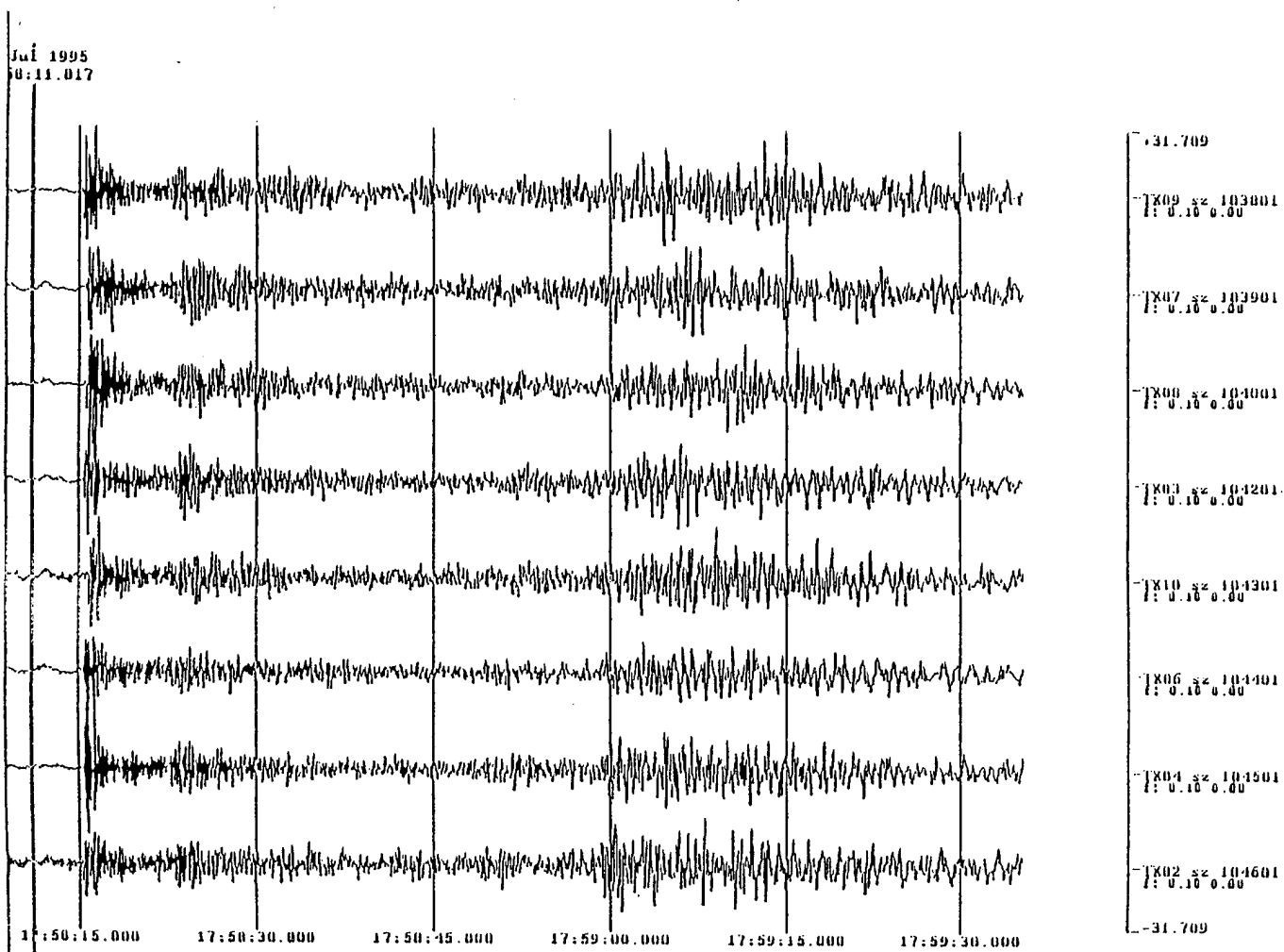


Figure B21 TXAR waveforms for an event on 25 July 1995.  $Z=111^\circ$ ,  $D=308$  km,  
mb=2.5.



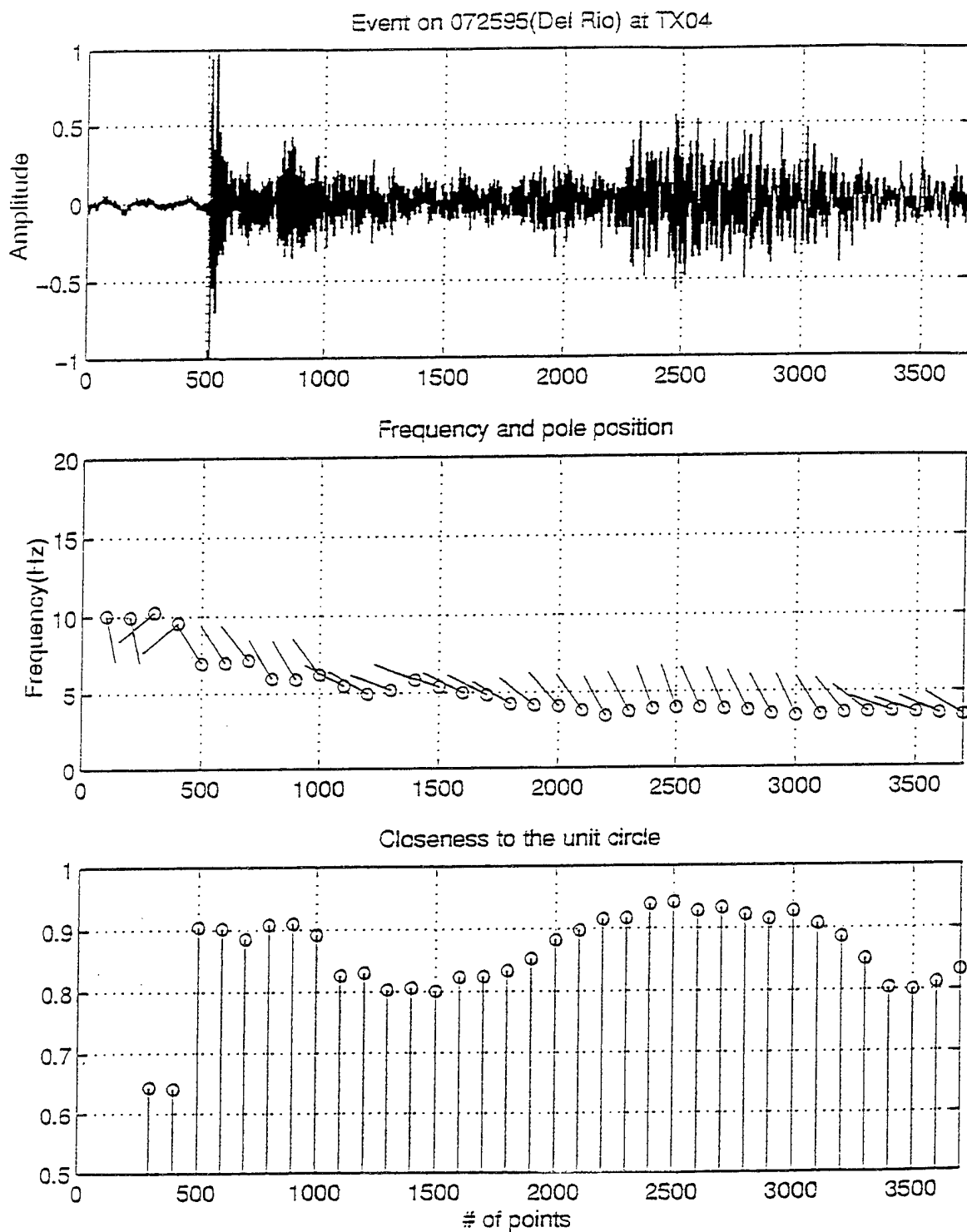


Figure B22. AR(3) moving window display for the event shown in Figure B21. This pattern of pole positions is indicative of an explosion.

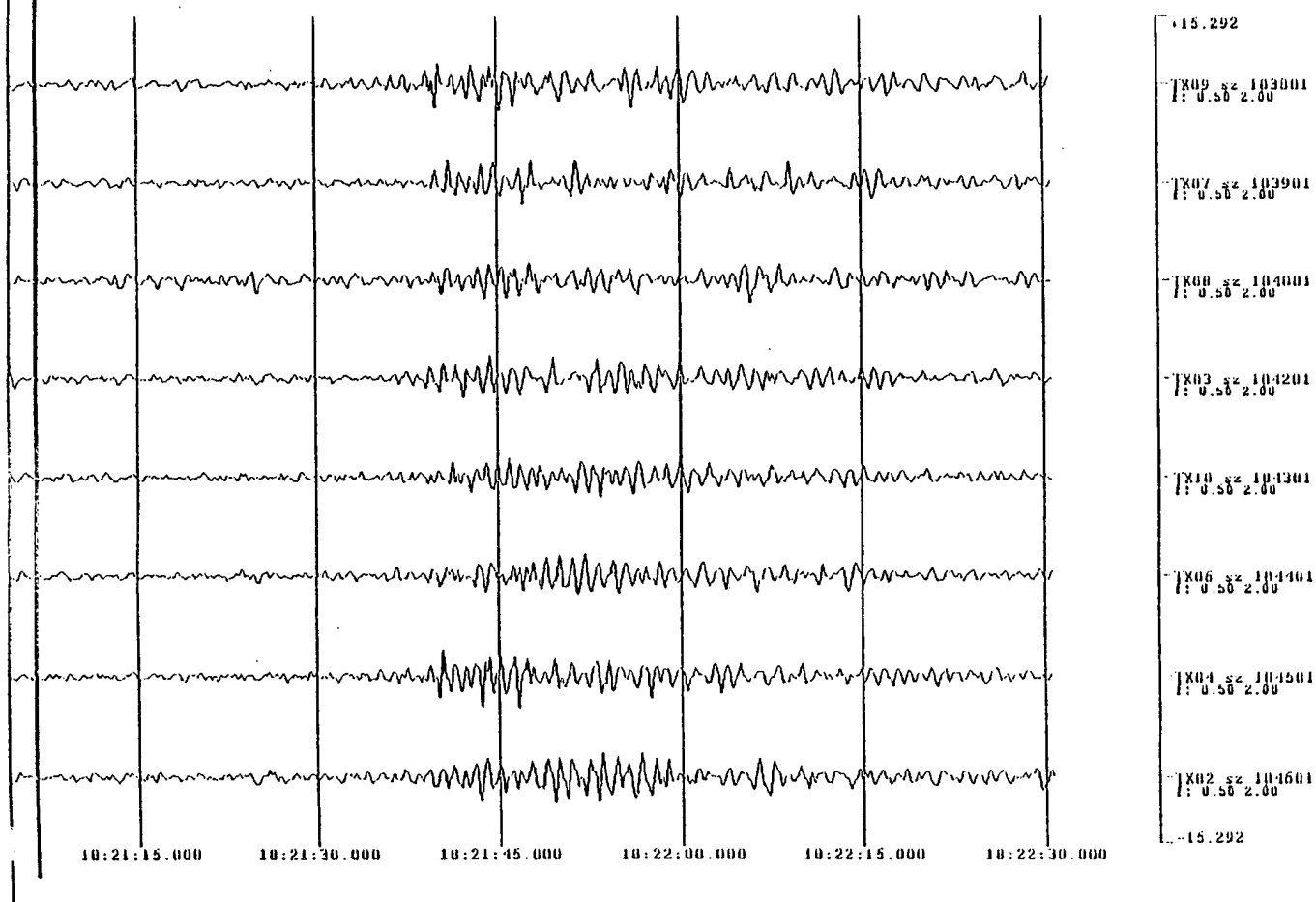
Jul 1995  
11:06.404

Figure B23. TXAR waveforms at the expected time of arrival of acoustic waves from the explosion shown in Figures B21 and B22.

25 Jul 1995  
10:21:03.007

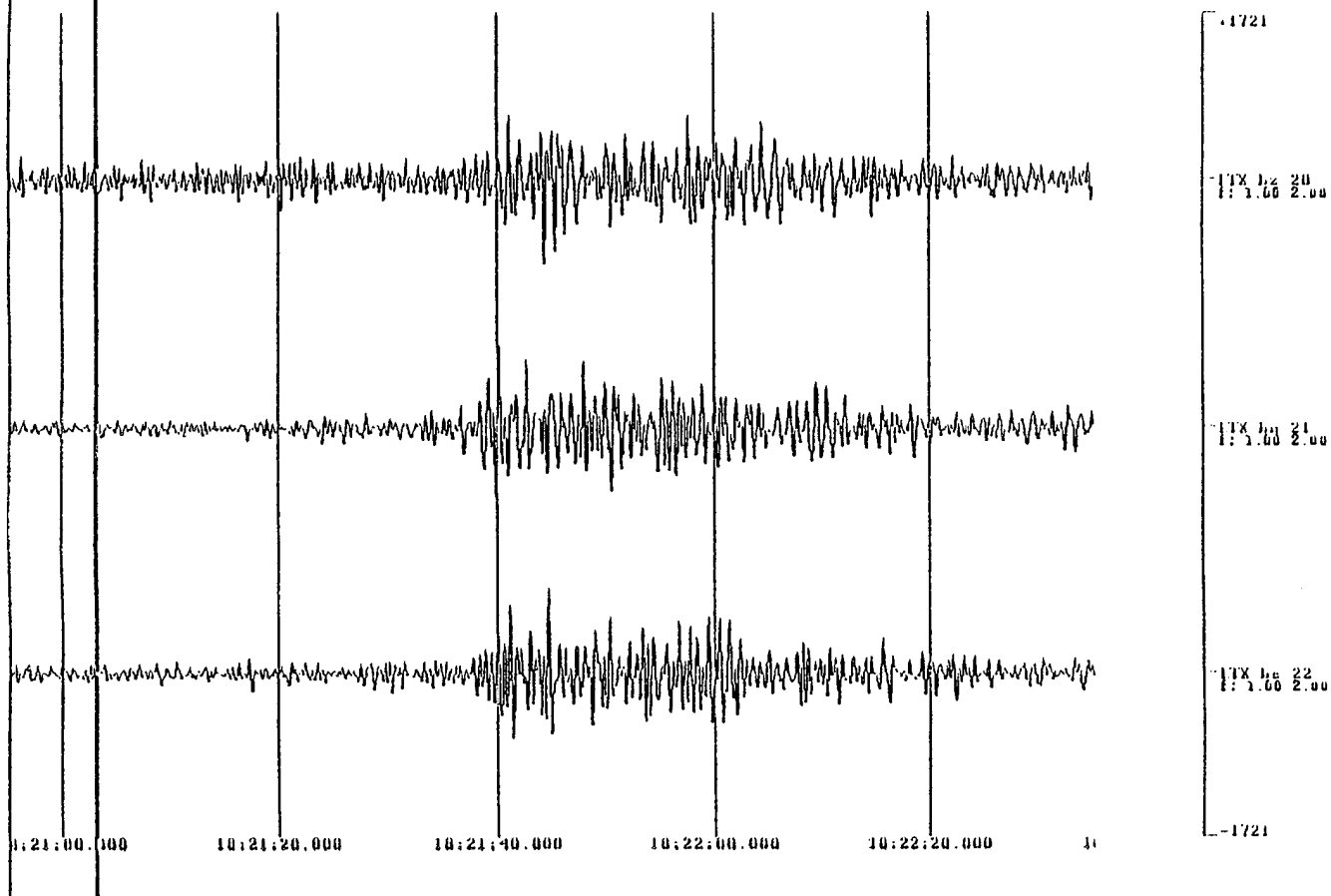


Figure B24 TXAR 3-component broadband waveforms for the acoustic arrival shown in Figure B23.

On 25 July 1995 a larger event from the Villa Unión region ( $m_b$  2.5) was recorded at TXAR (Figure B21). The AR(3) moving window display seen in Figure B22 is indicative of a commercial explosion. Figure B23 and B24 show the seismo-acoustic arrivals from this explosion at the time appropriate for the acoustic arrival, confirming the characterization of this event as a mining blast. Again had data from an acoustic array been available at TXAR, an even stronger conclusion as to the nature of this event could have been reached.

## CONCLUSIONS

Collocation of seismic and infrasonic arrays should provide seismo-acoustic synergy useful for identifying surface explosions. This capability will allow numerous commercial explosions expected to be observed by the IMS to be identified. Current plans call for the installation of a single infrasonic pipe array at TXAR that can be used to lower the detection threshold of surface explosions at regional distances. A four-station infrasonic array will be installed at Pinedale, Wyoming (PDAR) by Dr. R. Whittaker from Los Alamos National Laboratory. This installation will serve as a prototype for the collocated seismic-infrasonic stations called for in CD/NTB/WP.225. It is anticipated that identification of explosions seen at TXAR and PDAR will be significantly aided by the synergistic use of seismic and acoustic data.

## REFERENCES

- Donn, W.L., H. Dalins, V. McCarty, M. Ewing and G. Kaschak (1971) Air-Coupled Seismic Waves at Long Range from Apollo Launchings, *Geophys. Jour. R. Astron. Soc.*, **26**, 161-171.
- McDonald, John A., E.J. Douze, and Eugene Herrin (1971) The structure of atmospheric turbulence and its application to the design of pipe array, *Geophys. Jour. R. Astron. Soc.*, **26**, 99-109.
- Pierce, Allen D., and Joe W. Posey (1971) Theory of the excitation and propagation of Lamb's atmospheric edge mode from nuclear explosions, *Geophys. Jour. R. Astron. Soc.*, **26**, 34-368

Sorrells, Gordon G. (1971) A preliminary investigation into the relationship between long-period noise and local fluctuations in the atmospheric pressure field, *Geophy. Jour. R. Astron. Soc.*, **26**, 71-82.

Sorrells, G.G. and T.T. Goforth (1973) Low-frequency earth motion generated by slowly propagating partially organized pressure fields, *Bull. Seis. Soc. A.*, **63**, 1583-1601.

#### ACKNOWLEDGEMENTS

Ileana Tibuleac, Chris Hayward, Jessie Bonner, G.G. Sorrells, Paul Golden and Valeriu Burlacu all contributed to this study. The work was supported by the Defense Advanced Research Projects Agency under Phillips Laboratory Contract Number F19628-93-C-0057 and Midwest Environmental Consultants, Inc., under a contract from Phillips Laboratory.

## APPENDIX C -- SEISMO-ACOUSTIC METHODS FOR THE DETECTION OF ACOUSTIC WAVES

Gordon G. Sorrells

### EXECUTIVE SUMMARY

The detection of an acoustic signal and its association with a given seismic event provides a simple method for the unambiguous identification of uncontained explosions. The key to the successful utilization of this approach is the consistent detection of the associated acoustic signal. The bandwidth of most acoustic signals that may be associated with the detected seismic signals of low yield uncontained explosions is expected to be 0.5 to 5 hertz and their pressure amplitudes in this bandwidth are likely to be relatively small outside the source region. Therefore, the best opportunities for the successful practical application of the method are currently believed to be at near regional to regional distances and are likely to be realized only with acoustic monitoring systems that provide a low detection threshold in the bandwidth of interest. While acoustic signals are conventionally detected through the use of infrasonic monitoring systems, there are valid reasons to believe that short period vertical seismograph systems may also be used for this purpose and may provide lower detection thresholds during adverse surface wind conditions. Therefore the near term objectives of the seismo-acoustics research task are to analyze simultaneously acquired seismic and infrasonic data in order to:

1. Experimentally determine the relative sensitivity of the infrasonic and seismic detection thresholds for short period acoustic signals to variations in local wind conditions.

2. Investigate the possibility that short period acoustic waves generated by quarry blasts and other types of uncontained explosions are detectable at near regional to regional distances, through the use of infrasonic systems, seismic systems, or some combination of the outputs of both systems.

Progress made during this reporting period towards the fulfillment of these objectives is summarized in the following paragraphs.

The capability to calculate theoretical seismo-acoustic transfer functions has been significantly enhanced. The results of trial calculations with the upgraded code predict that acoustic waves with pressure amplitudes of about a  $\mu$ bar in the 1-10 hertz bandwidth should be produce detectable seismo-acoustic signals at seismically quiet sites.

Preliminary estimates of infrasonic and seismo-acoustic background noise levels indicates that the infrasonic detection threshold is extremely sensitive to local surface wind conditions. In contrast, the seismo-acoustic detection threshold appears to be virtually independent of these same conditions at frequencies less than about 6 hertz. While the infrasonic system enjoys a 10-12 db detection threshold advantage over a vertical seismograph in the 0.5-5.0 hertz bandwidth during calm periods, this advantage vanishes in the 1.0-5.0 hertz bandwidth and falls to the seismograph system during windy periods. These results suggest that a stable, relatively low threshold can be maintained regardless of surface wind conditions by selectively using either or both systems for acoustic signal detection.

A code which estimates the zero lag correlation coefficient for two inputs in a moving window has been written tested, and calibrated for one configuration. The initial application of this code to selected records of the output of the pressure transducer and the TX01 short period vertical seismograph have yielded very promising results. Three seismo-acoustic detections were made by the code, two of which were clearly associated with near regional seismic events detected at TXAR. The association of both seismic and seismo-acoustic detections for a single event strongly implies an explosive origin. Thus the preliminary results of this experiment suggests that seismo-acoustic signal detection and its subsequent association with a seismic event may prove to be a useful method for the identification of low yield explosive sources.

## 1. Background

There is a continuing requirement to develop improved methods for the positive identification of the seismic signals generated by low yield explosions. In those cases where the explosive source is uncontained, such as a quarry blast or a low altitude atmospheric explosion, the observed seismic signal will be followed by an associated acoustic signal. Thus, in principle, the detection of an acoustic signal and its association with a given seismic event provides a simple method for the unambiguous identification of uncontained explosions. The key to the successful utilization of this approach is the consistent detection of the associated acoustic signal. The bandwidth of most acoustic signals that may be associated with the detected seismic signals of low yield uncontained explosions is expected to be 0.5 to 5 hertz and their pressure amplitudes in this bandwidth are likely to be relatively small outside the source region. Therefore, the best opportunities for the successful practical application of the method are currently believed to be at near regional to regional distances and are likely to be realized only with acoustic monitoring systems that provide a low detection threshold in the bandwidth of interest.

Acoustic signals are conventionally detected through the use of infrasonic monitoring systems. During calm periods, the detection thresholds of these systems are typically of the order of a  $\mu$ bar or less at frequencies greater than 0.5 hertz. However, since the pressure fluctuations caused by local surface winds tend to scale as the cube of the mean wind speed (Bedard et al, 1992) windy period infrasonic detection thresholds can exceed 10  $\mu$ bars in this bandwidth. Thus, there is a need to investigate alternative acoustic signal detection systems which are less sensitive to wind noise. In this regard, it has been shown that the passage of an acoustic signal locally generates earth motion which may be detectable on the outputs of short period vertical seismographs at frequencies greater than about 0.5 to 1.0 hertz. This earth motion will be referred to as the "seismo-acoustic" signal in the following discussion and in future reports. Since short period vertical seismographs are usually deployed at shallow depths in order to minimize wind noise, it is possible that the seismo-acoustic detection threshold may be significantly lower than the infrasonic detection threshold during periods of adverse wind



conditions. Thus, through the combined use of infrasonic and seismic monitoring systems it may be possible to maintain a relatively low acoustic signal detection threshold in the bandwidth of interest during both calm and windy periods.

The goals of this research task are to investigate this possibility and to critically assess the use of associated acoustic and/or seismo-acoustic signals to identify the seismic signals generated by uncontained explosive sources. The near term technical objectives of this research task are summarized below.

## 2.Objectives

The near term objectives of the seismo-acoustics research task are to analyze simultaneously acquired seismic and infrasonic data in order to:

2.1. Experimentally determine the relative sensitivity of the infrasonic and seismic detection thresholds for short period acoustic signals to variations in local wind conditions at TXAR.

2.2. Investigate the possibility that short period acoustic waves generated by quarry blasts and other types of uncontained explosions are detectable at near regional to regional distances, through the use of infrasonic systems, seismic systems, or some combination of the outputs of both systems.

Progress towards the fulfillment of these objectives is summarized in the following paragraphs.

## 3. Results to date

**3.1 Seismo-Acoustic Transfer Functions** It follows from Sorrells and Goforth(1973) that if  $P(w)$  is the spectrum of a plane acoustic wave which propagates with a horizontal phase velocity,  $c$ , then the  $j$ th component of the velocity spectrum of the seismo-acoustic signal,  $U_{j,t}$ , is given by

$$U_{j,t}(w,z;c) = iwG_j(w/c,z)P(w) \quad j=1,3 \quad (1)$$

where  $G_j$  is the  $j$ th component of the seismo-acoustic displacement transfer function. During this reporting period, the existing MATLAB code for the calculation of seismo-acoustic transfer functions was upgraded to calculate either velocity or displacement transfer functions for selectable bandwidths, depths, acoustic phase velocities, and multi-layered earth models. Examples of the outputs of the upgraded code are shown in Figure C1.

The two curves shown in Figure C1a are the moduli of the vertical velocity seismo-acoustic transfer functions for acoustic signals with horizontal phase velocities of 0.33 and 0.66 km/sec., calculated for a depth of 0.007 km. at TXAR. The earth model used for the calculations is shown in Figure C1b. It is based upon results obtained by Sandige-Bodoh (1989) and approximates the shallow seismic velocity and density structure beneath the TXAR seismic array. The data shown in Figure D1a illustrate several important features of the vertical velocity transfer functions in "hard rock" geologic environments. First of all, notice that for frequencies,  $f$ , such that

$$f \ll c/2pz \quad (2)$$

the transfer functions are approximately flat and scale linearly with  $c$ . Thus, other factors being equal, the seismo-acoustic detection threshold at frequencies less than a few hertz, is expected to increase approximately linearly with the horizontal phase velocity of the impinging acoustic wave. It should also be observed that at frequencies which fail to satisfy the inequality above the transfer functions will, as a general rule, attenuate exponentially as a function of increasing frequency. It has been shown by Sorrells (1971) that the attenuation rate is virtually independent of the elastic properties of the medium and functionally dependent only upon the magnitude of the ratio of the observation depth to the seismo-acoustic wavelength. Since seismo-acoustic wavelengths are generally less than 100 meters at frequencies greater than a few hertz, substantial signal attenuation will be encountered at moderate to high frequencies if the sensor deployment depth exceeds a few tens of meters. This phenomenon must be kept in mind if short period vertical seismographs are to be used to detect both seismic and seismo-acoustic signals. Finally, it is important to notice that the magnitude of the 0.33 km/sec. transfer function is greater than about 2 nm/sec/ $\mu$ bar at

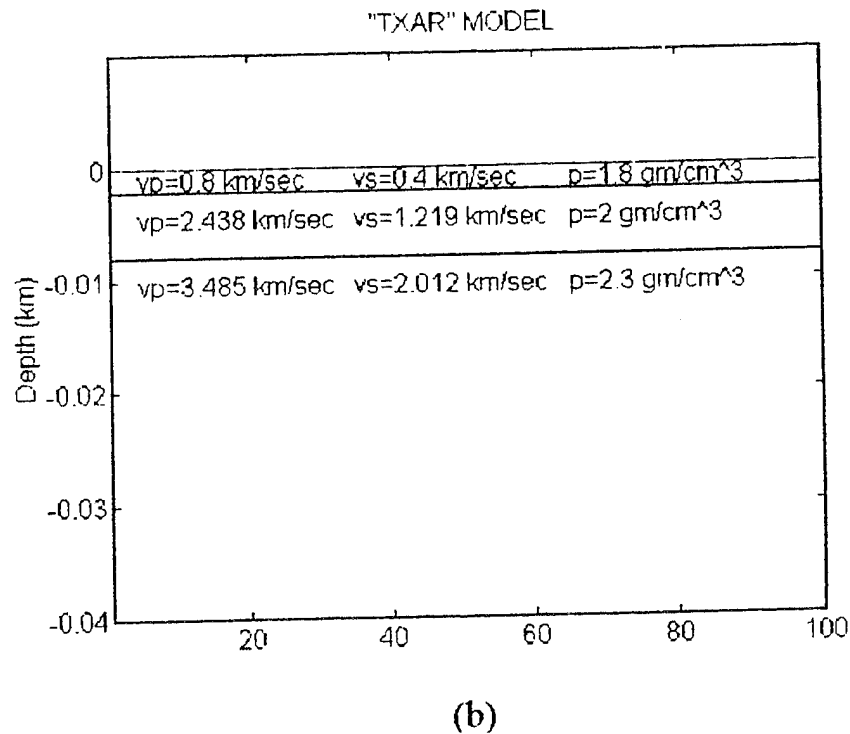
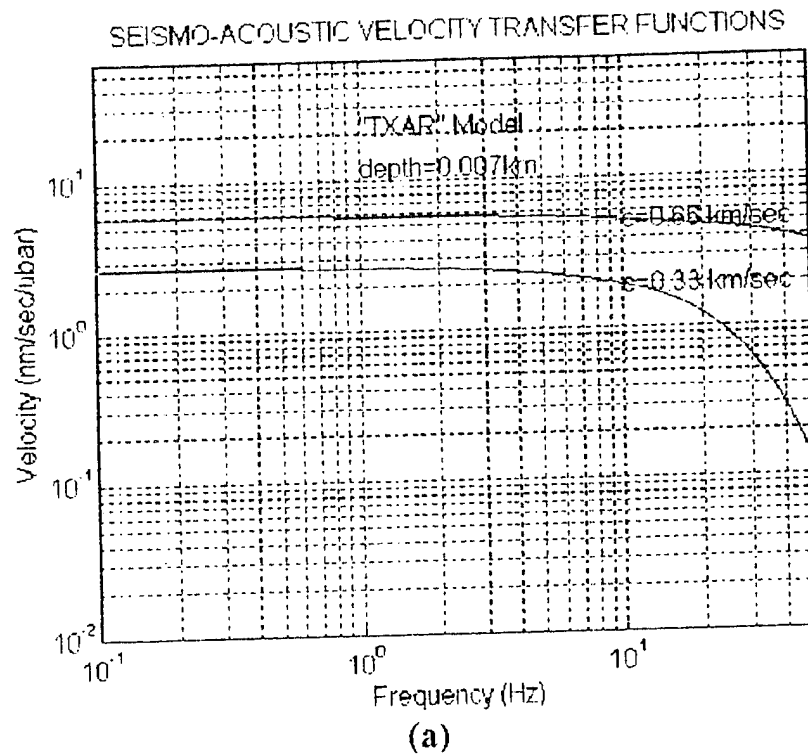


Figure C1a. Comparison of the moduli of vertical velocity seismo-acoustic transfer functions for acoustic-wave velocities of 0.33 and 0.66 km/sec and a depth of 0.007 km at TXAR. Figure C1b. The shallow seismic velocity and density structure at TXAR (from Sandidge-Bodoh, 1989).

frequencies less than 10 hertz. Since the background noise levels at seismically quiet sites at frequencies greater than 1 hertz are typically less than few nm/sec, this result implies that the seismo-acoustic detection threshold at quiet sites can be of the order of a  $\mu$ bar or less in the 1-10 hertz bandwidth if the sensors are deployed at depths less than a few 10's of meters. This phenomenon is examined in greater detail with specific reference to TXAR in the following paragraphs.

### **3.2 Comparison of Acoustic and Seismo-Acoustic Background Noise Levels at TXAR**

An infrasonic monitoring system was fabricated and deployed at TXAR in late October 1995. The system consists of a differential pressure transducer coupled to a noise reducing pipe array. According to manufacturer specifications, the response of the differential pressure transducer is flat from dc to 200 hertz. It is coupled to a pipe array whose geometry consists of 6 symmetrically deployed legs, each 50 feet in length, which extend radially from a central collection point. In order to improve the opportunities for the detection and identification of short period acoustic and seismo-acoustic signals, the central collection point is located within 50 feet of the borehole containing the TX01 short period vertical seismograph system. The output of the infrasonic monitoring system is sampled at the rate of 40 samples per second and is simultaneously transmitted with the seismic data acquired at TXAR to SMU and CSS for storage and subsequent processing and analysis. During this reporting period studies were undertaken to investigate the differences in infrasonic and seismo-acoustic background noise levels during various sets of local wind conditions at TXAR. The preliminary results of these studies are summarized in the following paragraphs.

Spectral estimates of the infrasonic noise power representative of locally calm and windy atmospheric conditions are compared in Figure D2a. These data have been corrected for the system response of the pressure transducer and have been plotted in db relative to  $1 \mu\text{bar}^2/\text{hertz}$ . Notice that the change from locally calm to locally windy atmospheric conditions results in a wide band increase in the infrasonic noise power of some 20 to 30 dB. In the 0.5-5.0 hertz bandwidth the change from calm to windy conditions results in an increase

the rms background noise levels from 0.8  $\mu$ bars to 13.3  $\mu$ bars. It may be inferred from these results that the short period infrasonic detection threshold at TXAR will be seriously degraded during periods of locally moderate to high surface wind speeds.

Spectral estimates of the equivalent seismo-acoustic noise power observed during the identical atmospheric conditions referred to earlier are compared in Figure C2b. For the purposes of this report the equivalent seismo-acoustic noise power is defined to be the estimated vertical seismic noise power corrected for system response and divided by the squared modulus of the vertical velocity seismo-acoustic transfer function. This definition is directly analogous to the definition of system noise viewed at the output of a transducer. Insofar as acoustic wave detection is concerned, seismic earth noise is the "system noise" of a seismo-acoustic transducer whose properties are determined by the local seismic velocity and density structure as well as the horizontal phase velocity of the impinging acoustic wave. For the spectral estimates shown in Figure C2b it has been assumed that the 0.33 km/sec transfer function shown in Figure C1a correctly describes the local seismo-acoustic response at TXAR. Observe that the change from locally calm to windy conditions has little significant impact on the seismo-acoustic noise power at frequencies less than about 6 hertz.. In particular, it was found that in the 0.5-5.0 bandwidth, the rms seismo-acoustic background noise was 2.9  $\mu$ bars and 3.0  $\mu$ bars during the calm and windy periods, respectively. This difference is significantly less than the expected estimation errors. Therefore, it may be inferred from these results that the short period seismo-acoustic detection threshold will be virtually independent of the atmospheric turbulence associated with the local surface winds.

The rms infrasonic and seismo-acoustic noise levels observed during these initial studies are summarized and compared to similar measurements in the 1.0-5.0 bandwidth in Table C1 below. The preliminary results summarized in this table suggests that a relatively low stable acoustic detection threshold may be sustained at TXAR by using infrasonic observations in the 0.5-5.0 hertz bandwidth during calm periods and seismo-acoustic observations in the 1-5.0 hertz bandwidth during windy period.

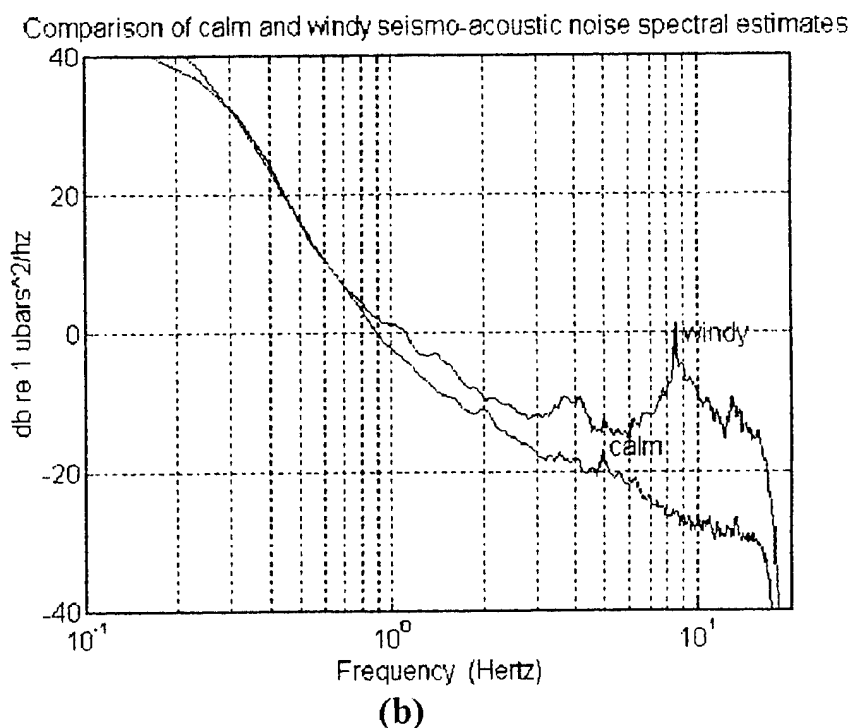
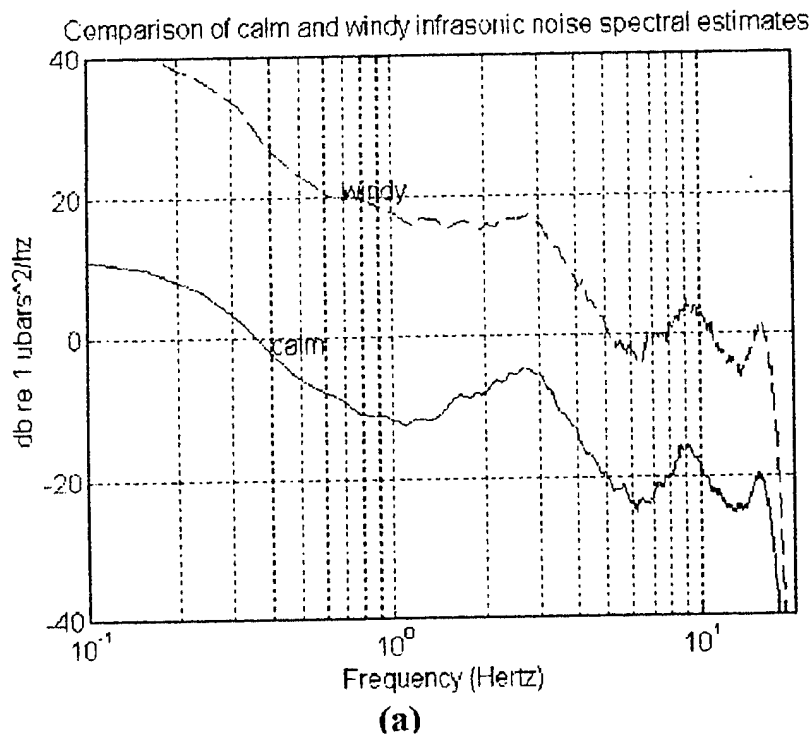


Figure C2a. Comparison of spectral estimates of the infrasonic noise power observed during calm and windy conditions at TXAR. Figure C2b. Comparison of spectral estimates of the equivalent seismo-acoustic noise power observed during identical conditions referred to in figure C2a.

Table C1. Comparison of the rms infrasonic and seismo-acoustic background noise levels in the 0.5-5.0 Hz and 1.0-5.0 bandwidths at TXAR. Units are in  $\mu$ bars

	0.5-5.0 Bandwidth		1.0-5.0 Bandwidth	
	calm	windy	calm	windy
Infrasonic Noise	0.8	13.3	0.8	10.7
Seismo-Acoustic Noise	2.9	3.0	0.6	0.9

### 3.3 Seismo-acoustic Identification of Quarry and Mine Blasts

Since infrasonic and seismic noise in the short period signal bandwidth are derived from mutually independent sources, observations of the two fields should be expected to be statistically incoherent. This expectation is confirmed by the results shown in Figure C3, where the estimated coherence between the outputs of the pressure transducer and short period vertical seismograph at TX01 are plotted as a function of frequency in the 0.1-10 hertz bandwidth.

The data used for these calculations were acquired in the calm period referenced above. Similar results were obtained for observations made during the windy period referenced above. Thus, it may be concluded that the outputs of the pressure transducer and TX01 vertical seismograph will be uncorrelated in the absence of an acoustic signal. On the other hand, it follows from equation 1 that these outputs should be correlated in the presence of an acoustic signal. Since the two monitoring systems are horizontally separated by less than 50 feet, estimation of the zero lag correlation coefficient should provide the data necessary to detect the presence or absence of an acoustic signal. During this reporting period a MATLAB code was written to estimate the zero lag correlation coefficient between two input data sequences. In its current configuration, the code accepts data records of selectable lengths from the outputs of the pressure transducer and the TX01 short period vertical seismograph. The inputs are filtered to pass data in the 2-8 hertz bandwidth, then estimates of the normalized zero lag correlation coefficient are made in a 5 second window which is sequentially shifted forward in one second intervals. The output of

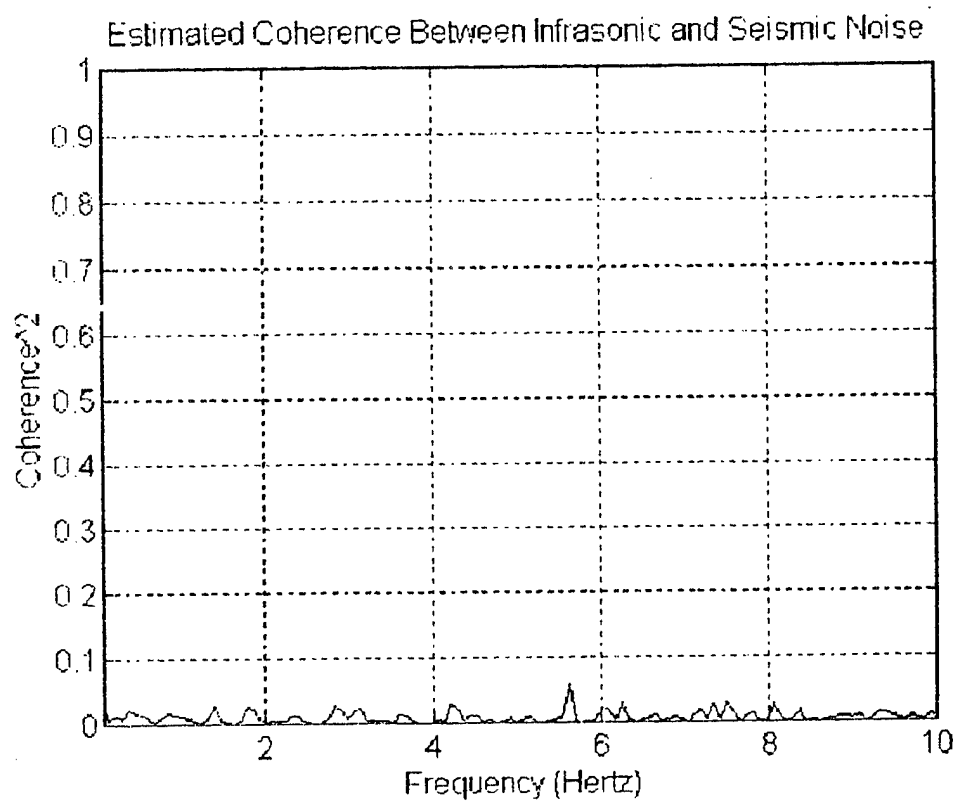


Figure C3. Estimated coherence between observations of infrasonic and seismic noise during locally calm atmospheric conditions at TXAR.



the code is a time series whose amplitudes are found in the interval [-1,1] and whose sample points are separated by 1 second in input record time.

The provisional criteria used for the identification of an acoustic signal using this particular configuration are that:

1. The sign of the correlation coefficient must be negative.
2. The magnitude of the correlation coefficient must be greater than 0.35

The first criterion simply reflects the fact that a local increase in atmospheric pressure applied at the surface of the earth produces negative vertical earth movements at a point located beneath the surface. The second criterion was determined experimentally by running the correlator code continually on two randomly correlated time series for a simulated 24 hour period. The results of this test indicated that by setting the correlator at -0.35 the probability of a false alarm will be less than 0.001.

In order to associate an acoustic detection with a seismic signal, one additional constraint is imposed: the apparent group velocity,  $v_g$ , when referenced to the estimated origin time and distance of the seismic event must satisfy the condition that;

$$0.24 \text{ km/sec} < v_g < 0.36 \text{ km/sec} \quad (3)$$

Initial tests of the correlator code have yielded promising results. In its first application to real data on day 1995\_311 two of three acoustic event detections made by the code were associated with two low magnitude seismic events located about 140-150 kilometers south of TXAR. An example of one of these signals is shown in the upper panel of Figure C4. The output of the correlator code for the same time period is plotted in the lower panel. The solid horizontal line in the lower panel identifies the acoustic detection threshold for the correlator code. Notice that the correlator code output crosses the detection threshold about 7 minutes after the arrival of the seismic signal shown in the upper panel. The value of the correlation coefficient at its

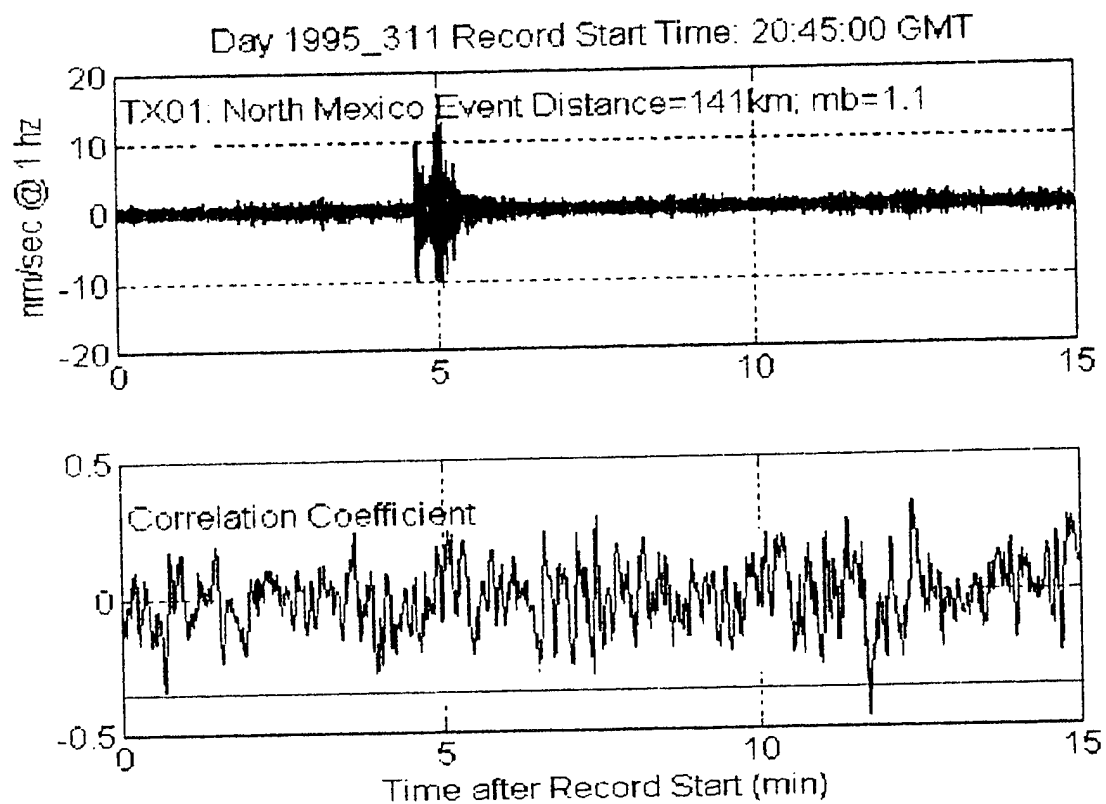


Figure C4. An example of the seismo-acoustic correlator code to identify the seismic signals generated by uncontained explosions. Upper Panel: Short-period vertical seismogram of a near regional seismic event detected at TXAR. Lower Panel: Output of the seismo-acoustic correlator code for the same time interval (see text for additional detail).

minimum point beyond the detection threshold is -0.46 which clearly satisfies the criteria for an acoustic signal detection. The group velocity referenced to the estimated origin time and distance of the seismic event shown in the upper panel was found to be 0.30 km./sec. It is concluded, therefore, that the seismic and acoustic signals are associated and the source of both is a low yield uncontained explosion.

#### 4.0 Summary of Results and Conclusions

The Seismo-Acoustic research task has yielded the following results and inferences during the current reporting period.

1. The capability to calculate theoretical transfer functions has been significantly enhanced. The results of trial calculations with the upgraded code predict that acoustic waves with pressure amplitudes of about a  $\mu$ bar in the 1-10 hertz bandwidth should produce detectable seismo-acoustic signals at seismically quiet sites.

2. Preliminary estimates of infrasonic and seismo-acoustic background noise levels indicates that the infrasonic detection threshold is extremely sensitive to local surface wind conditions. In contrast, the seismo-acoustic detection threshold appears to be virtually independent of these same conditions at frequencies less than about 6 hertz. While the infrasonic system enjoys a 10-12 db detection threshold advantage over a vertical seismograph in the 0.5-5.0 hertz bandwidth during calm periods, this advantage vanishes in the 1.0-5.0 hertz bandwidth and falls to the seismograph system during windy periods. These results suggest that a stable, relatively low threshold can be maintained regardless of surface wind conditions by selectively using either or both systems for acoustic signal detection.

3. A code which estimates the zero lag correlation coefficient for two inputs in a moving window has been written tested, and calibrated for one configuration. The initial application of this code to selected records of the output of the pressure transducer and the TX01 short period vertical seismograph have yielded very promising results. Three seismo-acoustic detections were made by the code, two of which were clearly associated with

near regional seismic events detected at TXAR. The association of both seismic and seismo-acoustic detections with a single event strongly implies an explosive origin. Thus the preliminary results of this experiment suggests that a seismo-acoustic signal detection and its subsequent association with a seismic event may prove to be a useful method for the identification of low yield explosive sources.

#### 4.0 References

- Bedard, A.J., R.W. Whittaker, G.E. Greene, P. Mutschlecner, R.T. Nishiyama, and M. Davidson (1992) Measurements of pressure fluctuations near the surface of the earth, Tenth Symposium on Turbulence and Diffusion 29 Sept-2 Oct 1992, Portland OR, *Am. Meteor. Soc.* 293-296
- Sandige-Bodoh, Victoria L (1989) Investigating the effects fractures have on seismic wave velocities at the Lajitas, Texas seismic stations. GL-TR-89-0153, Geophysics Laboratory, United States Air Force Systems Command, Hanscom Air Force Base, MA 01731, ADA215943.
- Sorrells, Gordon G. (1971) A preliminary investigation into the relationship between long-period noise and local fluctuations in the atmospheric pressure field, *Geophys. Jour. R. Astron. Soc.*, 26, 71-82.
- Sorrells, G. G. and T. T. Goforth (1973) Low-frequency earth motion generated by slowly propagating partially organized pressure fields, *Bull. Seis. Soc. Am.*, 63, 1583-1601.

Prof. Thomas Ahrens  
Seismological Lab, 252-21  
Division of Geological & Planetary Sciences  
California Institute of Technology  
Pasadena, CA 91125

Prof. Keiiti Aki  
Center for Earth Sciences  
University of Southern California  
University Park  
Los Angeles, CA 90089-0741

Prof. Shelton Alexander  
Geosciences Department  
403 Deike Building  
The Pennsylvania State University  
University Park, PA 16802

Dr. Thomas C. Bache, Jr.  
Science Applications Int'l Corp.  
10260 Campus Point Drive  
San Diego, CA 92121 (2 copies)

Prof. Muawia Barazangi  
Cornell University  
Institute for the Study of the Continent  
3126 SNEE Hall  
Ithaca, NY 14853

Dr. Douglas R. Baumgardt  
ENSCO, Inc  
5400 Port Royal Road  
Springfield, VA 22151-2388

Dr. T.J. Bennett  
S-CUBED  
A Division of Maxwell Laboratories  
11800 Sunrise Valley Drive, Suite 1212  
Reston, VA 22091

Dr. Robert Blandford  
AFTAC/TT, Center for Seismic Studies  
1300 North 17th Street  
Suite 1450  
Arlington, VA 22209-2308

Dr. Stephen Bratt  
ARPA/NMRO  
3701 North Fairfax Drive  
Arlington, VA 22203-1714

Mr. Dale Breeding  
Sandia National Laboratories  
Organization 9236, MS 0655  
Albuquerque, NM 87185

Dr. Jerry Carter  
Center for Seismic Studies  
1300 North 17th Street  
Suite 1450  
Arlington, VA 22209-2308

Mr Robert Cockerham  
Arms Control & Disarmament Agency  
320 21st Street North West  
Room 5741  
Washington, DC 20451,

Dr. Zoltan Der  
ENSCO, Inc.  
5400 Port Royal Road  
Springfield, VA 22151-2388

Dr. Stanley K. Dickinson  
AFOSR/NM  
110 Duncan Avenue  
Suite B115  
Bolling AFB, DC 20332-6448

Dr. Petr Firbas  
Institute of Physics of the Earth  
Masaryk University Brno  
Jecna 29a  
612 46 Brno, Czech Republic

Dr. Mark D. Fisk  
Mission Research Corporation  
8560 Cinderbed Rd.  
Suite 700  
Newington, VA 22122

Dr. Cliff Frolich  
Institute of Geophysics  
8701 North Mopac  
Austin, TX 78759

Dr. Holly Given  
IGPP, A-025  
Scripps Institute of Oceanography  
University of California, San Diego  
La Jolla, CA 92093

Dr. Jeffrey W. Given  
SAIC  
10260 Campus Point Drive  
San Diego, CA 92121

Dan N. Hagedon  
Pacific Northwest Laboratories  
Battelle Boulevard  
Richland, WA 99352

Dr. James Hannon  
Lawrence Livermore National Laboratory  
P.O. Box 808, L-205  
Livermore, CA 94550

Dr. Roger Hansen  
University of Colorado, JSPC  
Campus Box 583  
Boulder, CO 80309

Prof. David G. Harkrider  
Phillips Laboratory  
Earth Sciences Division, PL/GPE  
29 Randolph Road  
Hanscom AFB, MA 01731-3010

Prof. Danny Harvey  
University of Colorado, JSPC  
Campus Box 583  
Boulder, CO 80309

Prof. Donald V. Helmberger  
Division of Geological & Planetary Sciences  
California Institute of Technology  
Pasadena, CA 91125

Prof. Eugene Herrin  
Geophysical Laboratory  
Southern Methodist University  
Dallas, TX 75275

Prof. Robert B. Herrmann  
Department of Earth & Atmospheric Sciences  
St. Louis University  
St. Louis, MO 63156

Prof. Lane R. Johnson  
Seismographic Station  
University of California  
Berkeley, CA 94720

Prof. Thomas H. Jordan  
Department of Earth, Atmospheric &  
Planetary Sciences  
Massachusetts Institute of Technology  
Cambridge, MA 02139

Mr. Robert C. Kemerait  
ENSCO, Inc.  
445 Pineda Court  
Melbourne, FL 32940

U.S. Dept of Energy  
Max Koontz, NN-20, GA-033  
Office of Research and Develop.  
1000 Independence Avenue  
Washington, DC 20585

Dr. Richard LaCoss  
MIT Lincoln Laboratory, M-200B  
P.O. Box 73  
Lexington, MA 02173-0073

Prof. Charles A. Langston  
Geosciences Department  
403 Deike Building  
The Pennsylvania State University  
University Park, PA 16802

Jim Lawson, Chief Geophysicist  
Oklahoma Geological Survey  
Oklahoma Geophysical Observatory  
P.O. Box 8  
Leonard, OK 74043-0008

Prof. Thorne Lay  
Institute of Tectonics  
Earth Science Board  
University of California, Santa Cruz  
Santa Cruz, CA 95064

Dr. William Leith  
U.S. Geological Survey  
Mail Stop 928  
Reston, VA 22092

Mr. James F. Lewkowicz  
Phillips Laboratory/GPE  
29 Randolph Road  
Hanscom AFB, MA 01731-3010( 2 copies)

Dr. Gary McCartor  
Department of Physics  
Southern Methodist University  
Dallas, TX 75275

Prof. Thomas V. McEvilly  
Seismographic Station  
University of California  
Berkeley, CA 94720

Dr. Keith L. McLaughlin  
S-CUBED  
A Division of Maxwell Laboratory  
P.O. Box 1620  
La Jolla, CA 92038-1620

Prof. Bernard Minster  
IGPP, A-025  
Scripps Institute of Oceanography  
University of California, San Diego  
La Jolla, CA 92093

Prof. Brian J. Mitchell  
Department of Earth & Atmospheric Sciences  
St. Louis University  
St. Louis, MO 63156

Mr. Jack Murphy  
S-CUBED  
A Division of Maxwell Laboratory  
11800 Sunrise Valley Drive, Suite 1212  
Reston, VA 22091 (2 Copies)

Dr. Keith K. Nakanishi  
Lawrence Livermore National Laboratory  
L-025  
P.O. Box 808  
Livermore, CA 94550

Prof. John A. Orcutt  
IGPP, A-025  
Scripps Institute of Oceanography  
University of California, San Diego  
La Jolla, CA 92093

Dr. Howard Patton  
Lawrence Livermore National Laboratory  
L-025  
P.O. Box 808  
Livermore, CA 94550

Dr. Frank Pilotte  
HQ AFTAC/TT  
1030 South Highway A1A  
Patrick AFB, FL 32925-3002

Dr. Jay J. Pulli  
Radix Systems, Inc.  
6 Taft Court  
Rockville, MD 20850

Prof. Paul G. Richards  
Lamont-Doherty Earth Observatory  
of Columbia University  
Palisades, NY 10964

Mr. Wilmer Rivers  
Teledyne Geotech  
1300 17th St N #1450  
Arlington, VA 22209-3803

Dr. Alan S. Ryall, Jr.  
Lawrence Livermore National Laboratory  
P.O. Box 808, L-205  
Livermore, CA 94550

Dr. Chandan K. Saikia  
Woodward Clyde- Consultants  
566 El Dorado Street  
Pasadena, CA 91101

Mr. Dogan Seber  
Cornell University  
Inst. for the Study of the Continent  
3130 SNEE Hall  
Ithaca, NY 14853-1504

Secretary of the Air Force  
(SAFRD)  
Washington, DC 20330

Office of the Secretary of Defense  
DDR&E  
Washington, DC 20330

Thomas J. Sereno, Jr.  
Science Application Int'l Corp.  
10260 Campus Point Drive  
San Diego, CA 92121

Dr. Michael Shore  
Defense Nuclear Agency/SPSS  
6801 Telegraph Road  
Alexandria, VA 22310

Prof. David G. Simpson  
IRIS, Inc.  
1616 North Fort Myer Drive  
Suite 1050  
Arlington, VA 22209

Dr. Jeffrey Stevens  
S-CUBED  
A Division of Maxwell Laboratory  
P.O. Box 1620  
La Jolla, CA 92038-1620

Prof. Brian Stump  
Los Alamos National Laboratory  
EES-3  
Mail Stop C-335  
Los Alamos, NM 87545

Prof. Tuncay Taymaz  
Istanbul Technical University  
Dept. of Geophysical Engineering  
Mining Faculty  
Maslak-80626, Istanbul Turkey

Phillips Laboratory  
ATTN: GPE  
29 Randolph Road  
Hanscom AFB, MA 01731-3010

Prof. M. Nafi Toksoz  
Earth Resources Lab  
Massachusetts Institute of Technology  
42 Carleton Street  
Cambridge, MA 02142

Phillips Laboratory  
ATTN: TSML  
5 Wright Street  
Hanscom AFB, MA 01731-3004

Dr. Larry Turnbull  
CIA-OSWR/NED  
Washington, DC 20505

Phillips Laboratory  
ATTN: PL/SUL  
3550 Aberdeen Ave SE  
Kirtland, NM 87117-5776 (2 copies)

Dr. Karl Veith  
EG&G  
2341 Jefferson Davis Highway  
Suite 801  
Arlington, VA 22202-3809

Dr. Michel Campillo  
Observatoire de Grenoble  
I.R.I.G.M.-B.P. 53  
38041 Grenoble, FRANCE

Prof. Terry C. Wallace  
Department of Geosciences  
Building #77  
University of Arizona  
Tucson, AZ 85721

Dr. Kin Yip Chun  
Geophysics Division  
Physics Department  
University of Toronto  
Ontario, CANADA

Dr. William Wortman  
Mission Research Corporation  
8560 Cinderbed Road  
Suite 700  
Newington, VA 22122

Prof. Hans-Peter Harjes  
Institute for Geophysics  
Ruhr University/Bochum  
P.O. Box 102148  
4630 Bochum 1, GERMANY

ARPA, OASB/Library  
3701 North Fairfax Drive  
Arlington, VA 22203-1714

Prof. Eystein Husebye  
IFJF  
Jordskjelvstasjonen  
Allegaten, 5007 BERGEN NORWAY

HQ DNA  
ATTN: Technical Library  
Washington, DC 20305

David Jepsen  
Acting Head, Nuclear Monitoring Section  
Bureau of Mineral Resources  
Geology and Geophysics  
G.P.O. Box 378, Canberra, AUSTRALIA

**Defense Technical Information Center**  
**8725 John J. Kingman Road**  
**Ft Belvoir, VA 22060-6218**  
**(2 copies)**

Ms. Eva Johannisson  
Senior Research Officer  
FOA  
S-172 90 Sundbyberg, SWEDEN

TACTEC  
Battelle Memorial Institute  
505 King Avenue  
Columbus, OH 43201 (Final Report)

Dr. Peter Marshall  
Procurement Executive  
Ministry of Defense  
Blacknest, Brimpton  
Reading FG7-FRS, UNITED KINGDOM



Dr. Bernard Massinon, Dr. Pierre Mechler  
Societe Radiomana  
27 rue Claude Bernard  
75005 Paris, FRANCE (2 Copies)

Dr. Svein Mykkeltveit  
NTNT/NORSAR  
P.O. Box 51  
N-2007 Kjeller, NORWAY (3 Copies)

Dr. Jorg Schlittenhardt  
Federal Institute for Geosciences & Nat'l Res.  
Postfach 510153  
D-30631 Hannover , GERMANY

Dr. Johannes Schweitzer  
Institute of Geophysics  
Ruhr University/Bochum  
P.O. Box 1102148  
4360 Bochum 1, GERMANY

Trust & Verify  
VERTIC  
Carrara House  
20 Embankment Place  
London WC2N 6NN, ENGLAND